2012-09-13

Experimental study of imbibition mechanisms in heavy oil waterflooding using etched glass micromodel

Mei, Songyi

UNIVERSITY OF CALGARY

Experimental Study of Imbibition Mechanisms in Heavy Oil Waterflooding Using Etched Glass Micromodel

by

Songyi Mei

A THESIS

SUBMITTED TO THE FACULTY OF GRADUATE STUDIES

IN PARTIAL FULFILMENT OF THE REQUIREMENTS FOR THE

DEGREE OF MASTER OF SCIENCE

DEPARTMENT OF CHEMICAL AND PETROLEUM ENGINEERING

CALGARY, ALBERTA

SEPTEMBER, 2012

Abstract

Waterflooding in heavy oil reservoirs has an almost 50 years history in western Canada, but its recovery mechanisms, especially in the situation of a high oil to water viscosity ratio, are still not well understood. This thesis studied the water imbibition mechanisms in the process of heavy oil waterflooding, and their effects on oil recovery using a glass made micromodel.

In a water-wet environment, waterflooding (water displacing oil) represents a process of water imbibition. This water imbibition experimental study was conducted with varying water injection rates and oil viscosities. The effects of time, viscosity ratio and water injection rate on imbibition rate were studied. The recovery factor was proportional to the square root of time, and it also had a definite relationship with oil viscosity even though it was not linear. The effects of injection rate on imbibition rate were complicated. Images of the imbibition process were recorded and analyzed. Water broke through quickly because of water fingering. A significant amount of oil was produced during the post-breakthrough period under high water cuts. In the cases of low rate water injection, water imbibed into the original oil region perpendicularly to the water channel. At this stage, capillary forces were the key factor. Water film thickening, snap-off and oil refilling were the main mechanisms that made water imbibition work. Emulsification was also another important mechanism observed, with W/O emulsions primarily being formed.

Acknowledgements

There are a number of people without whom this thesis might not have been written, and to whom I am greatly indebted.

I am heartily thankful to my supervisor, Dr. Apostolos Kantzas, whose guidance, encouragement, great patience and support from the initial to the final level enabled me to develop an understanding of the subject.

I would like to thank my mentor Dr. Jonathan Bryan, for his guidance and friendship.

I owe my deepest gratitude to all the staff and students at TIPM Laboratory. The help of Mr. Jun Gao, Ms. Xiaoli (Lilly) Yu, Mr. Zhengyin (Jim) Wang, Ms. Jihong (Nancy) Zhang and Mr. Israel Nandez were greatly appreciated.

I would like to show my gratitude to NSERC and the Canada Research Chair in Energy and Imaging for financial support.

There have been many others who have given me a hand through some difficult times and to these persons I express my heartfelt thanks. To my friends who have shared the long time at the university with me (particularly Ziqiang (Kevin) Guo, Yi (Louise) Liu, Miss Jia (Maris) Mei, Dr. Xiaodong Zhou, Miss Xiaoqing Wang and Lin Li). To my family for always being there to encourage me.

Dedication

This dissertation is lovingly dedicated to my parents (Qiyou Mei and Xingfeng Liu), my sister (Ni Mei) and my brother-in-law (Zhongtao Cai). For having been a source of encouragement, inspiration and moral support to me throughout my life.

Table of Contents

List of Tables

List of Figures

List of Symbols, Abbreviations and Nomenclature

Symbols	Definition
A	Area
A_c	Area under the capillary pressure curve
A_i	Area open to imbibition in the i^{th} direction
A_0	Area of oil zone
A_w	Area of water zone
b	Width
C	Constant
C^*	Wettability constant
d	Drop diameter
D	Diameter of the sandpack
E(η)	Dimensionless function of imbibition rate
f	Calibration factor for the spinning drop tensiometer
F_s	Shape factor
g	Gravity acceleration
h	Height
I_{sc}	Instability number
k	Permeability
k_{re}^*	Relative permeability pseudo-function
k_{ro}^*	Relative permeability to oil phase at the S_{wf}
k_{rw}^*	Relative permeability to water phase at the S_{wf}
K_{wor}	Permeability to water at the S_{or}
l_{Ai}	Distance the imbibition front travelled from the imbibition face to the no-flow boundary
L	Length
L’	Recovery limit
L_c	Modified characteristic length
Ls	Characteristic length
M	Mobility ratio
n	Viscosity ratio exponent
n_r	Rotation rate
N_{ca}	Capillary number
N_g	Gravity number
P	Pressure
PV	Pore volume
P_c	Capillary pressure
P_c^*	Capillary pressure at S_{wf}
q_t	Constant pumping rate
$q_{free\text{-}spo\text{-}im}$	Initial displacement rate in the free spontaneous imbibition
Q	Flow rate
$Q_i(t)$	Volume of oil originally in place
$Q_o(t)$	Volume of oil produced up to the time t
r	Radius

R	Recovery
R_{bt}	Breakthrough Recovery
S_o	Oil saturation
$S_{o\text{-}bt}$	Oil saturation at breakthrough
S_{oi}	Initial oil saturation
S_{or}	Residual oil saturation
S_w	Water saturation
S_{wi}	Initial water saturation
S_{wf}	Water saturation behind the imbibition front
t	Time
t_D	Dimensionless time
V	Volume
V_b	Bulk volume of the matrix
X	Distance
X_{Ai}	Distance from imbibition face to the center of the matrix
α	Dip angle
ΔP	Differential pressure
ΔR	Incremental recovery
$\Delta\rho$	Density difference
η	Square root of oil to water viscosity ratio
θ	Contact angle
λ	Dimensionless empirical constant
μ	Viscosity
μ_e	effective viscosity of the oil and water phases
μ_{gm}	Geometric mean of the water and oil viscosity
μ_g	Viscosity of gas
μ_l	Viscosity of liquid
μ_m	Mean viscosity of gas-liquid system
μ_o	Viscosity of oil
μ_w	Viscosity of water
υ	Velocity
$\upsilon_{free\text{-}spo\text{-}im}$	Initial Darcy velocity in free spontaneous imbibition
ρ	Density
ρ_o	Density of oil
ρ_w	Density of water
σ	Interfacial tension
σ_e	Effective interfacial tension
σ_{ow}	Interfacial tension between oil and water
Ø	Porosity

Subscripts

m	Mean value
o	Oil
w	Water

Abbreviations

1A	Fluids pair: oil #1 and water #A
A1	Fluids pair: water #A and oil #1
CA	Complete Capillary Number
CSS	Cyclic steam stimulation
CHOPS	Cold heavy oil production with sand
IFT	Interfacial tension
RF	Recovery factor
SAGD	Steam assisted gravity drainage
W/O	Water in oil emulsion

CHAPTER ONE: INTRODUCTION

1.1 Research Background

Heavy oil is defined as any liquid petroleum with the API gravity ranging from 10°- 20°, and the viscosity ranging from 50mPa.s - 50,000mPa.s. It is referred to as "heavy" because its density or specific gravity is higher than that of light oil. Crude bitumen is a type of extra heavy oil that does not flow to the producer at reservoir conditions. The crude bitumen and the rock material it is found in, together with any other associated mineral substances other than natural gas, are called oil sands.

In western Canada and in the Orinoco heavy oil belt of Venezuela, there are huge reserves of heavy oil and bitumen. According to the report ST98-2010 (ERCB, 2010), in Alberta alone, there are about 26.99 billion cubic meters remaining established reserves of crude bitumen. Table 1.1 summarizes the established reserves and annual production in 2009. And about 21.55 billion cubic meters, or about 80 percent of the remaining established reserves is considered to be recoverable by in-situ methods. With a rising worldwide consumption of oil and declining light oil reserves, Canada will be one of the most important oil sources for the world. The heavy oil deposits in Alberta alone, account for approximately 2 percent of the total oil sand resource base. This small fraction, as the resource base is huge, is an absolutely significant amount of oil that is available for recovery.

Table 1.1: Alberta oil reserves and production in December, 2009

remaining established reserves	crude bitumen	26,992 $\times 10^6$ m^3
	conventional	228 $\times 10^6$ m^3
annual production (2009)	crude bitumen	86 $\times 10^6$ m^3
	conventional	27 $\times 10^6$ m^3

Heavy oil reservoirs are often found in high permeability, high porosity, and weakly consolidated or unconsolidated sand deposits. Due to its high viscosity, heavy oil may not flow easily at reservoir conditions.

At the initial reservoir conditions, the oil may contain dissolved gas that can provide energy for driving oil. In some cases, the oil formation may connect with active boundary or underlying aquifer, which can provide full or partial pressure support for the reservoir. Sometimes, in thick or high inclination-angle reservoirs, gravity can also act as a significant force to drive oil. Most of the in-situ recoverable resource is developed by primary and thermal methods. In 2009, 31 percent of in situ heavy oil and bitumen production in Alberta was recovered by primary production, and primary production has been growing since 2003 and increased by 11 percent from 2008 to 2009 (ERCB, 2010). The production of sand in primary production is inevitable, and this sand production will result in the generation of high permeability “wormholes network” (Tremblay et al., 1997). This process is known as CHOPS (cold heavy oil production with sand). In addition to wormhole, “foamy oil flow” which results from gas evolution in the heavy oil, is another important mechanism in this process (Maini, 2001). The recovery factor of primary production is about 5 percent (ERCB, 2010), that means most oil is left in the reservoir. Secondary or advanced recovery methods are usually considered for the

potential of further development. These methods mainly include waterflooding, solvent injection, chemical flooding, CSS (cyclic steam stimulation) and SAGD (steam assistant gravity drainage).

Waterflooding, among those secondary and enhanced oil recovery methods, is inexpensive and easier to operate. Many reservoirs in Alberta and Saskatchewan are relatively thin or considered to be marginal, so expensive methods will likely not be applicable. Waterflooding is becoming increasingly important in recovering heavy oil. Unfortunately, for heavy oil waterflooding systems, due to high oil viscosity, oil recovery is expected to be very low (Brice et al., 2008). Heavy oil waterfloods, in despite of poor recovery, have been carried out in Alberta and Saskatchewan for the past 50 years (Miller, 2006).

In the literature, most reports are focused on the operation and performance of heavy oil waterflooding (Miller, 2006; Vittoratos et al., 2010). In contrast, there is much less information regarding its mechanisms. Recently, Mai has investigated the mechanisms of heavy oil recovery by low rate waterflooding, in the report, the relative significance of viscous and capillary forces in heavy oil systems was studied, and water imbibition was believed to make a great contribution to the oil production after water breakthrough (Mai and Kantzas, 2010). Water imbibition is the main target of this thesis. The development of understanding of the mechanisms in heavy oil waterflooding will be covered in Chapter Two.

1.2 Research Objective and Methodology

The main focus of this research is to determine the role the water imbibition plays in the process of heavy oil waterflooding. An experimental study was conducted using etched-glass micromodel under laboratory conditions. What contribution the imbibition makes on the oil recovery is the main question this research seeks to answer. Imbibition, according to the advancing direction, can be classified as co-current and counter-current. Film thickening, snap-off, oil-refilling, emulsifying and any other mechanisms are strongly related to water imbibition. This research also seeks to investigate several factors that have important effects on the water imbibition process. Specifically, imbibition time, viscosity ratio and injection rate are interesting factors. Imbibition rate is a function of time, so finding the relationship between imbibition rate and time is another objective of this thesis.

A micromodel, which is made of etched glasses, was used as porous media. Pore level fluids distribution and flow mechanisms were studied. The oil recovery and fluid saturations at different stages during waterflooding were measured using both image analysis and mass balance. The images of the process were recorded using a high resolution camera. Images and other dynamic experimental data, such as injection rate, production rate and differential pressure variation, were analyzed. A maximum flow rate in the micromodel was set, and the flow rate was well controlled to make sure the experiments were performed within the capillary dominated flow regime. Based on direct observations through transparent micromodel, visual evidences of water imbibition in the process of heavy oil waterflooding were also provided.

The operation strategy of heavy oil waterflooding attracted lots of attention. Some common opinions, such as gas saturation control and voidage replacement ratio control, were obtained. However, the mechanisms behind the strategy were still unknown. To correlate substantial mechanisms with operation strategy is also an objective of this research.

At low water injection rate, especially after water breakthrough, capillary forces are believed to play an important role in oil propagation and oil production. Last but not the least, to study the balance between viscous forces and capillary forces is another objective of this study. Instability number and capillary number were used for the forces analysis.

CHAPTER TWO: LITERATURE REVIEW

2.1 Mechanisms in Heavy Oil Waterflooding

For conventional oil reservoirs, waterflooding, known as a secondary recovery method, is the most popular technique for oil recovery. The performance of conventional waterflooding can be accurately described and predicted by the Buckley-Leverett equation (Buckley and Leverett, 1942). For heavy oil waterflooding, ordinary water without additives is injected into a heavy oil reservoir. This will result in a so-called high mobility ratio or adverse mobility ratio waterflooding. As this process is much more complex than conventional waterflooding, the theoretical and operational knowledge of conventional waterflooding is not applicable for heavy oil waterflooding (Miller, 2006). Currently, such dynamic is not fully described in a theory or simulation framework.

In the literature, the mechanisms of oil flow in the process of heavy oil waterflooding are found to be pressure support, solution gas drive, imbibition, drag, emulsification, gravity effect (Chen et al., 1991; Smith, 1992; Chen et al., 1999; Farouq-Ali, 2000; Vittoratos et al., 2006; Miller, 2006; Fischer et al., 2006; Mai, 2008).

2.1.1 Pressure Support

As waterflooding is usually performed at the conclusion of primary depletion, it means the reservoir pressure is decreased to a low level. Drive energy is necessary for further oil production (Smith, 1992). Water injection is considered to be a manner of energy maintenance or pressure support. In the unstable process of heavy oil waterflooding, water injection is more like of a pair of hands surrounding and squeezing the oil out of

the pores. Pressure in the water phase is supported and is transferred to the oil phase. Pressure drives both water and oil phases toward a pressure sink at the producers independently. However, the formation of water fingers, which leads to early water breakthrough, is inevitable due to the poor mobility ratio (Perkins et al., 1969). Before water breakthrough, viscous forces induced by pressure support are considered to be the dominant drive force.

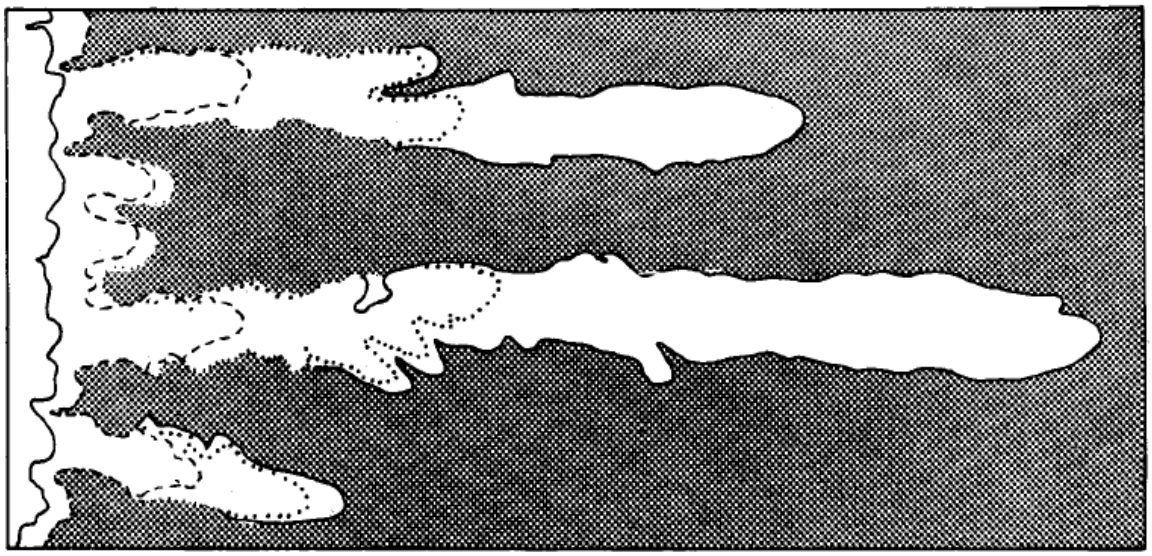

Figure 2.1: Viscous fingering pattern with viscosity ratio of 146
(Perkins et al., 1969)

When water breakthrough occurs, the injector and producer are connected through high permeability water channels. These preferential communication paths result in the low differential pressure between the injector and the producer. Maintaining large reservoir pressure and high injection rate has been repeatedly reported to merely circulate water (Vittoratos et al., 2006). From this perspective, pressure support through high rate water injection is difficult and uneconomical to maintain.

Smith pointed out that gas control could be one of mechanisms of heavy oil waterflooding (Smith, 1992). To keep the gas saturation small but non-zero through water injection, can make full use of the internal solution gas drive energy. Actually, in order to meet the condition of appropriate gas saturation, the reservoir pressure should be held around the related bubble point. Therefore, this is a natural process of pressure support.

2.1.2 Solution Gas Drive

As the reservoir pressure decreases, solution gas comes out of the hydrocarbon phase. As to the reservoir pressure maintenance condition, liberated gas may become a continuous phase and move independently of oil. The expanded volume of gas will squeeze oil into the producer. The gas bubbles formed in the reservoir tend to block small pore throats, and there can be a displacement of the flow from the smaller pores to the larger ones. Also from water filled pores to oil/gas filled ones if the reservoir rock is in the condition of water wet. The moving of oil and less gas as a mixture phase is beneficial to oil recovery. However, the rapid drainage of continuous gas phase is considered to be a waste of reservoir energy (Smith, 1988; 1992).

Vittoratos pointed out that the most effective use of solution gas drive is for pushing the oil into the nearby portions of the communication path. In heavy oil waterflooding systems, as the pressure declines below the bubble point, gas bubbles will be nucleated. This will result in the formation of foamy oil (gas-in-oil foam). Expansion of oil and gas phases will squeeze foamy oil into the nearby water path, through where foamy oil will be driven toward the production well by the water injected (Vittoratos et al., 2006).

2.1.3 Imbibition

Imbibition is the process by which a wetting fluid displaces a non-wetting fluid out of a porous medium. Waterflooding in a water wet porous medium is considered to be a water imbibition process. The development of water imbibition theory will be discussed in detail in the section 2.2.

2.1.4 Drag

In water-wet porous media, water as the wetting phase tends to occupy small pores and throats. In the case of low water saturation, water films present between oil phase and the pore walls, and water may only be able to flow in the form of thickening films (Yuster, 1951; Dullien, 1979). Water here is hydraulically connected to oil that is flowing in the center of the pores, and this will result in the apparent slip of oil. This effect is so-called "lubrication" effect (Yuster, 1951; Dullien, 1979). Thickening and slippage at the oil-water interface in the water-wet porous medium result in the squeezing and dragging of the hydrocarbon phase to the pressure sink producer (Smith, 1992).

2.1.5 Emulsification

In heavy oil thermal recovery, emulsification of water into the oil phase was widely investigated (Farouq-Ali, 1989; Vittoratos, 1990; Chen et al., 1991; Bennion et al., 1993). Previously, it was believed that the W/O emulsions form only at restrictions in and around the wellbore, but not in the reservoir. Subsequently, Chen presented both laboratory and field evidence for the in-situ formation and flow of emulsions, and he also conducted a series of co-injection experiments to study the factors causing emulsification

of water into bitumen (Chen et al. 1991; 1999). It must be noted that these experiments were performed at temperatures greater than 60^0C. That temperature may be in the scope of a hot water flood.

Smith presented that, in heavy oil waterflooding, some of the hydrocarbon became suspended in the water phase as a result of the formation of in-situ emulsions. The weak emulsions or micro-emulsions were effective in transporting oil and in improving displacement (Smith, 1992). In this process, some chemical fractions of heavy oils were believed to be native surfactants or co-surfactants, which can contribute to emulsification. The salinity of water and contact time were believed to be two other important factors as well.

Vittoratos analyzed the field production data of Milne Point Unit in the Alaska North Slope (Vittoratos et al., 2006). The reservoir, with in-situ oil viscosity ranging from 20mPa.s to 220mPa.s, was recovered by waterflooding. Vittoratos developed a conceptual model to explain the empirical observations. The model envisioned the injected water initially forming a preferred communication path between the injector and producer, wherein the injected water mixes with the oil to form water-in-oil emulsions that were then driven to the producer. The results of the model and the production data were in agreement. However, so far, no experiment, which was operated at ambient temperature, has provided evidence for this model. Additionally, in this model, the function of solution gas should be further investigated as most waterflooding projects were operated in conditions of relative low pressure.

2.1.6 Gravity Effect

The density of heavy oil is very close to that of water, so the gravity effect is weak in the heavy oil – water system. However, when a free gas phase forms, gravity drainage in heavy oil waterflooding will help the oil phase film spread on the water phase, and this film spreading tends to decrease oil saturation in the gas zone (Smith, 1992).

2.2 Water Imbibition

In a water wet reservoir, water imbibition is the process of water invading into the porous media originally occupied by the non-wetting phase. According to the flow direction, imbibition can be classified into co-current imbibition and counter-current imbibition. In co-current imbibition, oil moves in the same direction as that of water. However, in counter-current imbibition, oil and water move in opposite directions. Capillary pressure is the dominant factor for water imbibition.

Conventionally, many studies on imbibition have focused on naturally fractured reservoirs, where water is imbibed into the rock matrix blocks from the fractures to displace gas or oil (Bourbiaux and Kalaydjian, 1990). The effects of boundary condition, oil viscosity and many other parameters on water imbibition rate in fracture systems have been mentioned in many publications. However, there are many fewer reports about water imbibition in the process of heavy oil waterflooding in the literature. The water imbibition mechanisms in the fracture-matrix system and in heavy oil waterflooding system are discussed separately in the following sections.

2.2.1 Imbibition in Naturally Fractured Reservoir

2.2.1.1 Aronofsky's Equation

As early as 1958, Aronofsky et al. pointed out that imbibition may become a significant element of the production mechanism in a fractured reservoir with a great number of large fractures (Aronofsky et al., 1958). From the laboratory data collected, they gave a model to describe the variation of oil production rate with time, and the model was in the form of an equation:

$$\frac{Qo(t)}{Qi(t)} = L'(1 - e^{-\lambda t}) \qquad \text{Eqn (2.1)}$$

Where, $Qo(t)$ is the volume of oil produced up to the time t

$Qi(t)$ is the volume of oil originally in place

λ is a constant giving the rate of convergence

L' is the limit toward which the recovery converges.

Aronofsky et al. compared this model with actual field data, and selected best fit λ value with a least squares method. However, for some fractured reservoirs which are not well known, the λ value is then found empirically. They also found that oil production from water imbibition in a fractured reservoir may be a very lengthy process.

2.2.1.2 Scaling Method

In order to use the result of imbibition testing on small cores to predict field performance and on the basis of Rapoport's equation (Rapoport, 1955) and Leverett's dimensionless J-function, Mattax and Kyte (Mattax and Kyte, 1962) proposed a dimensionless scaling parameter:

$$t_D = t \cdot \sqrt{\frac{k}{\emptyset}} \cdot \frac{\sigma}{\mu_w L^2} \qquad \text{Eqn (2.2)}$$

Where, t_D is dimensionless time,

t is imbibition time

L is a characteristic linear dimension of the matrix block.

This scaling parameter allows the imbibition performance of any system of varying dimensions and rock properties to fit into a single "S-shaped" curve where the recovery can be predicted.

Mattax and Kyte (1962) found that if imbibition oil recovery is plotted against this dimensionless scaling parameter, the same recovery curve will be obtained for the model and for all matrix blocks of the same rock type and geometry. In this scaling parameter, they ignored the gravity effects. On the other hand, they took different rock and fluid properties into consideration, such as block size, permeability, porosity, interfacial tension and viscosity. They did not provide a general definition of the characteristic length L, which was a dominant factor in scale up.

Kazemi et al. presented a shape factor, F_s, to combine the effects of matrix sizes, shapes and boundary conditions (Kazemi et al., 1992):

$$F_s = \frac{1}{V_b} \sum_{i=1}^{n} \frac{A_i}{X_{A_i}} \qquad \text{Eqn (2.3)}$$

Where, V_b is bulk volume of the matrix

A_i is the area open to imbibition at the ith direction

X_{Ai} is the distance from A_i to the center of the matrix

n is the total number of surfaces open to imbibition.

A characteristic length, L_s, is defined as,

$$L_s = \sqrt{\frac{1}{F_s}} = \sqrt{V_b \Big/ \sum_{i=1}^{n} \frac{A_i}{X_{A_i}}} \qquad \text{Eqn (2.4)}$$

Substitute this characteristic length into Mattax and Kyte scaling equation: Equation 2.2, the dimensionless time will be modified to:

$$t_{D1} = t \cdot \sqrt{\frac{k}{\emptyset}} \cdot \frac{\sigma \cdot F_s}{\mu_w} \qquad \text{Eqn (2.5)}$$

The applicability of the characteristic length defined by Equation 2.4 was tested using the data reported by Hamon and Vidal (Hamon and Vidal, 1986); Ma et al. found it didn't fit well in the one-end-open (Figure 2.2, OEO) systems (Ma et al., 1997). So they proposed a modified characteristic length, L_c:

$$L_c = \sqrt{\frac{V_b}{\sum_{i=1}^{n} A_i \Big/ l_{A_i}}} \qquad \text{Eqn (2.6)}$$

Where, l_{Ai} is the distance that the imbibition front travels from the imbibition face to the no-flow boundary.

Substituting this characteristic length L_c into Mattax and Kyte scaling Equation 2.2, and then it yields the modified dimensionless time:

$$t_{D2} = C \cdot t \cdot \sqrt{\frac{k}{\emptyset}} \cdot \frac{\sigma}{\mu_w} \cdot \frac{1}{L_c^2} \qquad \text{Eqn (2.7)}$$

Where, *C* is the unit conversion factor, is equal to 0.018849 if *t* is in mintues, *K* in md, Φ in fraction, σ in dynes/cm, μ_w in mPa.s, and L_c in cm.

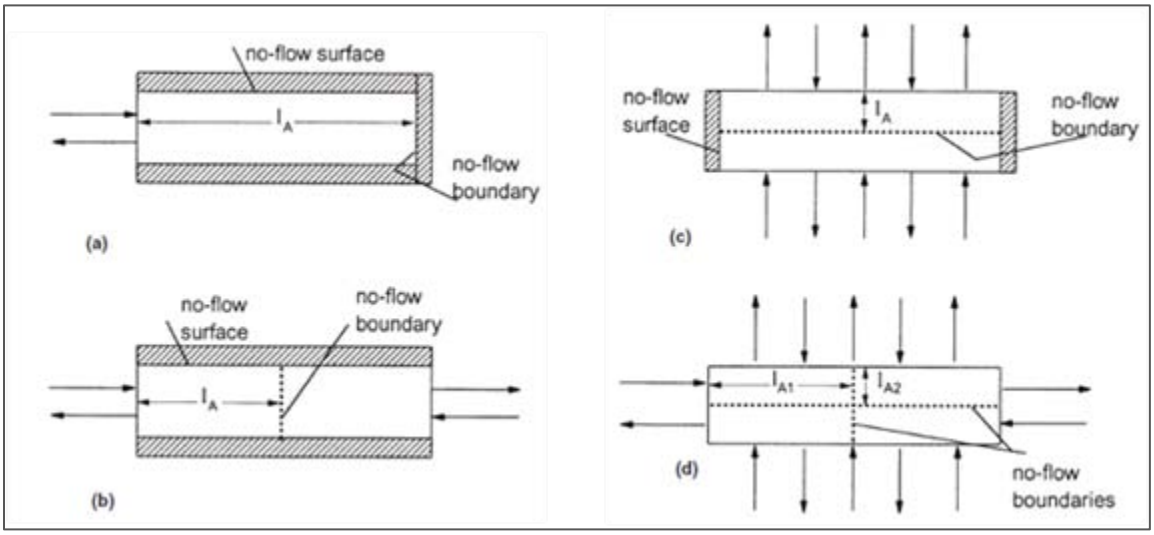

(a) OEO-one end open, 1D linear counter-current imbibition. (b) TEO-two end open, 1D linear counter-current imbibition. (c) TEC-two end closed, radial counter-current imbibition. (d)AFO-all faces open, 3D counter-current imbibition (Zhang et al., 1996; Ma et al., 1997).

Figure 2.2: Four boundary conditions of counter-current imbibition

Depending on the boundary conditions, l_{Ai} may be different from X_{Ai}, and this may result in a different L_c value compared with L_s. For the boundary condition of one end open that was shown in Fig. 2.2a, $l_{Ai} = 2X_{Ai}$, or $L_c = 1.414\ L_s$.

Previous scaling groups, Equation 2.2 - Equation 2.7, were based on the assumptions that the viscosity ratios were identical. Actually, the effects of fluid viscosity on imbibition rate should be and have been further investigated.

As early as 1959, Graham found that the rate of imbibition depended on fluid viscosities (Graham, et al., 1959). Later on, Blair described the counter-current water imbibition using transformed Darcy equations, which took capillary forces as the dominant factor (Blair, 1964). With these equations, imbibition rate of water into both linear and radial

systems were studied, and he drew a conclusion that the time required to imbibe a fixed volume of water of a certain viscosity is approximately proportional to the square root of the viscosity of the oil.

Ma et al. studied the influence of oil viscosity and oil/water viscosity ratio on imbibition rate (Ma et al., 1995). For water-oil systems, to account for different viscosity ratios of oil over water, they introduced the square root of viscosity ratio into Equation 2.7 and proposed a modified scaling group:

$$t_{D2} = C \cdot t \cdot \sqrt{\frac{k}{\emptyset}} \cdot \frac{\sigma}{\mu_w} \cdot \sqrt{\frac{\mu_w}{\mu_o}} \cdot \frac{1}{L_c^2} = C \cdot t \cdot \sqrt{\frac{k}{\emptyset}} \cdot \frac{\sigma}{\mu_{gm}} \cdot \frac{1}{L_c^2} \qquad \text{Eqn (2.8)}$$

$$\mu_{gm} = \sqrt{\mu_w \cdot \mu_o} \qquad \text{Eqn (2.9)}$$

Where, μ_{gm} is the geometric mean of the water viscosity and oil viscosity.

Considering that the effects of viscosity ratio on imbibition rate are complex, they even gave a general format of viscosity ratio term in Equation 2.8. Then a more generalized dimensionless scaling group was proposed:

$$t_{D3} = C \cdot t \cdot \sqrt{\frac{k}{\emptyset}} \cdot \frac{\sigma}{\mu_w} \cdot (\frac{\mu_w}{\mu_o})^n \cdot \frac{1}{L_c^2} \qquad \text{Eqn (2.10)}$$

Where, *n* is the viscosity ratio exponent.

Wang (Wang, 1999) conducted experimental studies on imbibition in air/refined oil-rock system, and proposed a different correlation for the mean viscosity of gas-liquid system as:

$$\mu_m = \mu_l^{3/4} \mu_g^{1/4}$$ Eqn (2.11)

Here the liquid is the wetting phase. And the difference between air viscosity and liquid viscosity is large. It also yielded a related scaling equation by substituting Equation 2.11 into Equation 2.8.

Equation 2.8 was also used to study the spontaneous imbibition from a weakly water wet system by Xie and Morrow (Xie and Morrow, 2001).

Li and Horne have published a more general scaling approach for spontaneous imbibition of both gas-liquid-rock system and oil-water-rock system (Li and Horne, 2004; 2006). For oil-water-rock systems, they combined many rock and fluid properties into the scaling parameter. The dimensionless time was expressed as follows:

$$t_{D4} = t \cdot \frac{k k_{re}^*}{\emptyset} \cdot \frac{P_c^*}{\mu_e} \cdot \frac{S_{wf} - S_{wi}}{L_c^2}$$ Eqn (2.12)

Where, k_{re}^* is the relative permeability pseudofunction associated with k_{ro}^* (the oil phase relative permeability at S_{wf}) and k_{rw}^*, μ_e is the effective viscosity of the oil and water phases, S_{wf} is the water saturation behind the imbibition front, S_{wi} is the initial water saturation in the core sample, k_{rw}^* is the water phase relative permeability at S_{wf}, P_c^* is the capillary pressure at S_{wf}.

Fischer et al. (Fischer et al., 2005; 2008) have modelled the effect of viscosity ratio on spontaneous imbibition. In the mathematical model, they gave a method to calculate the

characteristic length for each boundary condition separately. They described the relation between imbibition rate and viscosity ratio as a dimensionless function of viscosity ratio:

$$E(\eta) = \frac{a}{\frac{1}{b\eta} + b\eta} \qquad \text{Eqn (2.13)}$$

$$\eta = \sqrt{\frac{\mu_o}{\mu_w}} \qquad \text{Eqn (2.14)}$$

Where, *a* and *b* are dimensionless parameters in the function *E(η),* and they are functions of the matrix shape, matrix size, permeability and many other properties of the block. If *E(η)* is plotted as a function of *bη* in Cartesian coordinates, the curve, which is "asymmetric bell-shaped", has a maximum when *bη* is equal to 1. This means imbibition rate has the highest value at a certain viscosity ratio.

2.2.1.3 Co-current and Counter-current Imbibition

Imbibition can occur either co-currently or counter-currently. For co-current imbibition, the direction of oil movement is in the same as that of water propagation. In contrast, the direction of oil movement is opposite to that of water propagation for counter-current imbibition. Imbibition in water-wet matrix blocks of fractured reservoirs is commonly thought to be counter-current. However, Pooladi-Darvish and Firoozabadi observed that water did not fill up the fractures first before entering matrix as that was originally expected. They found that at early times, co-current imbibition played an important role until the matrix blocks were fully surrounded by water. At this time, water began to invade from all faces of the block, and then the imbibition process becomes counter-

current. They also pointed out that the recovery rate of co-current imbibition was better than that of counter-current (Pooladi-Darvish and Firoozabadi, 2000).

2.2.2 Water Imbibition in Heavy Oil-Water System

Mai and Kantzas (Mai, 2008; Mai and Kantzas, 2010) conducted a series of experimental studies of sandpack core floods to investigate the mechanisms of heavy oil recovery by waterflooding. Mai and Kantzas used CT scanners and Low Field NMR to find the evidences of water imbibition, and to quantify the contribution of water imbibition to oil recovery. They pointed out that capillary forces were important contributors to oil production after water breakthrough. It was further concluded that the significant oil recovery after water breakthrough was mainly due to water imbibition and film thickening. Especially, the function of water imbibition in oil recovery can be optimized at low water injection rates. They explained this conclusion as, at low injection rates, the active capillary forces resulted in the reduction of apparent relative permeability to water phase. They pointed out that, in heavy oil waterflooding, the main part of porous media were by passed and kept at original oil saturation when water broke through, and this situation left room for later water imbibition.

Nandez (Nandez, 2010) further investigated the mechanisms of imbibition in the process of heavy oil waterflooding. A series of sandpack core floods were conducted. Nandez pointed out that imbibition forces dominated the displacement after water breakthrough, and additional oil could be produced at low injection rates. He found that co-current imbibition dominated the process at early stage and counter-current imbibition dominated

at late stage. The main role of counter-current imbibition was that it can displace oil into water channels which were generated by water fingering. He also found that co-current imbibition was more efficient than counter-current imbibition.

Sohrabi et al. (Sohrabi et al., 2004) and Dong et al. (Dong et al., 2005) have investigated the water alternating gas injection process using micromodels. The initial water injection stage was a waterflooding process. Sohrabi et al. found that, in a strongly water-wet micromodel, during waterflooding, water films that were close to the walls of oil filled pores thicken progressively, leaving oil in the middle of the pore bodies by snap-off. Unfortunately, their studies did not offer much information for the mechanism of heavy oil waterflooding as the water injection period was very short. However, their studies indicated that the micromodel is a good tool to investigate mechanisms of heavy oil waterflooding.

In the operation of heavy oil waterflooding, water injection rate is one of the most important parameters. In the literature, the optimization of water rate was based on empirical methods. Adams (Adams, 1982) reported that shutting in water injection wells resulted in water cut reduction, but little change in oil production rate. Adams suggested this was because the drive-energy came from solution gas and rock compressibility. Smith (Smith, 1992) pointed out that changing injection and production rate likely improve sweep. Singhal (Singhal, 2009) compared oil responses of four different water strategies that were used in nine heavy oil pools in Alberta. These strategies included steady injection rate, declining injection rate, increasing injection rate and cyclic

variation in injection rate. Singhal found that periodic/cyclic variations in water injection rate can improve performance. Mai and Kantzas (Mai, 2008; Mai and Kantzas, 2010) experimentally investigated the production mechanisms under different water injection rates. They pointed out that after water breakthrough, waterfloods were more efficient under low injection rates, and capillary imbibition was largely responsible for water propagation and oil production. Above all, the water injection strategy has a significant influence on the performance of water imbibition.

2.3 Summary

The mechanisms of heavy oil waterflooding are more complicated than that of conventional light oil waterflooding. Heavy oil waterflooding has the disadvantageous characteristic of adverse mobility ratio. This process has not been fully described in a theoretical or simulation framework. The mechanisms of oil flow in heavy oil waterflooding are supposed to be: pressure support, solution gas drive, imbibition, drag, emulsification, gravity effect and so on. Most studies about mechanisms of imbibition were focused on natural fracture reservoirs. Unfortunately, the dimensionless scaling equation, which is based on the boundary condition and matrix block's shape, obtained in the fracture-matrix system, cannot be used for heavy oil-water system. However, some results, such as the effects of viscosity, may be applicable. Water imbibition is the main factor for oil recovery after water breakthrough, and low injection rate is beneficial for water imbibition. Water imbibition in heavy oil-water systems was studied recently. However, most of the research work conducted so far was through sandpack core displacement experiments, and no convincing evidence was provided to prove

imbibitions' existence and effects. Most of proposed mechanisms were based on assumptions or indirect observations. Besides, although water rate had drawn a lot of attention, how to determine the water injection rate for heavy oil waterflooding was based on empirical methods. It needs further investigation.

CHAPTER THREE: EXPERIMENTAL DESIGN

In this thesis, experimental studies were conducted to determine the effects of time, viscosity ratio and water injection rate on imbibition. Many oil and water samples were prepared. Their properties, such as density and viscosity, were measured. Based on the viscosity ratio, 5 pairs of these fluid samples were chosen to be used in the experimental study. The micromodel used in the experiments was made of etched glasses. Micromodel properties were carefully measured with different methods, such as mass balance and image analysis.

As etched-glass is fragile and micromodel has no regular connectors, special assemblies and equipments were needed for the experiment set up. One pore volume of the micromodel is only 0.822 cm^3, and the highest pressure the micromodel can stand is in the level of 6.9 kPa. A good flow rate controlling pump, a low pressure loss cylinder, a special differential pressure transducer and an analytical balance were used in the experiments.

Finally, a series of standard experimental procedures are designed and tested. These procedures include wettability alteration, primary drainage and secondary imbibition.

3.1 Fluid and Micromodel Properties

3.1.1 Oil Samples Basic Properties

The crude oil used in this thesis was provided from the Court pool (west central Saskatchewan). Totally, eleven model oils were prepared by mixing crude oil and

naphtha. These model oils were mixed by weight percentage control. The weight percentage of crude oil was varying from 0 to 100%. Viscosities of oil samples were in the range of 1.4mPa.s to 2830.2mPa.s (Table 3.1). Their densities were in the range of 0.7958g/cm^3 to 0.9675g/cm^3. A Brookfield Viscometer was used to measure some oil samples that have high viscosity. Several glass capillary viscometers were used for other less viscous oil samples and for water samples as well. A density meter which was manufactured by Anton Paar was used for both oil and water samples. All these measurements for oil and water samples were carried out at atmospheric pressure and room temperature of 23^{o}C.

Table 3.1: Oil samples composition and basic properties

#	Heavy oil (wt%)	Naphtha (wt%)	Density (g/cm^3)	Viscosity (mPa.s)
1	0	100	0.7958	1.4
2	10	90	0.8104	1.8
3	20	80	0.8258	2.9
4	30	70	0.8411	4.3
5	40	60	0.8573	10.0
6	50	50	0.8747	18.3
7	60	40	0.8928	39.3
8	70	30	0.9102	85.8
9	80	20	0.9286	341.7
10	90	10	0.9434	505.0
11	100	0	0.9675	2830.2

The colour of the oil phase varies from light brown to dark brown with increasing percentage of bitumen. And before injected into micromodel, the oil samples were filtered to remove any fine solid particles.

3.1.2 Water Phase Basic Properties

In this study, three types of water samples were prepared. One was distilled water, and the others were synthetic brines. Their composition, density and viscosity are listed in the Table 3.2. In the remaining part of this thesis, the abbreviation "1A" corresponds to the pair of oil sample #1 and water sample #A.

Table 3.2: Water samples component and basic properties

#	NaCl (wt%)	$CaCl_2 \cdot 2H_2O$ (wt%)	Density (g/cm^3)	Viscosity (mPa.s)
A	0	0	0.9971	0.9
B	2	0	1.0112	0.9
C	2	2	1.0243	1.0

In order to distinguish aqueous phase and glass matrix, the colour of the aqueous phase was dyed blue using the water soluble dye Methylene Blue. The aqueous phase was also filtered to remove any undissolved dye particles. The effect of dye on interfacial properties and wettability of experiment systems was simply ignored in the study.

3.1.3 Interfacial Properties

3.1.3.1 Interfacial Tension

Interfacial tensions were measured using the spinning drop method by using a KRUSS tensiometer. The interfacial tensions were in the range of 10.5mN/m to 15.7mN/m (in Table 3.3 and Figure 3.1).

Table 3.3: IFT measurement results

#	IFT, mN/m	#	IFT, mN/m	#	IFT, mN/m
1A	14.6	1B	13.5	1C	10.6
2A	14.1	2B	14.1	2C	12.1
3A	15.7	3B	11.7	3C	12.4
4A	12.7	4B	12.4	4C	12.9
5A	14.6	5B	12.1	5C	12.2
6A	13.5	6B	13.1	6C	12.2
7A	13.8	7B	11.5	7C	12.6
8A	13.3	8B	12.1	8C	10.5
9A	10.6	9B	12.5	9C	11.7
10A	15.5	10B	15.7	10C	13.8
11A	12.9	11B	14.3	11C	13.8

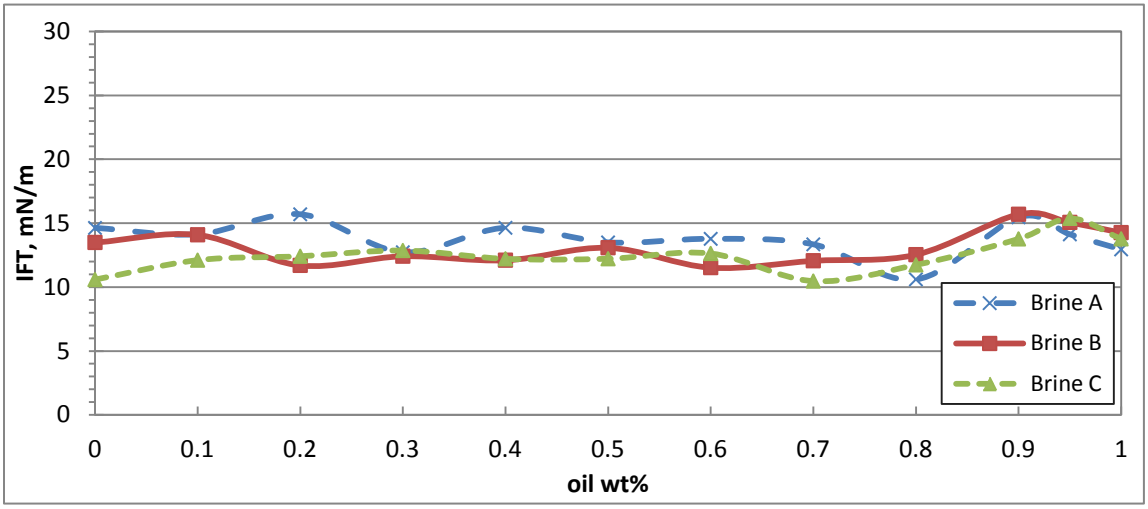

Figure 3.1: IFT of oil – water system using spinning drop method

3.1.3.2 Contact Angle of Oil-Water-Glass System

The contact angles of oil-water-glass system were measured by the drop geometry analysis method. The FTA200 contact angle analyzer equipped with a high resolution camera and a zoom microscope were used to capture the image. A PC was used to acquire the image and conduct the image analysis and calculation. For the pairs of 1A, 1B

and 1C, no contact angle could be measured as the oil sample #1 was transparent naphtha. According to the results in the Table 3.4 and Figure 3.2, contact angles of different pairs are in the range of 47^{o} to 59.9^{o}. No big difference exists among these values.

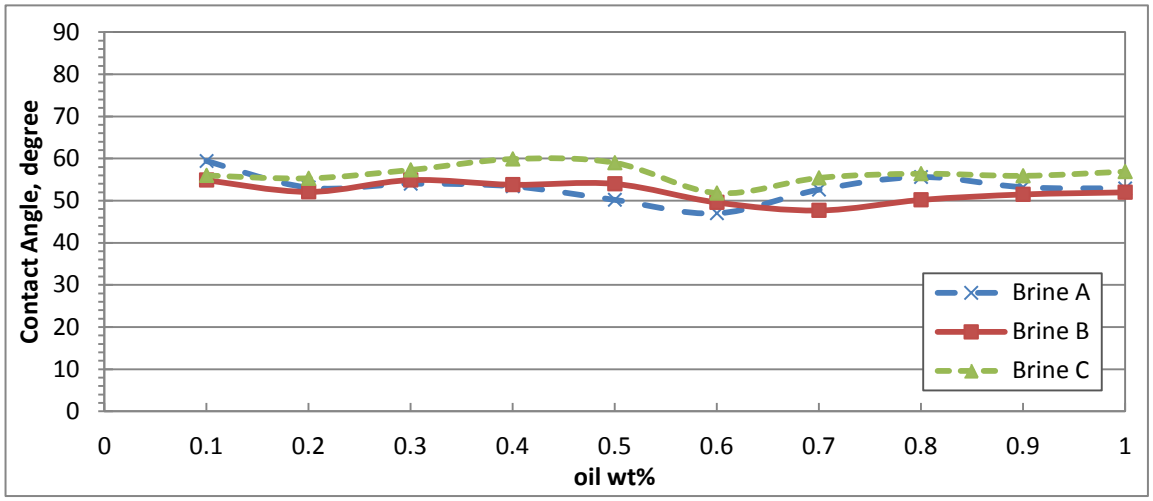

Figure 3.2: Results of contact angle measurement

Table 3.4: Contact angle measurement results

#	Contact Angle	#	Contact Angle	#	Contact Angle
1A	/	1B	/	1C	/
2A	59.4	2B	54.9	2C	56.0
3A	53.1	3B	52.1	3C	55.3
4A	54.0	4B	54.9	4C	57.3
5A	53.4	5B	53.8	5C	59.9
6A	50.2	6B	54.0	6C	59.0
7A	47.0	7B	49.6	7C	51.8
8A	52.6	8B	47.7	8C	55.4
9A	55.6	9B	50.2	9C	56.4
10A	53.2	10B	51.5	10C	55.9
11A	52.9	11B	52.0	11C	56.9

The results of above interfacial tension and contact angle measurements showed the values of different pairs were similar to each other. This indicated that, for this oil/water system, there was no evident relationship between the presence of variable salinity or divalent cations and possible changes to the fluid IFT values or rock wettability.

3.1.4 Micromodel Properties

In this thesis, an etched-glass micromodel was used as the porous media. Figure 3.3 shows the whole view of the micromodel. The micromodel patterns consist of pore bodies, pore throats and solid matrix. Because the structure of etched pore network is just several micra, and the pore walls and cover plates are all transparent glasses, micromodel was usually used as a strong tool to study flow and trap phenomenon at the pore level through visual observation. In the literature, micromodels were used for fluid displacement studies as early as 1960 (Mattax and Kyte, 1961). Numerous documents about etched-glass micromodel were published. Figure 3.4 shows the etched-glass micromodel patterns.

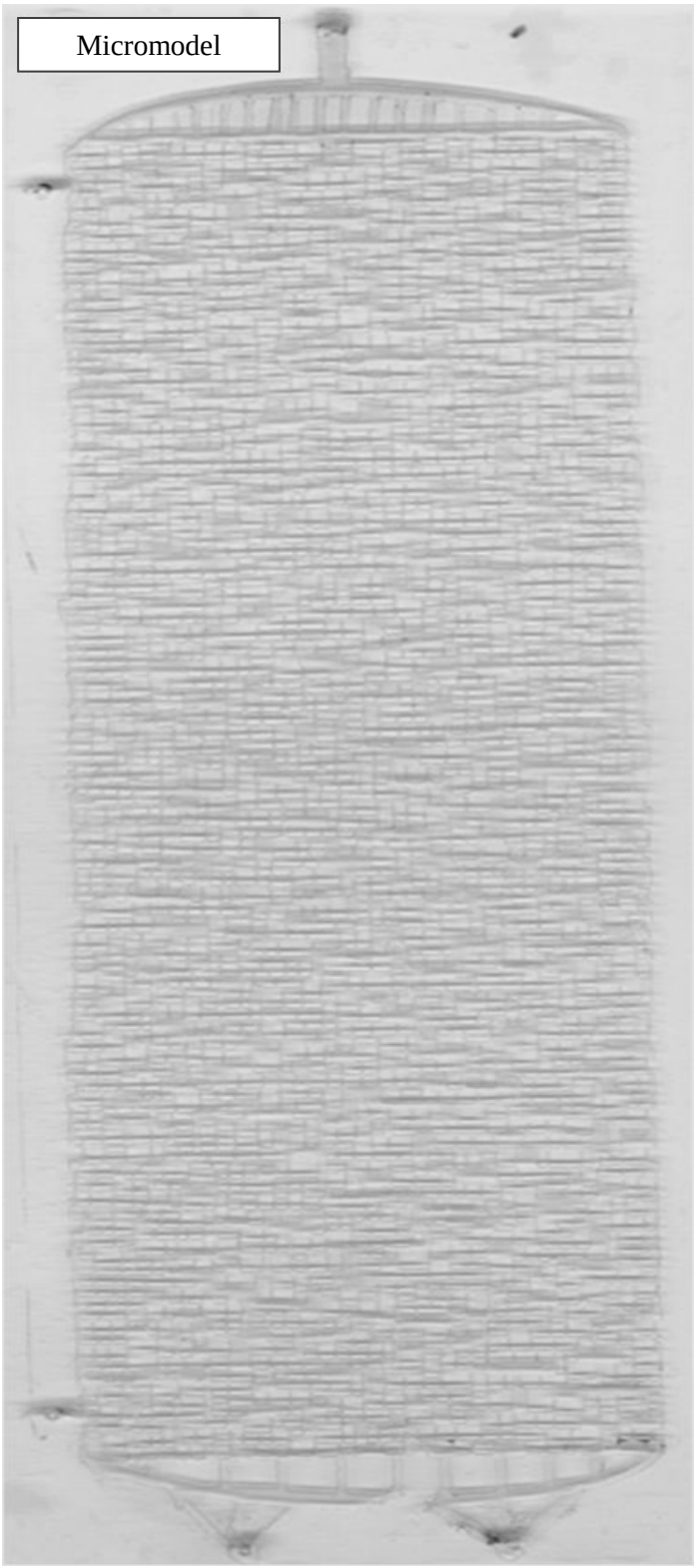

Figure 3.3: Micromodel structure

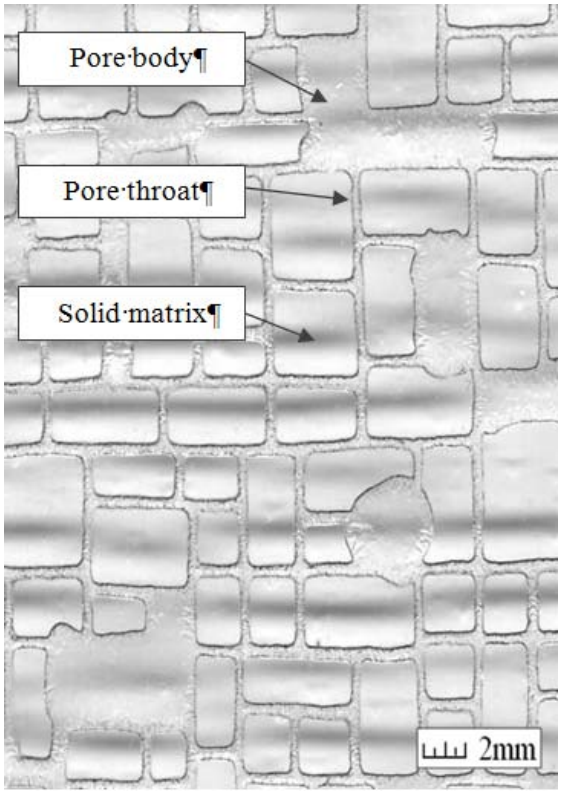

Figure 3.4: Micromodel patterns

The micromodel patterns were characterized by heterogeneities with a random distribution of pore bodies and pore throats. Some basic properties of the micromodel were obtained through image analysis. The images in the Figure 3.3 and 3.4 were captured with a high definition EPSON digital scanner. Table 3.5 gives the summary of micromodel properties. Where, the values of pore volume in the table were calculated based on the mass difference between the empty and the water saturated micromodel. Permeability here was the absolute permeability measured with the single phase flow of distilled water. The coordination number which reflects the connection of pore bodies with pore throats was a statistical value.

Table 3.5: Summary of micromodel properties

Properties	Micromodel
Length, cm	23.0
Width, cm	7.1
Height, cm	0.58
Depth of pores, micron	12.9
Porosity, %	39.0
Pore volume, cm^3	0.822
Pore body size*, $\times 10^{-12} m^3$	17.8
Pore throat size*, $\times 10^{-12} m^3$	1.96
Permeability, Darcy	16.6
Coordination number*	4

* mean value and measured by Romero-Zeron (2004);

The values in Table 3.5 are consistent with those in the literature (Romero-Zeron, 2004). The obvious difference was permeability, and this resulted from the different calculation of cross-sectional area. The value of permeability will be very small if the whole height of micromodel was considered as the thickness of porous media. In the calculation of this thesis, 10 times of the depth of pore structure was considered as the thickness of the permeable porous media.

The micromodel had five ports. Two were used for fluid injection, one was used as a production port, and the remaining two were used for differential pressure measurement. The micromodel was placed between two acrylic frames. In the upper frame, five holes which match well with the five ports on the micromodel were drilled. These holes were used to set up lines with micromodel. Between the micromodel and the upper frame, O-rings were placed to work as seal components.

3.2 Experiment Set-up

The process of water imbibition with imposed differential pressure is termed forced imbibition. The process of water imbibition without differential pressure is termed spontaneous imbibition. In heavy oil reservoir waterflooding, water is always injected continuously. This results in a continuous differential pressure forced imbibition. However, after water breakthrough, especially at the condition of low rate water injection, the differential pressure reduces to an extremely low level, so spontaneous imbibition is believed to play an important role at this situation. In order to investigate these two types of imbibition, two types of experiments were designed.

3.2.1 Forced Imbibition

Figure 3.5 is the schematic of the micromodel setup. A high accuracy Teledyne ISCO syringe pump was used to control fluid flow rate into the micromodel. The minimal injection rate is set at 1µl/hr. Within micromodel, 1µl/hr was equivalent to an interstitial velocity of approximate 0.0042 m/d. A Validyne differential pressure transducer was used to measure the differential pressure between the pressure ports on micromodel. In the experimental study, the maximum differential pressure was set at 2.7 kPa (pressure gradient < 38kPa/m). Figure 3.6 shows the assembly of the micromodel. As the operation pressure was low, plastic lines and nuts were used for the purpose of better operation control. A low pressure loss piston cylinder which was made of plastic, shown in Figure 3.7, was used for accurate injection rate control. The volume of this cylinder was approximately 76 cm^3. An analytical balance was used to weigh the produced fluids, and

the weight of water in the produced fluids was measured through a low field NMR. And thus the subtraction of the weights was the mass of produced oil.

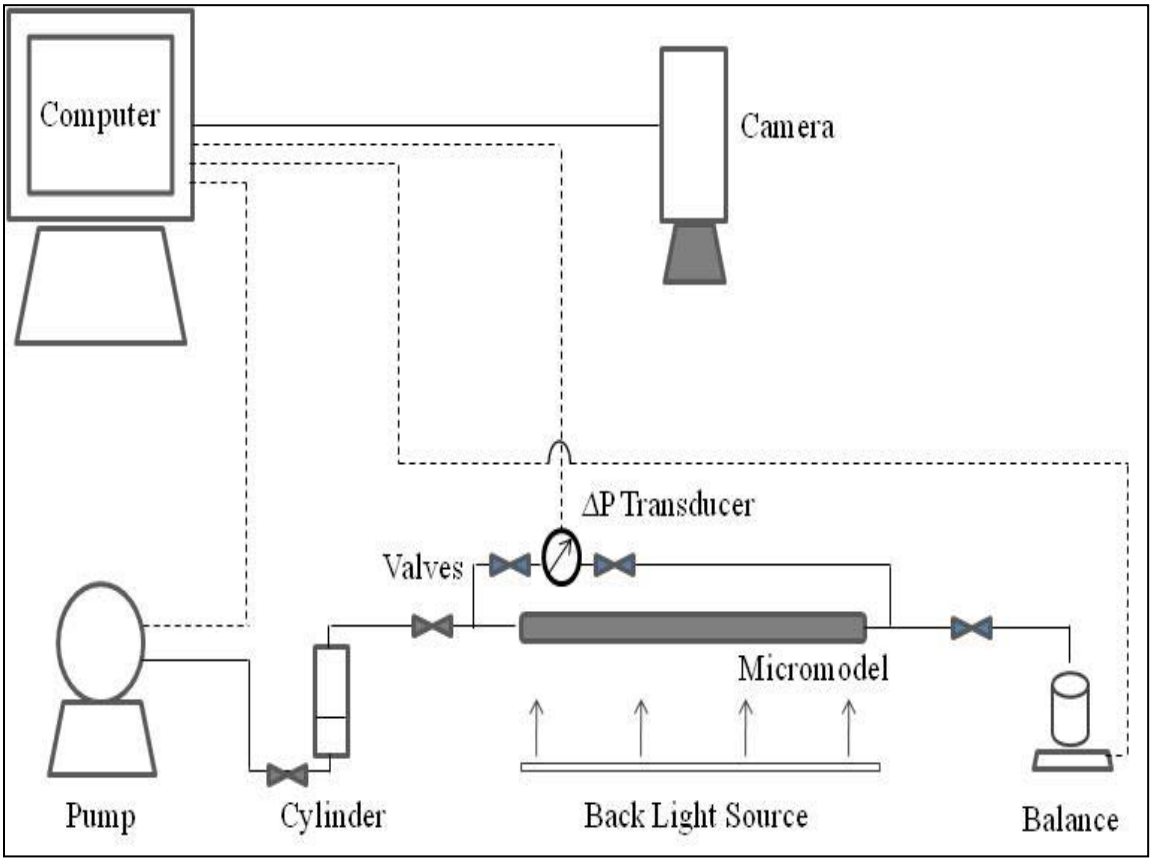

Figure 3.5: Schematic of the experiment (forced imbibition)

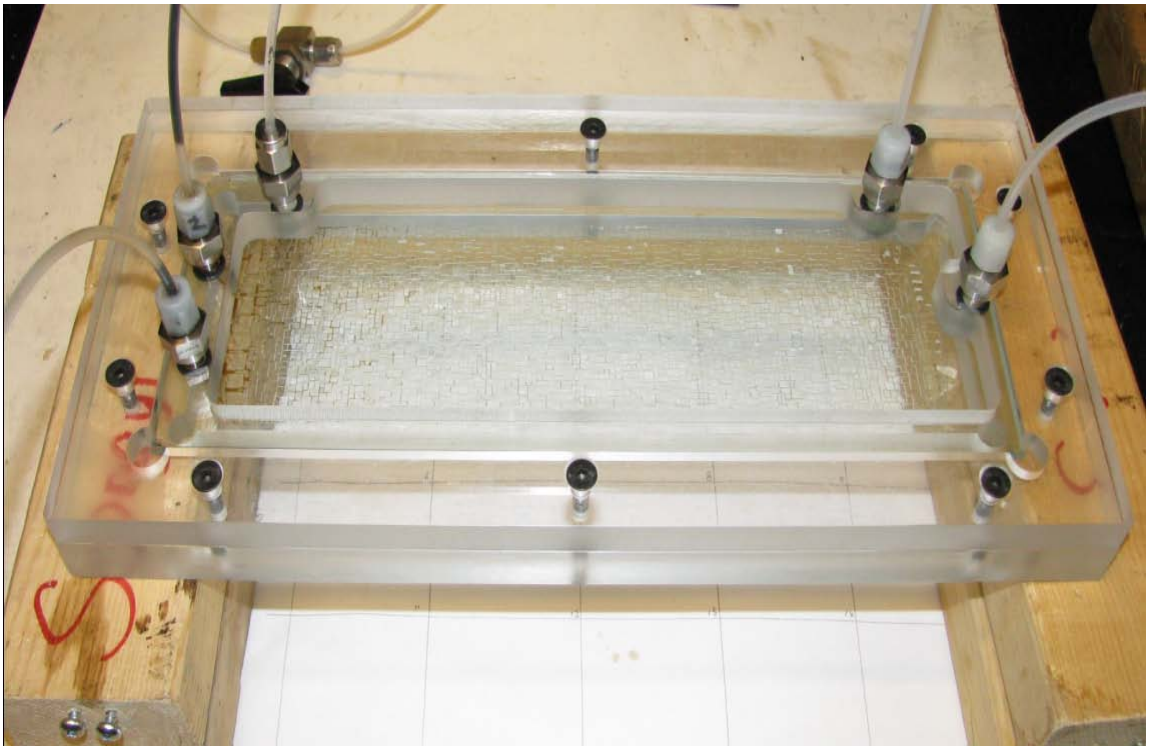

Figure 3.6: Micromodel assembly (forced imbibition)

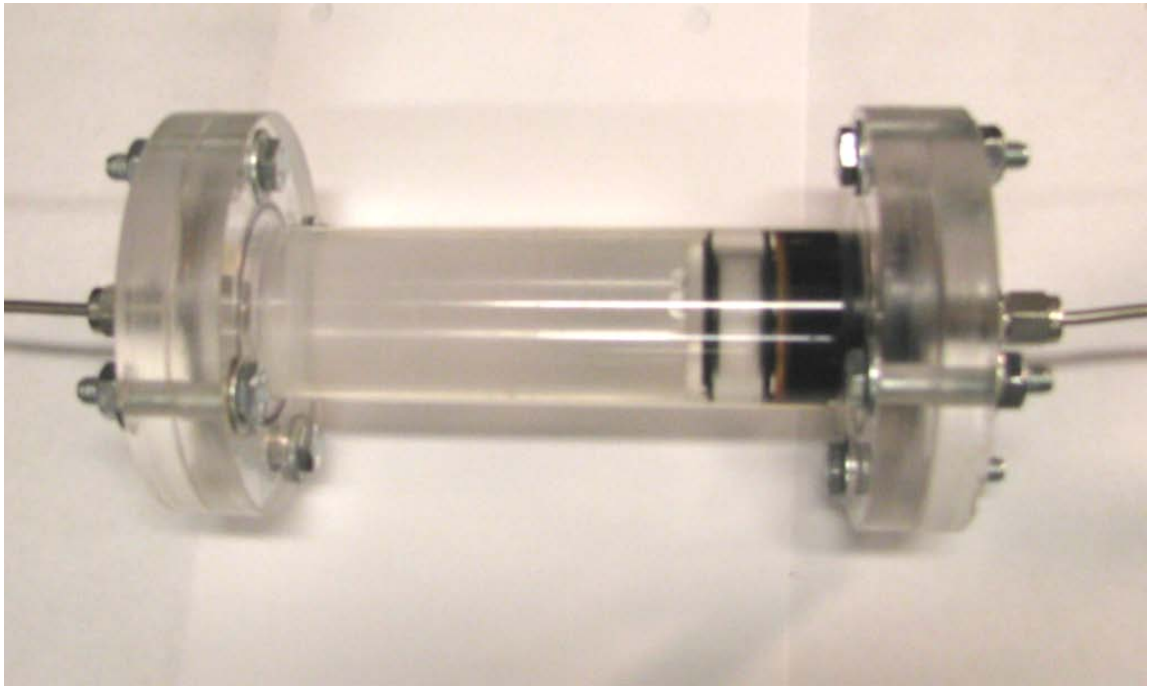

Figure 3.7: Small volume piston cylinder

3.2.2 Spontaneous Imbibition

Figure 3.8 is the schematic of the micromodel set up for spontaneous imbibition. As no water was injected into micromodel during the imbibition process, no pump was used after water being saturated. The fluid surfaces at inlet and outlet were horizontal, so the differential pressure between the inlet and outlet no longer existed, and no transducer was used. Figure 3.9 shows the assembly of the micromodel. Connected to the outlet, a capillary tube was used to measure the volume of oil produced.

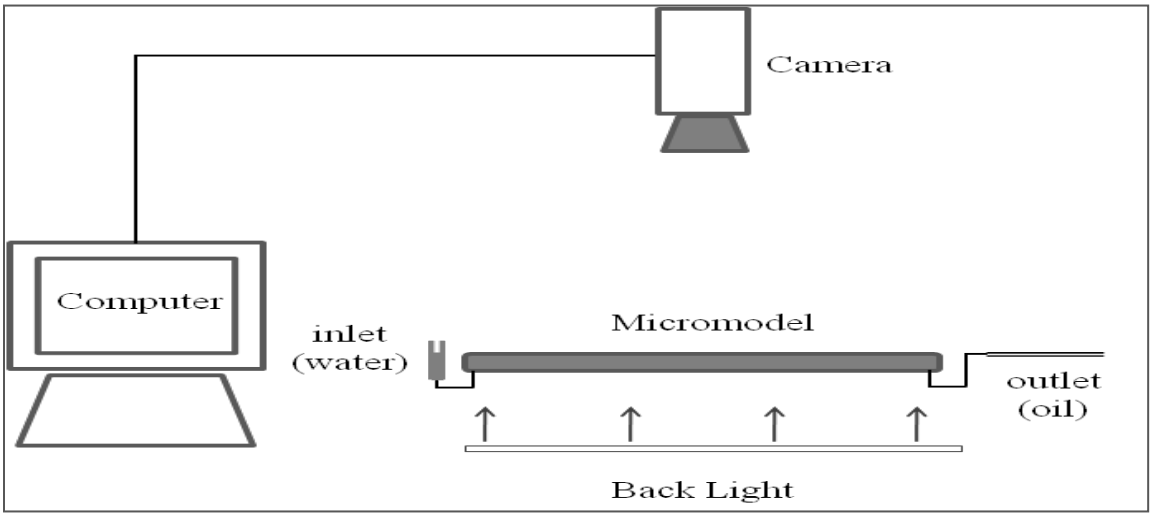

Figure 3.8: Schematic of the experiment (spontaneous imbibition)

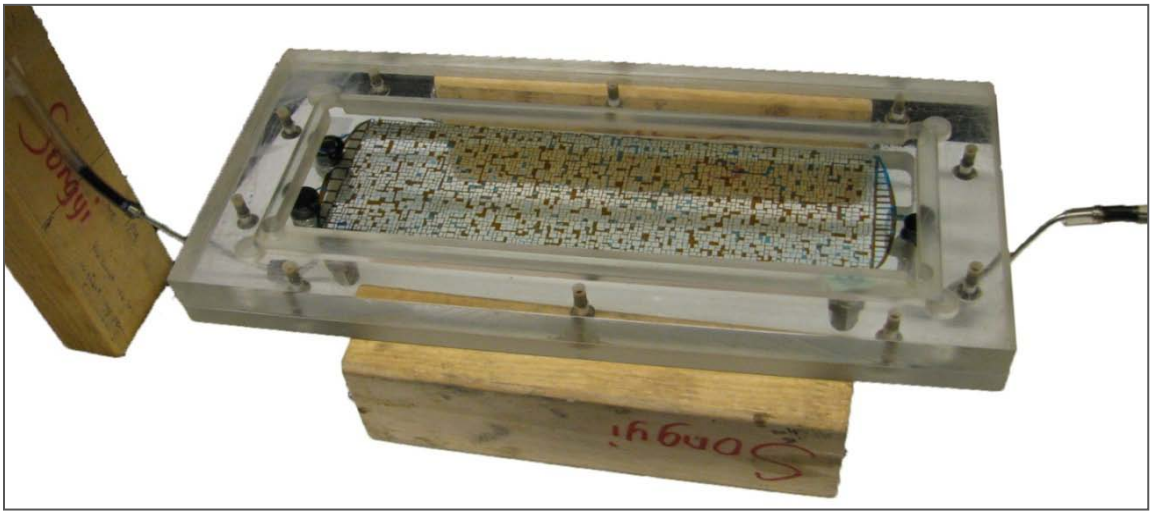

Figure 3.9: Micromodel assembly (spontaneous imbibition)

3.3 Experimental Procedures

3.3.1 Treatment of Micromodel Wettability

Imbibition is the process of a wetting phase invading into the porous media previously occupied by a non-wetting phase. In order to trigger water imbibition, the micromodel should be water wet. In this study, every experiment was conducted in the condition of water wet. A standard procedure was created for the treatment of micromodel wettability.

The procedure of treating the etched-glass micromodel to be water-wet is listed as follows:

(1) Rinse the micromodel with toluene to eliminate any organic material. Using a vacuum system to remove the residual fluid.

(2) Rinse the micromodel with acetone using a vacuum system to remove the residual fluid.

(3) Repeat step one and two.

(4) Rinse the micromodel with distilled water using a vacuum system to remove the residual fluid.

(5) Rinse the micromodel with hydrochloric acid solution (15 volume %) and then soak it in HCl solution for 2 hours, using a vacuum system to remove the residual solution.

(6) Rinse the micromodel with distilled water using a vacuum system to remove the residual water.

(7) Rinse the micromodel with acetone using a vacuum system to remove the residual acetone.

(8) Place the micromodel in an oven and let it dry at 150^{o}C for at least one hour.

3.3.2 Primary Drainage Process

This primary drainage process was carried out at atmospheric pressure and room temperature of 23^{o}C. Water was injected at a low constant rate. Then a drainage process followed. One oil sample with a certain viscosity was injected also at a low constant rate, until irreducible water saturation was reached. The procedure of this process is listed as follows:

(1) Before the saturation of water (or brine), the micromodel is evacuated for several minutes to prevent air trapping in the model, and at the same time, a leak test is conducted with the evacuated micromodel.

(2) Saturate the micromodel with water, and make sure the water saturation is above 99.9%.

(3) The absolute permeability to water is calculated applying Darcy's law.

(4) The syringe pump is turned on and the oil sample starts to be injected into the micromodel. Make sure the differential pressure should be less than 2.7 kPa.

(5) The produced fluids are collected in vials and then weighed. The differential pressure across the micromodel is also recorded.

(6) Stop the pump when 5 pore volumes of oil sample have been injected.

(7) The initial water saturation is calculated with both the methods of mass balance and image analysis, and effective permeability to the oil phase at S_{wi} is calculated applying Darcy's law.

(8) During the process, high resolution images and videos of different sections of the micromodel are captured and recorded.

3.3.3 Secondary Imbibition (Waterflooding) Process

This waterflooding process was also carried out at atmospheric pressure and room temperature of 23^{o}C. Water was injected at a low constant rate before water breakthrough. After water breakthrough, in some cases when studying imbibition at low injection rate, the injection rate was decreased. This is illustrated in Chapter 4. A standard cleaning procedure was also generated. This procedure is as follows:

(1) Keep the oil saturated micromodel static for a minimum of one day to allow enough time for capillary forces equilibrium.
(2) The syringe pump is turned on and water starts injected into the micromodel. Make sure the differential pressure should be less than 2.7 kPa.
(3) The produced fluids are collected in vials and then weighed. The differential pressure across the micromodel is also recorded.
(4) Record the time when water breakthrough happened, and high resolution images of micromodel are captured and recorded.
(5) Injection rate may need to be changed after water breakthrough.
(6) Stop the pump when 10 pore volumes of water or brine have been injected.
(7) The residual oil saturation is calculated with both the methods of mass balance and image analysis. Effective permeability to water phase at S_{or} is calculated applying Darcy's law.

(8) During the process, high resolution images and videos of different sections of the micromodel are captured and recorded.

(9) Data analysis is conducted using the methods of mass balance and image analysis.

(10) The procedure of micromodel cleaning is: firstly, rinse the micromodel with toluene to eliminate any residual oil and then using a vacuum system to remove liquids from the micromodel; secondly, rinse the micromodel with acetone and then using a vacuum system to remove liquid from the micromodel. These processes should be repeated several times.

3.3.4 Free Spontaneous Imbibition Process

Spontaneous imbibition is defined as a process by which a wetting phase is imbibed into the porous media by capillary action. In free spontaneous imbibition experiment, no viscous forces were imposed on fluids. This process was also carried out at atmospheric pressure and room temperature of 23^{o}C. Water imbibed into the micromodel from the input port. At the outlet, oil flowed into a capillary tube which was used for volume measurement. The procedure is listed as follows:

(1) Keep the oil saturated micromodel static for a minimum of one day to allow enough time for capillary forces equilibrium.

(2) Slightly raise the water surface of the inlet.

(3) Lower the water level when water entered and occupied 5% area of the micromodel.

(4) Keep the fluids' level of the inlet and outlet at a horizontal level.

(5) During the process, high resolution images and videos of different sections of the micromodel are captured and recorded.

(6) Data analysis in this section is conducted only using the method of image analysis.

3.4 Experiment Parameters

3.4.1 Viscosity Ratio

The adverse mobility ratio, which is caused by extremely high oil viscosity, is the most important characteristic for heavy oil waterflooding. To simulate the process of heavy oil waterflooding, some high viscosity ratios were necessary in this experimental study. However, the micromodel which was made of fragile glasses was not able to stand high pressure, so an upper limit of viscosity ratio existed. To balance these two points, a set of viscosity ratios were selected (in bold in Table 3.6). At the same time, the related oil and water samples were also selected to be used in the experiment. The value of viscosity ratio and samples selected are shown in Table 3.6.

Table 3.6: Viscosity ratio of each sample pair

	Brine A	Brine B	Brine C
Oil #1	1.5	1.5	1.4
#2	2.0	2.0	1.9
#3	3.2	3.2	3.0
#4	4.8	4.8	4.5
#5	**11.1**	11.1	10.5
#6	20.3	20.3	19.1
#7	43.7	43.7	41.1
#8	**95.3**	95.3	89.7
#9	379.7	379.7	357.3
#10	**561.1**	561.1	528.1
#11	3144.7	3144.7	2959.5

3.4.2 Flow Rate

The injection rates of oil and water were in the range of a minimum of 10µl/hr to a maximum of 1,000µl/hr. Within the micromodel, 10µl/hr was equivalent to an interstitial velocity of 0.0672m/day.

In this thesis, considering the actual operation in the field and the feasibility in the experimental study, a rate of 100µl/hr was set as the flow rate for primary drainage process, and 3 patterns of flow rates were designed for the imbibition process:

(1) Constant flow rate. In this pattern, the flow rate did not change during the whole imbibition process. The rate of 10µl/hr was set as the low flow rate, and 1,000µl/hr as the highest flow rate.

(2) Varied flow rate. The flow rate, when water broke through the micromodel, was changed to a lower rate compared to the flow rate before water breakthrough. The rates before and after water breakthrough were both constant. Taking the test of A5-1000-10 as an example, the water injection rate at pre-breakthrough stage was 1,000µl/hr, and it was reduced to 10µl/hr at post-breakthrough stage.

(3) Varied flow rate with shut in period. This pattern was the same as the second pattern except that in this case there were shut in periods after water breakthrough. These shut in periods were set for fluids redistribution.

CHAPTER FOUR: RESULTS

This chapter presents the descriptions and observations of the performed experiments. The experiments shown and discussed in this chapter were designed to investigate key factors and mechanisms of water imbibition. The key factors investigated here include time, oil viscosity and water injection rate. The mechanisms investigated here include snap-off, film thickening, oil refilling, lubrication and emulsification. Results were mainly extracted from the forced imbibition experiments. A spontaneous imbibition experiment was considered to be the reference case or the extremely low rate situation. The image analysis method was presented in Appendix II in detail. Additional discussion of experimental results is presented in Chapter Five.

In order to yield the most accurate measurements and results, several waterflooding experiments were performed to tune the equipment and procedures. These steps were necessary because wettability treatment and saturation measurement were time consuming and complicated. It was very important and necessary to ensure that the micromodel was in strong water wet so that water imbibition can occur. A special procedure for wettability treatment was developed and tuned, and that procedure is described in Chapter Three. These early treatments and experiments also served as trouble shooting tests. Once the experimental procedures were defined, additional waterflooding experiments were conducted. In the forced imbibition experiments, water was injected. The injection rate may be constant or variable. In some cases, a non-water injection period may exist, and this period was termed shut-in period. In the spontaneous imbibition experiment, no water was injected. This experiment was designed to

investigate the water imbibition under the exclusive influence of capillary forces and to be used for comparison to forced imbibition.

First, the data of all water imbibition experiments are presented and discussed. Then, detailed analyses of these data and images captured during experiments are presented. Further analyses, such as differential pressure variance and operation strategy, are presented at the end of this chapter. Forces balance between viscous forces and capillary forces is analyzed in Chapter Five.

4.1 Results of Individual Experiments

For each experiment, oil recovery versus time, oil recovery versus PVs of water injected, pressure response, oil saturation profiles, water permeability at the end of waterflooding and some observations are presented.

The calculations of oil saturation and oil recovery are based on image analysis. Oil saturation is the fraction of the area where is occupied by oil over the whole permeable area where is occupied by oil or water.

$$s_o = \frac{A_o}{A_o + A_w} \qquad \text{Eqn (4.1)}$$

$$s_w = \frac{A_w}{A_o + A_w} = 1 - s_o$$

Where, A_o is the area of oil zone

A_w is the area of water zone.

The recovery factor (RF) is the fraction of the deduction of oil saturation over the initial oil saturation.

$$RF = \frac{S_{oi} - S_o}{S_{oi}} \qquad \text{Eqn (4.2)}$$

Where, S_{oi} is initial oil saturation.

Details on these calculations are presented in Appendix II.

4.1.1 Results of A5-10

A5 stands for the combination of water sample #A and oil sample #5. The value 10 stands for the water injection rate 10µl/hr. Based on the fluid combination, the viscosity ratio was μ_o/μ_w=11.1.

This is the smallest viscosity ratio among all experiments in this thesis. The water injection rate, 10µl/hr, was also the lowest among those of all forced imbibition experiments. The low injection rate resulted in very long waterflooding. From Figure 4.1, the abscissa showed that the water injection period lasted for nearly 22 days. From Figure 4.2, the abscissa showed that about 8.6 PVs of water was injected.

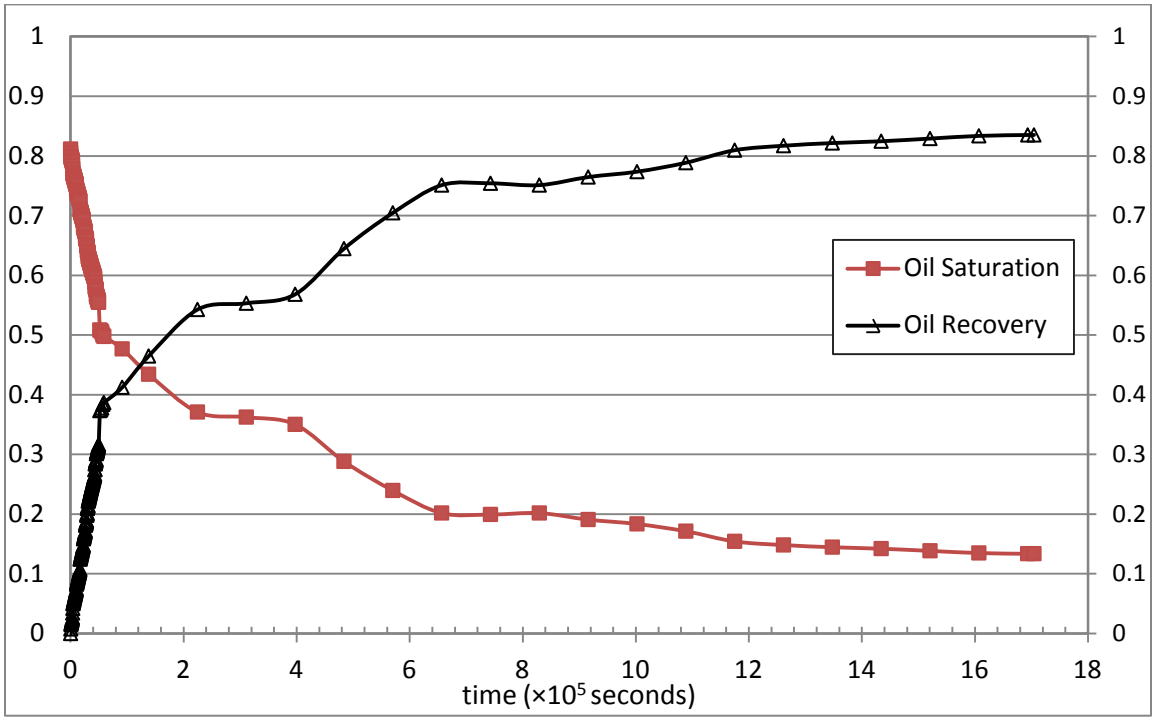

Figure 4.1: Recovery vs. time for A5-10

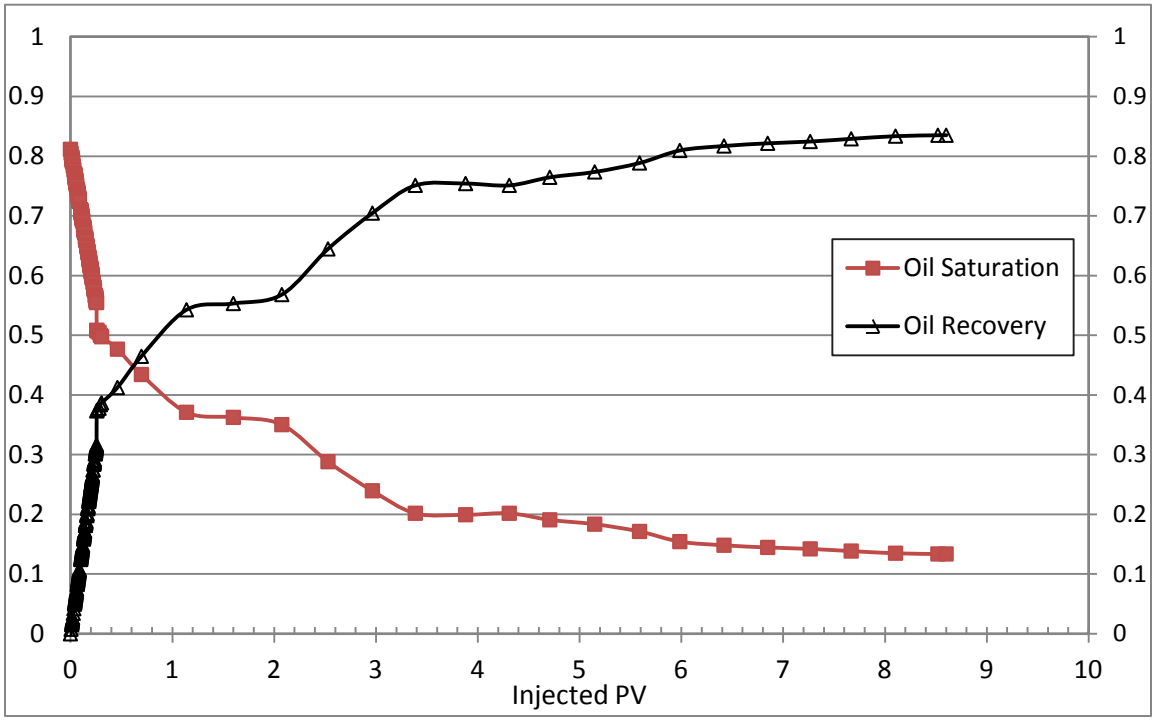

Figure 4.2: Recovery vs. PVs of water injected for A5-10

In Figure 4.1 and 4.2, the location of water breakthrough point can be estimated. Before water breakthrough, the volume of oil produced, which should be equal to the volume injected, can be extracted from the pump logging file, so the data points were denser than those after breakthrough. However, in this case, as something wrong happened with the pump volume signal collecting system, there was a gap at the end of pre-breakthrough period. Therefore, the breakthrough point is at the end of the straight line portion. Estimated from either curve in these figures, the time when breakthrough happened was close to 51,900 seconds. And the RF at that time was about 0.37. The final recovery was 0.835, and the water permeability at the end of waterflooding was 3.0 D. The relative permeability to water at residual oil saturation was 0.18.

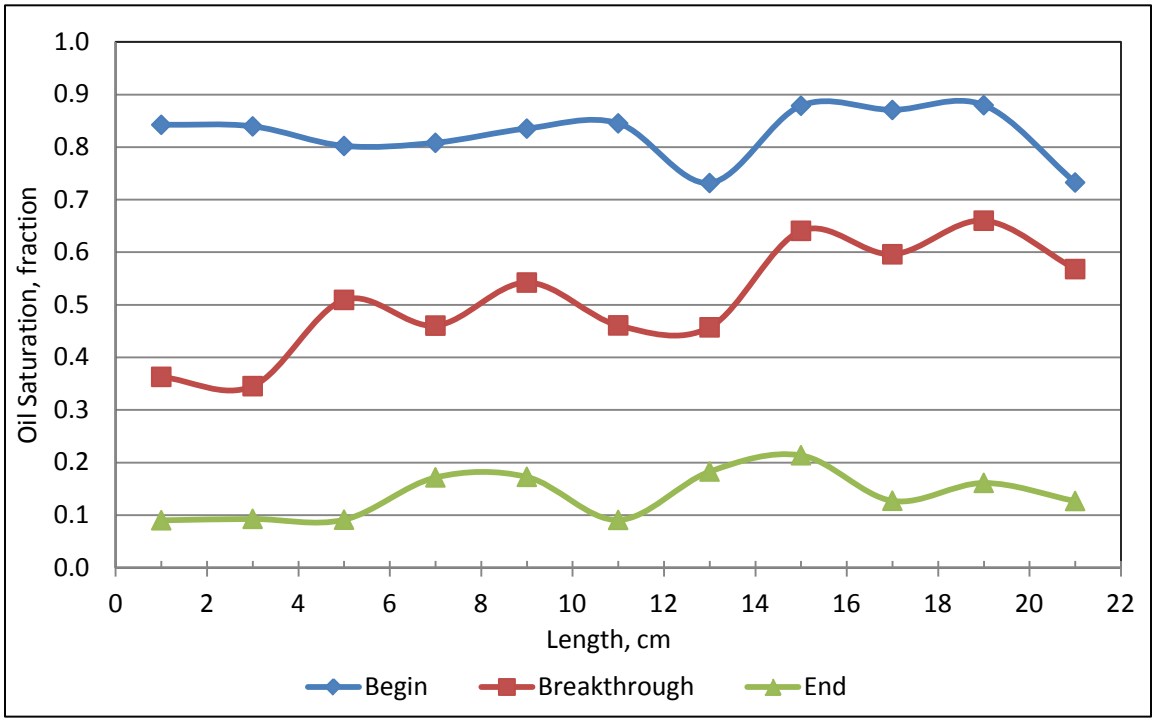

Figure 4.3: Oil saturation profiles during waterflooding for A5-10

Figure 4.3 shows local values of oil saturation along the length of micromodel. The left side is the inlet of the micromodel. These values were calculated using image analysis method. As it can be observed in this figure, oil saturation decreases practically uniformly along the length from the initial oil saturation to breakthrough oil saturation, and from breakthrough saturation to residual oil saturation. More analysis about saturation profile data is presented in Chapter Five.

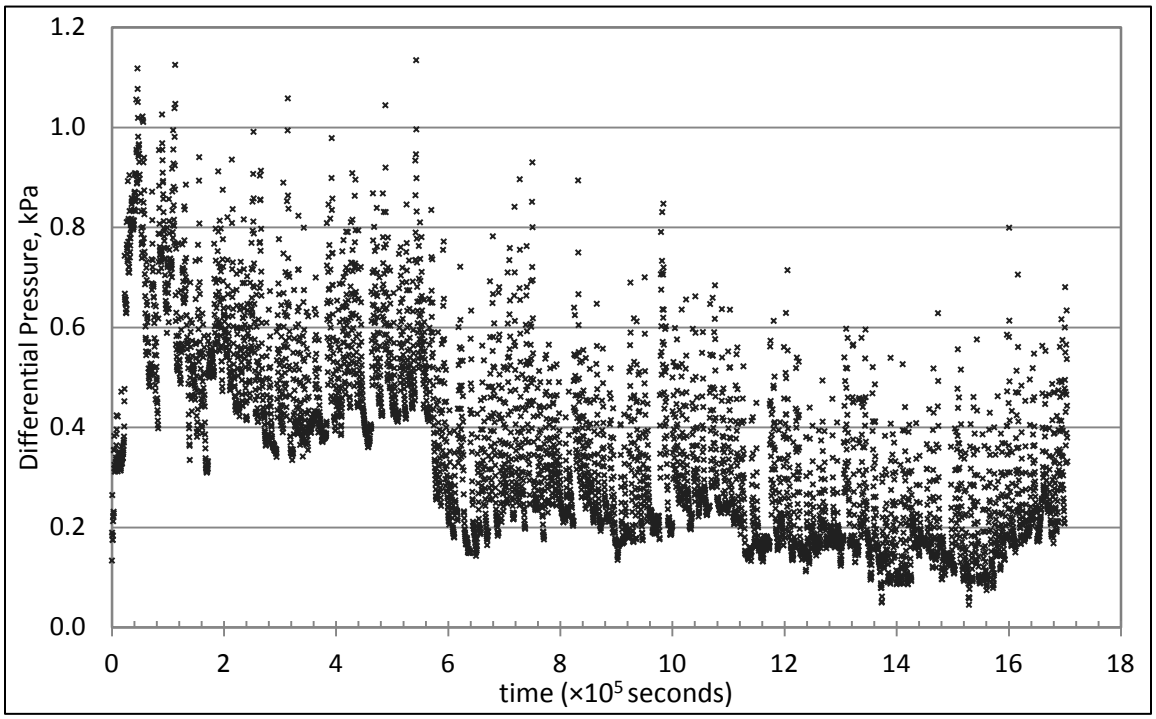

Figure 4.4: Differential pressure response for A5-10

The differential pressures data collected during the experiment are presented in Figure 4.4. Differential pressure was measured using a digital differential pressure transducer. At early times, the differential pressure increased sharply. At the time of water breakthrough, the differential pressure reached a peak value. After that, it began to

decline. A variance existed at about 536,700 seconds. Before that time, the differential pressure was above 0.4 kPa. And right after that, it suddenly declined to approximately 0.3 kPa. In the production response figure (Figure 4.1), significant amount of oil was produced around that time. After the time of 1,130,100 seconds, even though the differential pressure reduced to an extremely low value, about 0.1 kPa, additional 7% of original oil was eventually produced. Because the range of the differential pressure transducer is just 6.9 kPa, the measurement should be very accurate.

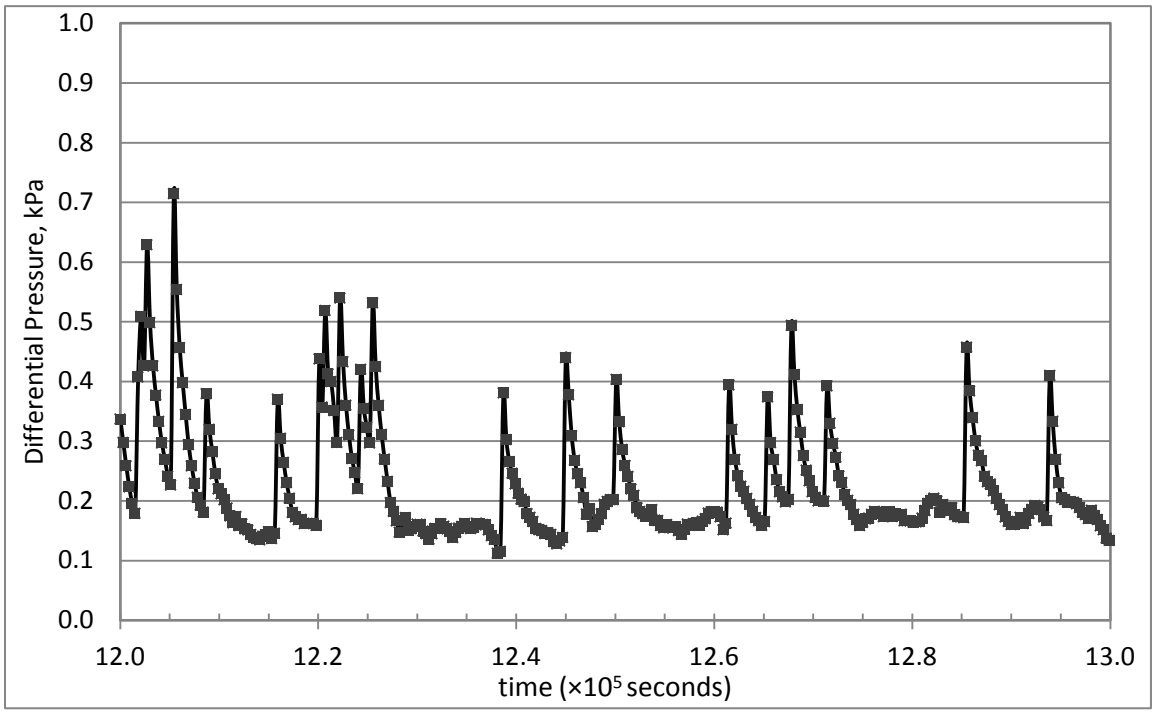

Figure 4.5: Differential pressure response in small scale (12-13×10^5 seconds)

Figure 4.5 shows the differential pressure in small scale. Only the portion located between 12-13×10^5 seconds is plotted in the figure. The maximal differential pressure is 0.71kPa, and the minimum is 0.13kPa. Differential pressure curve exhibits periodic

variation. More analysis about differential pressure data is presented in section 4.6 and Appendix III.

4.1.2 Results of A5-100

In this case, the same fluid samples were used as that in section 4.1.1. The water injection rate was increased to 100µl/hr.

In this case, the production performance is presented in Figure 4.6 and 4.7. The time when water breakthrough happened was around 7,800 seconds. And the RF at that time was about 0.36 which was very close to that of the case A5-10. The final recovery was 0.82, and the water permeability at the end of waterflooding was 3.3 D. The relative permeability to water at residual oil saturation was 0.20.

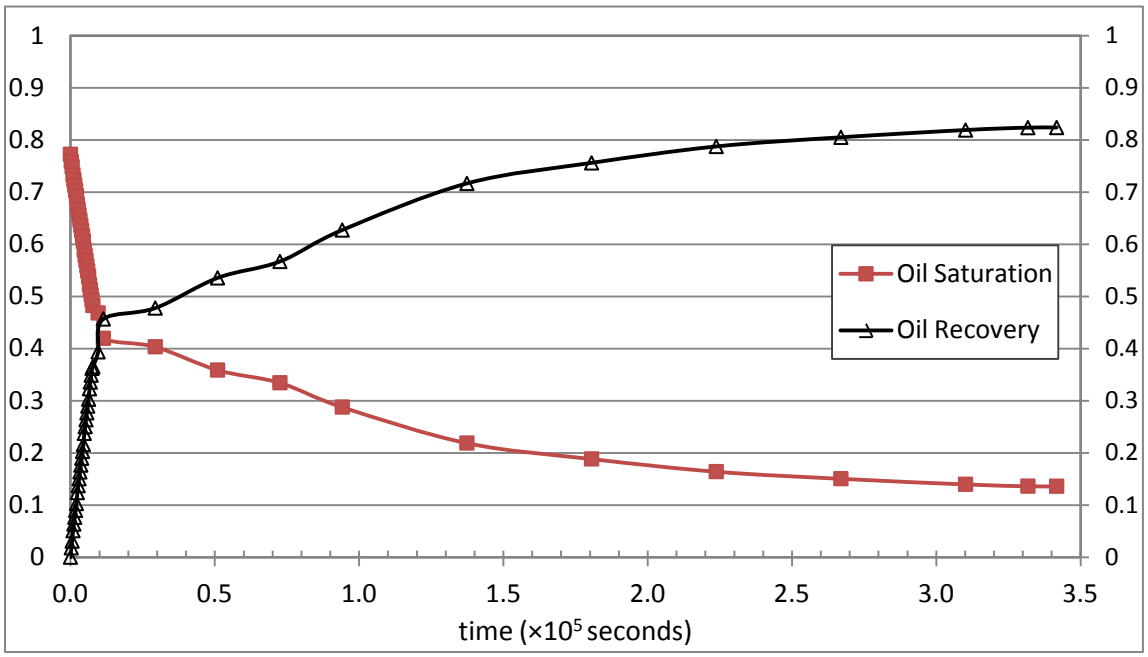

Figure 4.6: Recovery vs. time for A5-100

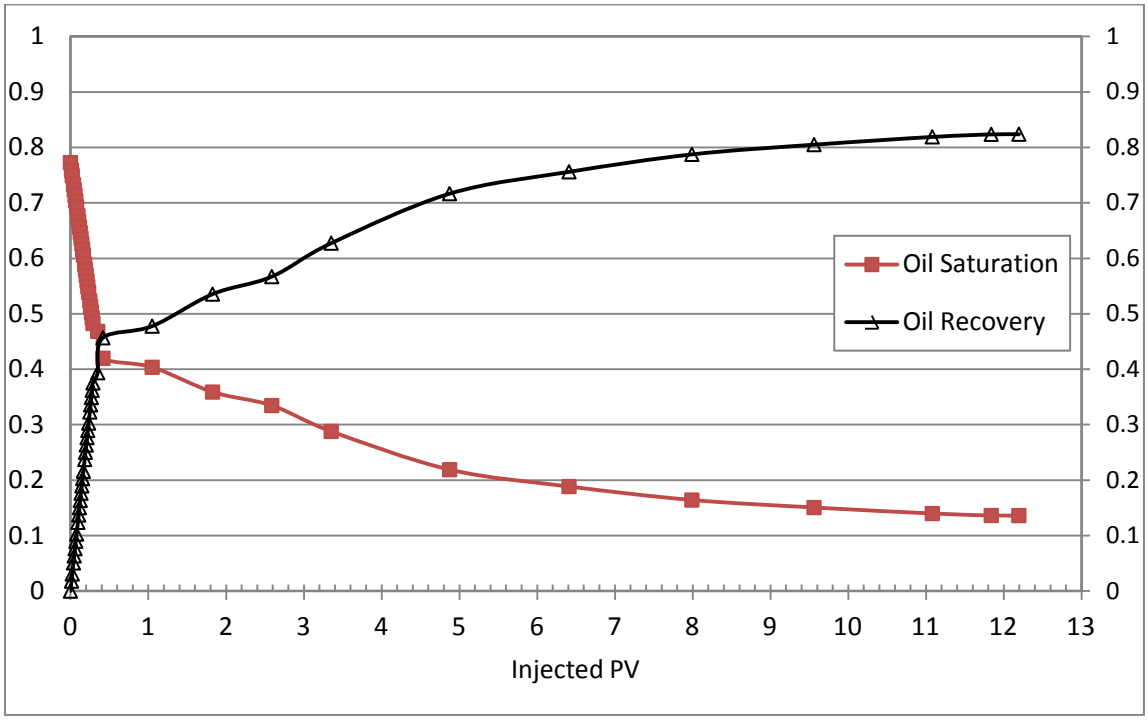

Figure 4.7: Recovery vs. PVs of water injected for A5-100

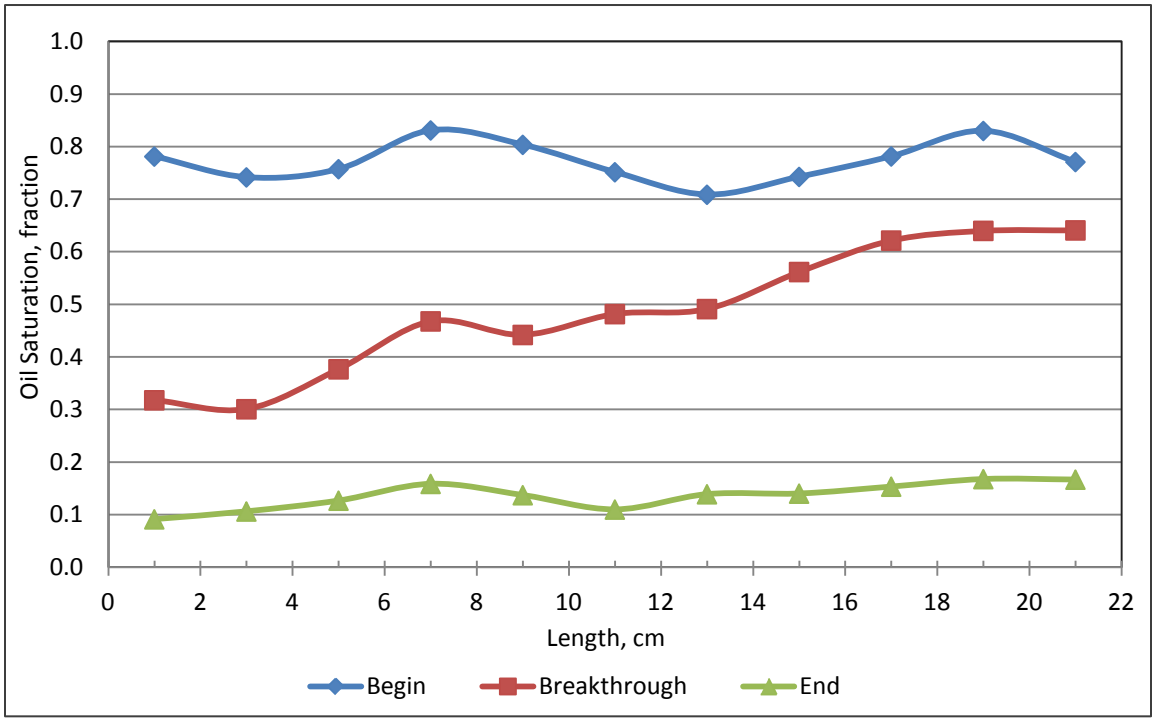

Figure 4.8: Oil saturation profiles during waterflooding for A5-100

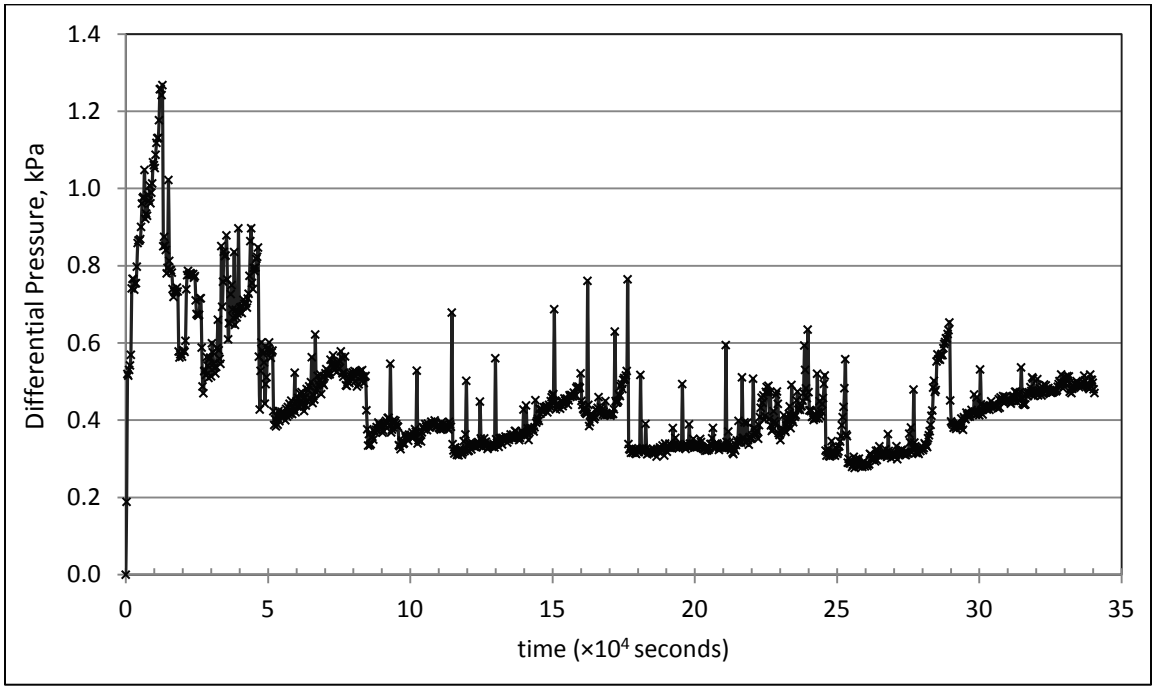

Figure 4.9: Differential pressure response for A5-100

Figure 4.8 shows oil saturation profile. The differential pressure collected during waterflooding is presented in Figure 4.9. More analysis and discussion about saturation profile and differential pressure will be presented in section 4.6 and Chapter Five.

4.1.3 Results of A5-100-10

In this case, the same fluid samples were used as that in section 4.1.1. However, the water injection rate was not a constant. It was 100µl/hr at first. And then it was reduced to 10µl/hr at the time of about 137,700 seconds.

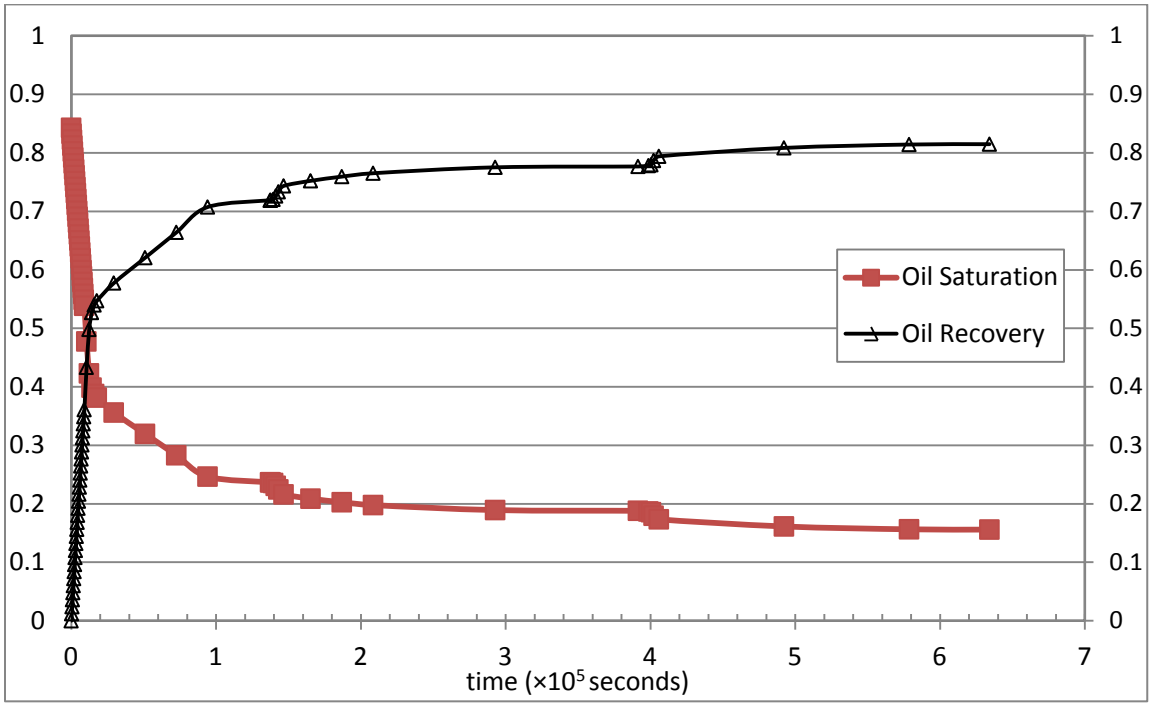

Figure 4.10: Recovery vs. time for A5-100-10

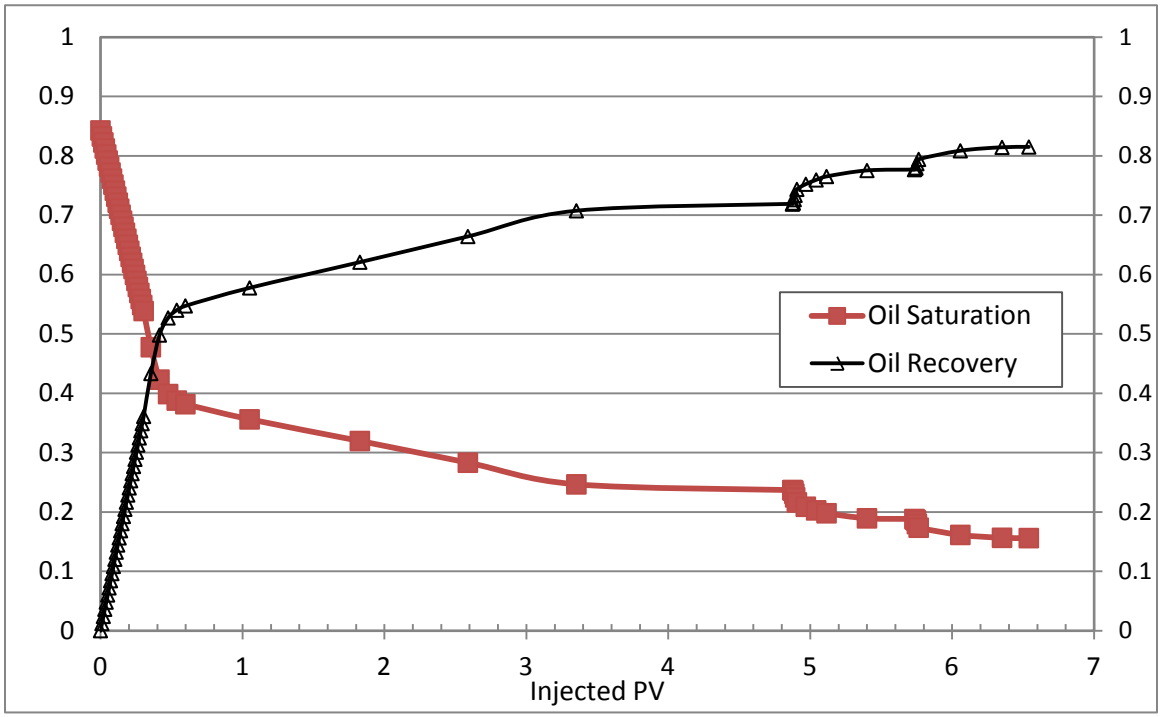

Figure 4.11: Recovery vs. PVs of water injected for A5-100-10

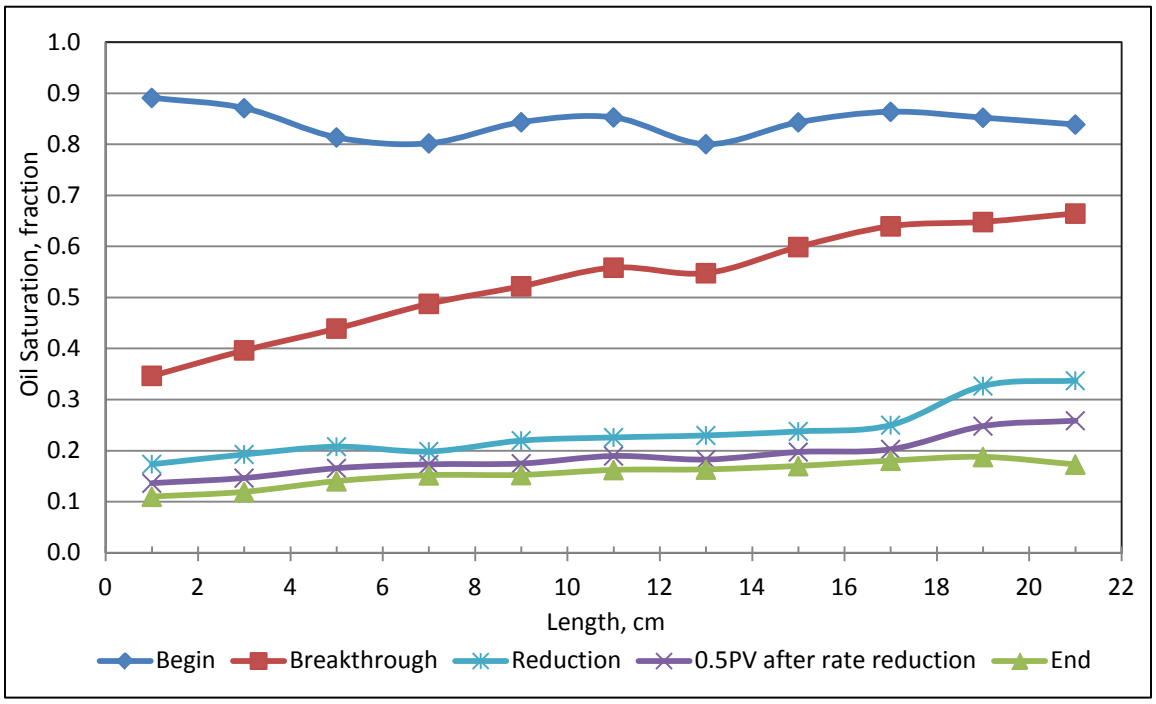

Figure 4.12: Oil saturation profiles during waterflooding for A5-100-10

In this case, the production performance is presented in Figure 4.10 and 4.11. The time when water breakthrough happened was around 9,000 seconds. And the RF at that time was about 0.36 which was very close to that of previous cases. The final recovery was 0.81, and the water permeability at the end of waterflooding was 2.8 D. Although the final recovery was slightly smaller than that of the case A5-100, the PVs injected were less. The relative permeability to water at residual oil saturation was 0.17.

Figure 4.12 shows oil saturation profile. The differential pressure was not collected due to technical problems.

4.1.4 Results of A5-500-10

In this case, the same fluid samples were used as that in section 4.1.1. The water injection rate was 500µl/hr at first, and then reduced to 10µl/hr at the time of 44,048 seconds.

In this case, the production performance is presented in Figure 4.13 and 4.14. The time when water breakthrough happened was around 1,620 seconds. And the RF at that time was about 0.32. The final recovery was 0.83. The water permeability at the end of waterflooding was 3.4D. The relative permeability to water at residual oil saturation was 0.20.

Figure 4.15 shows oil saturation profile. The differential pressure collected during waterflooding is presented in Figure 4.16. There is a gap on the pressure curve at the time when water injection rate is reduced.

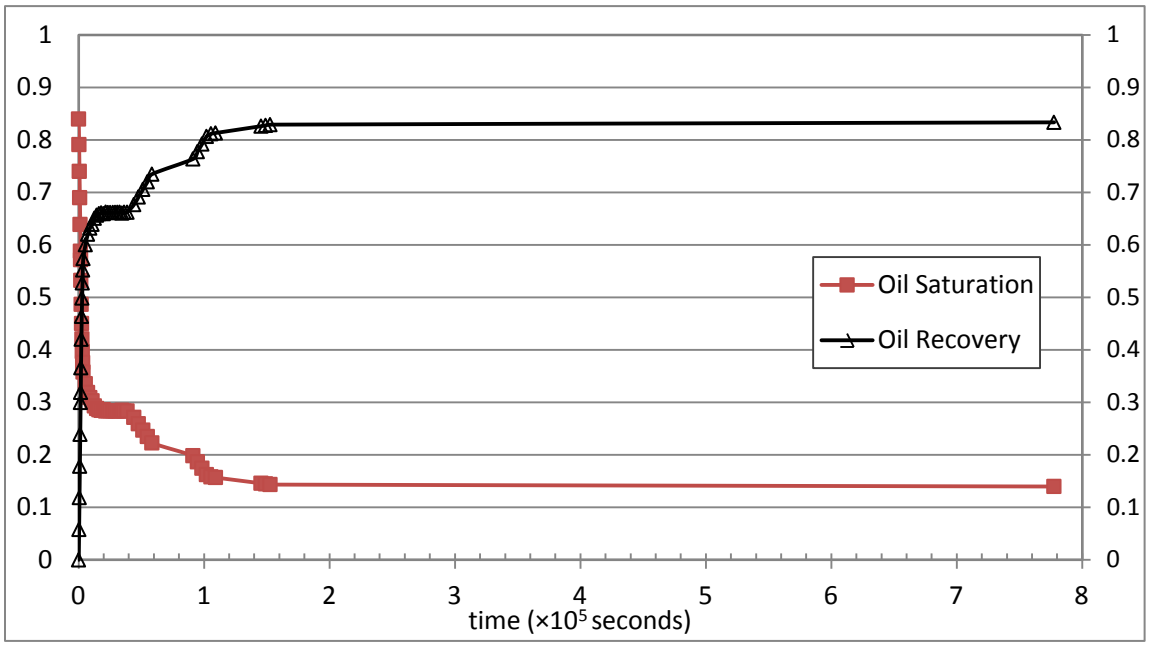

Figure 4.13: Recovery vs. time for A5-500-10

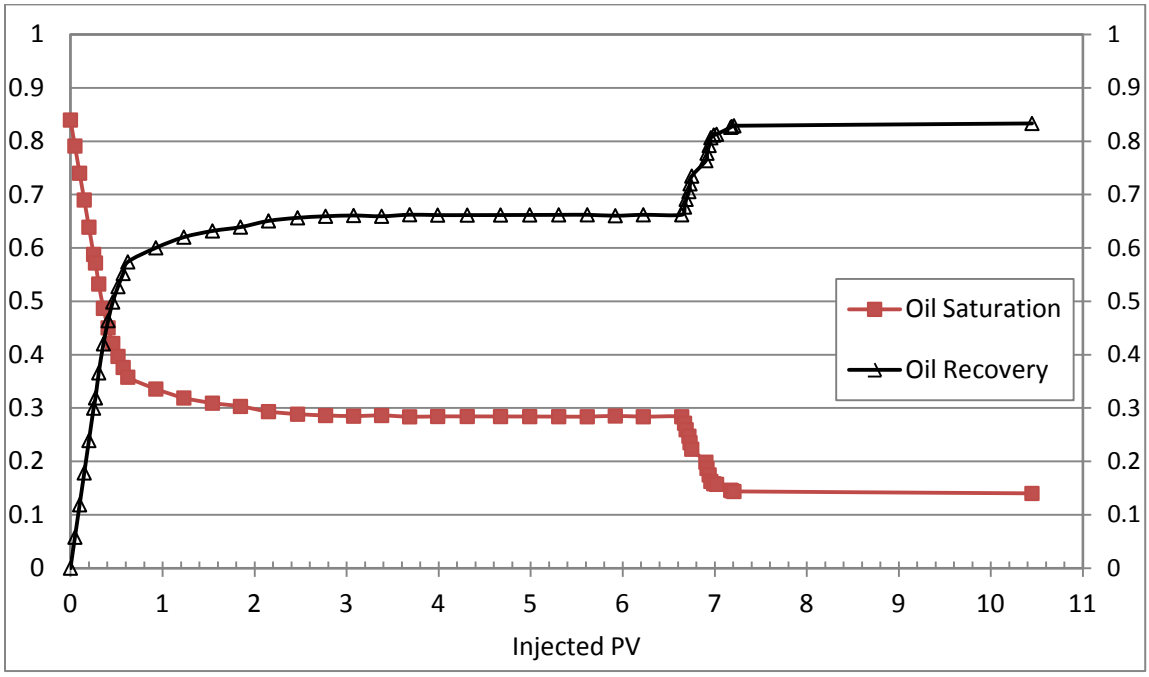

Figure 4.14: Recovery vs. PVs of water injected for A5-500-10

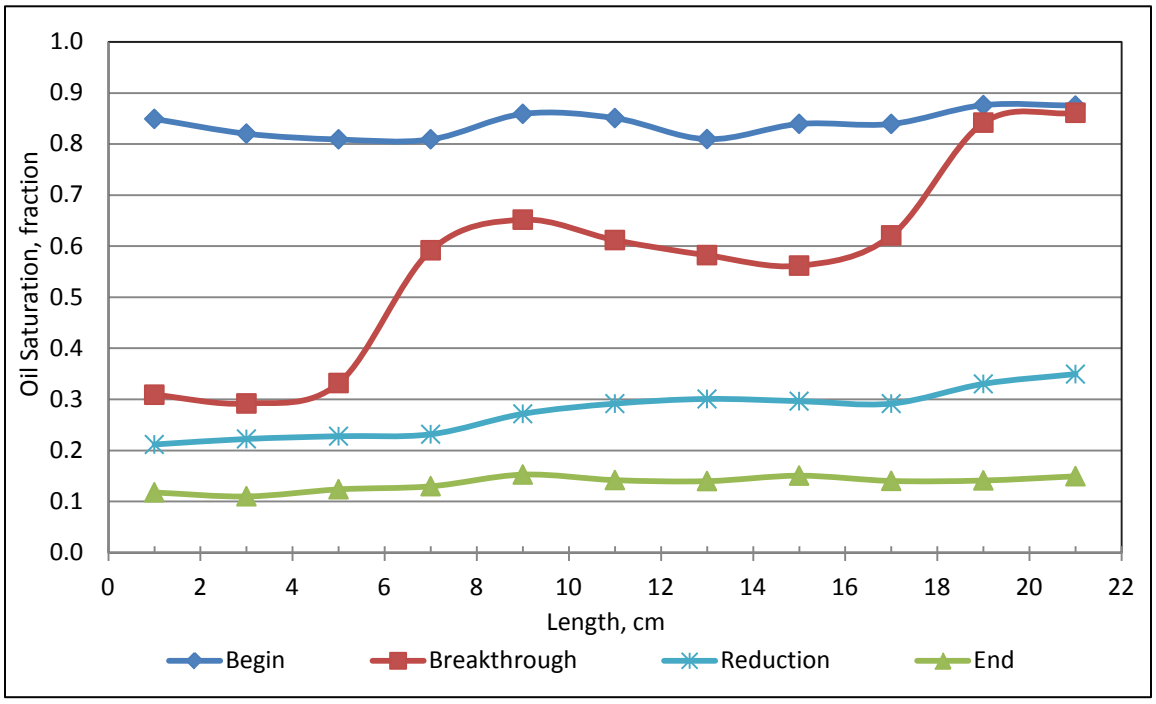

Figure 4.15: Oil saturation profiles during waterflooding for A5-500-10

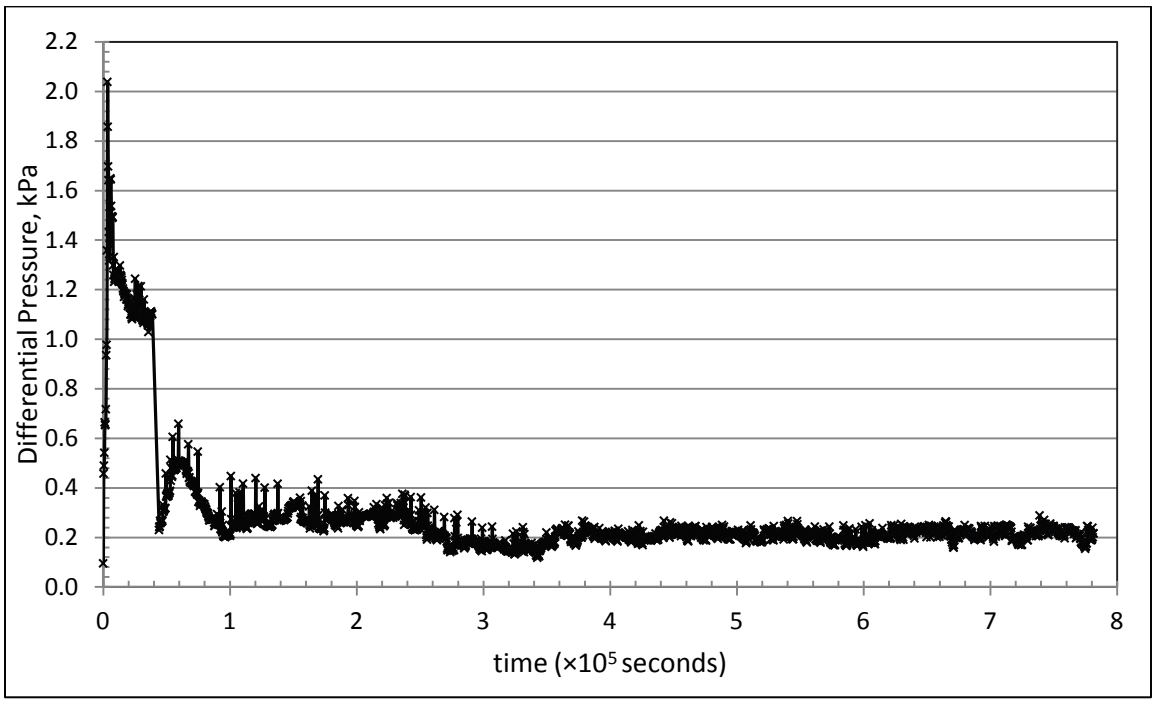

Figure 4.16: Differential pressure response for A5-500-10

4.1.5 Results of A5-1000-10

In this case, the same fluid samples were used as that in section 4.1.1. The water injection rate was the highest among the designed rates, and it was 1,000µl/hr. The rate was then reduced to 10µl/hr at the time of 34,689 seconds.

In this case, the time when water breakthrough happened was around 725 seconds. And the RF at that time was about 0.291. The final recovery was 0.82, and the water permeability at the end of waterflooding was 3.1D. The relative permeability to water at residual oil saturation was 0.19. In Figure 4.17, there was a horizontal stage between 20,237 seconds and 33,489 seconds on the curve of oil recovery versus time. That was because the pump stopped during that period. And this period was termed shut-in period.

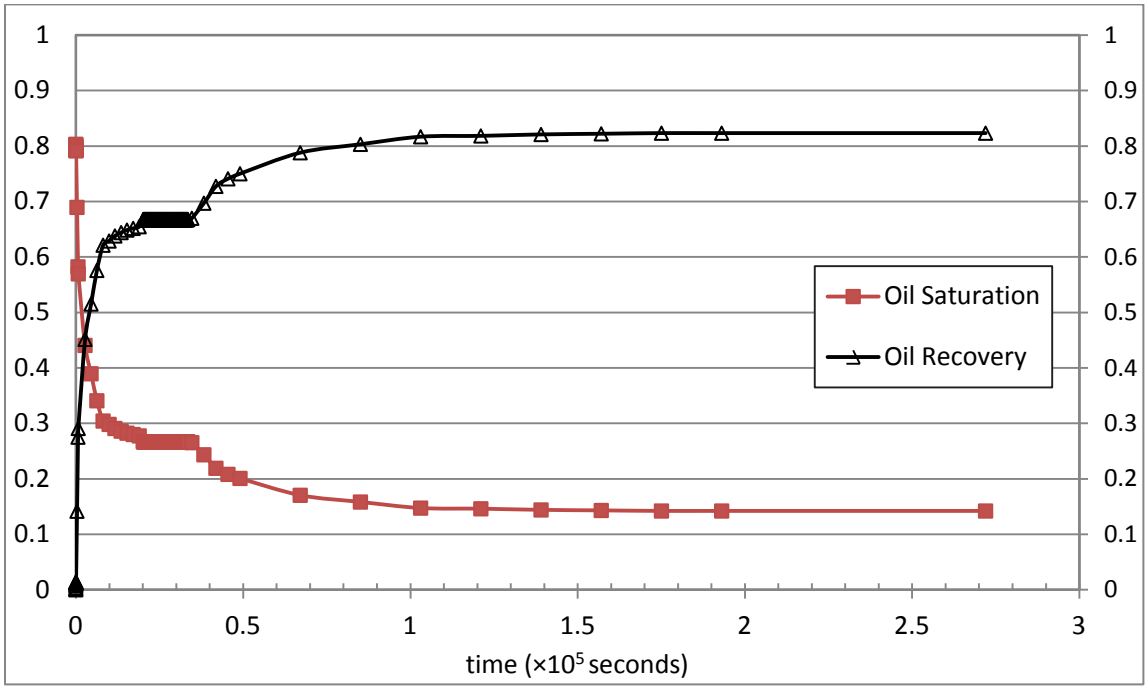

Figure 4.17: Recovery vs. time for A5-1000-10

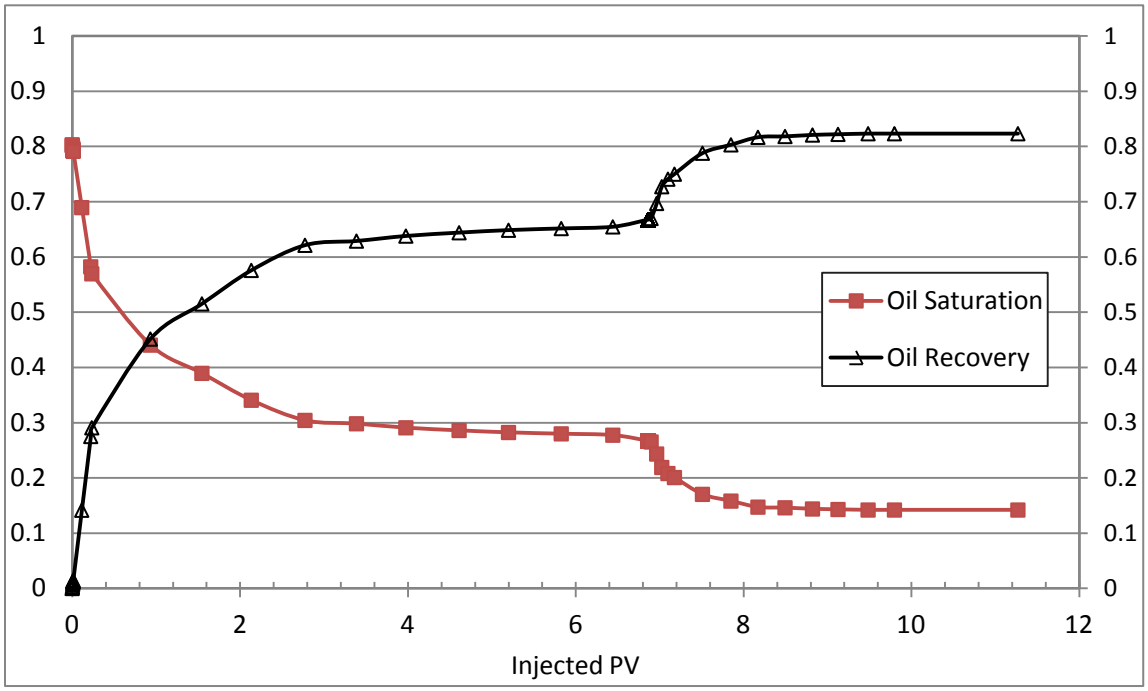

Figure 4.18: Recovery vs. PVs of water injected for A5-1000-10

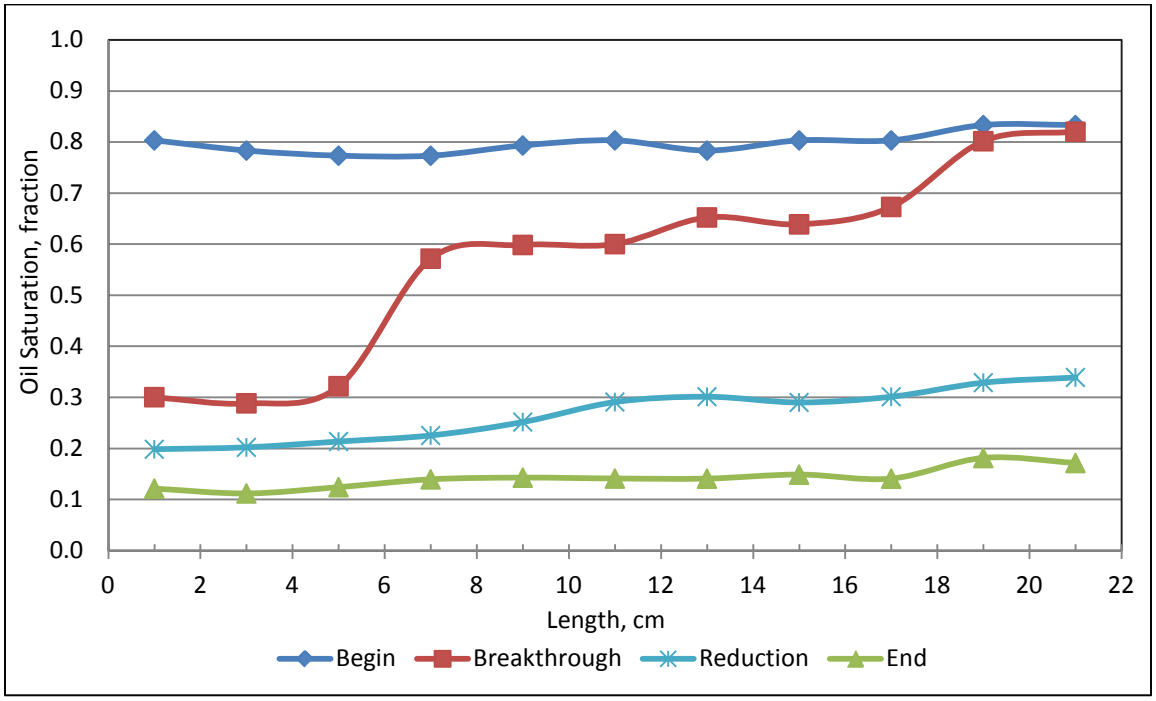

Figure 4.19: Oil saturation profiles during waterflooding for A5-1000-10

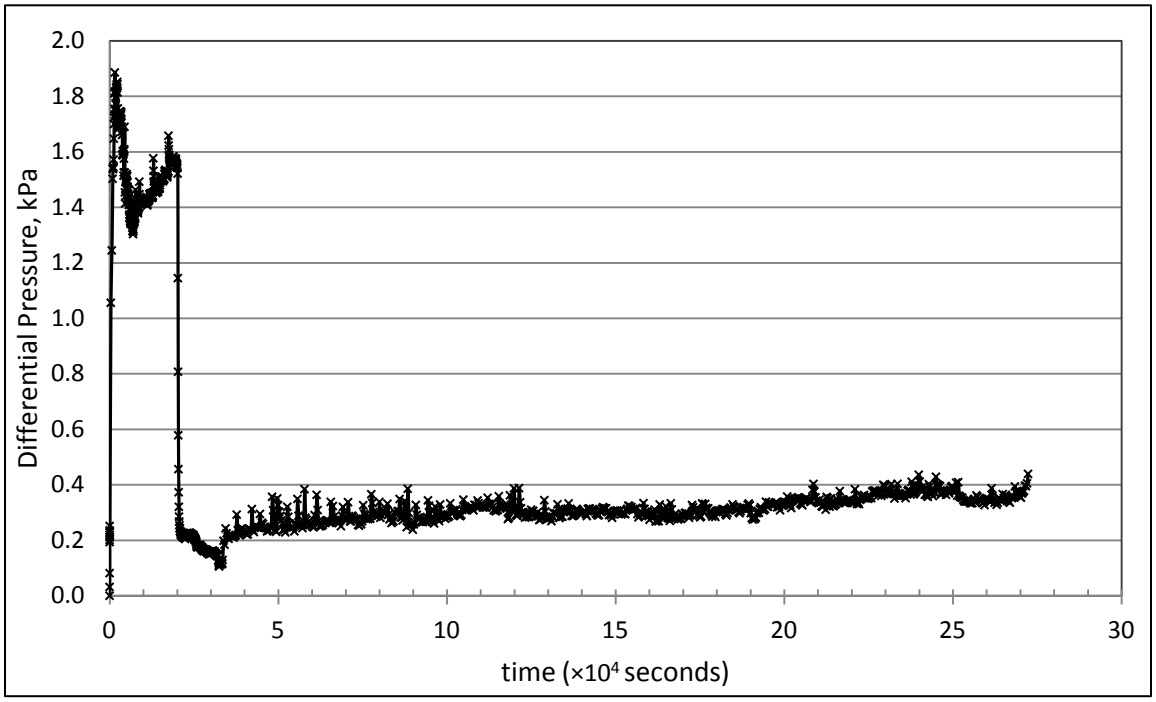

Figure 4.20: Differential pressure response for A5-1000-10

Figure 4.19 shows oil saturation profile. The differential pressure collected during waterflooding is presented in Figure 4.20. There is a long gap on the pressure curve at the time when water injection rate is reduced. That's because the injection was stopped for a while.

4.1.6 Results of A8-10

In this case, different oil sample was used. A8 stands for the combination of water sample #A and oil sample #8. The viscosity ratio was μ_o/μ_w=95.3. The water injection rate was constant, and it was 10µl/hr.

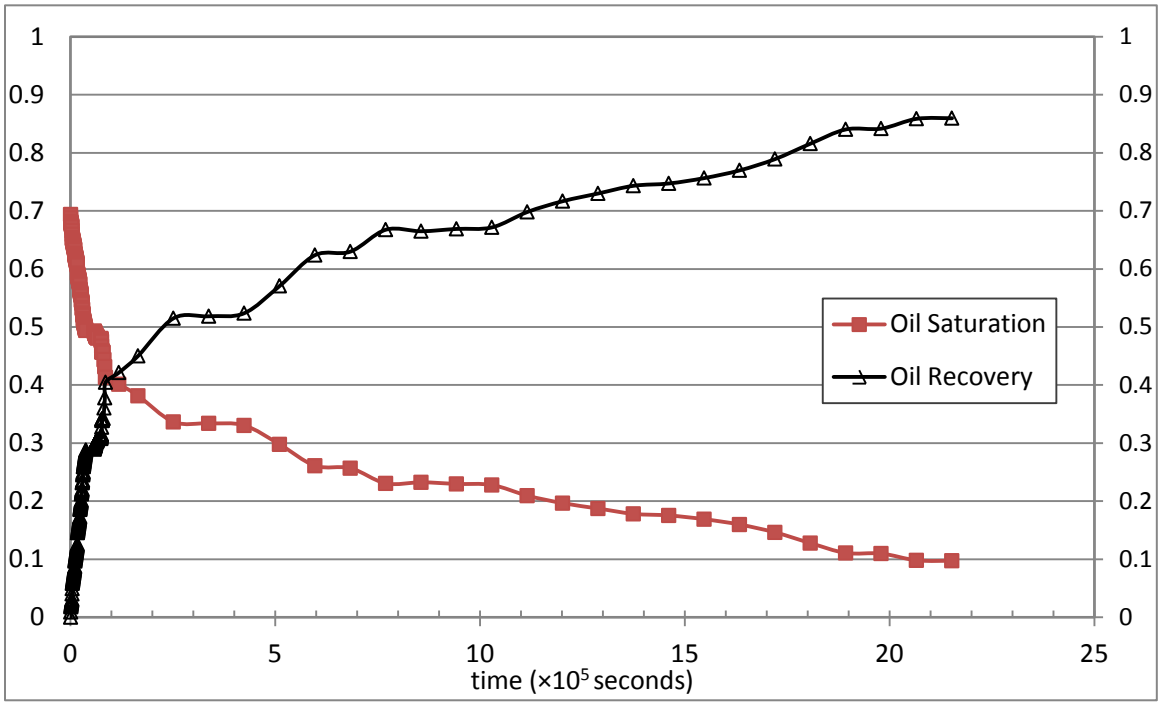

Figure 4.21: Recovery vs. time for A8-10

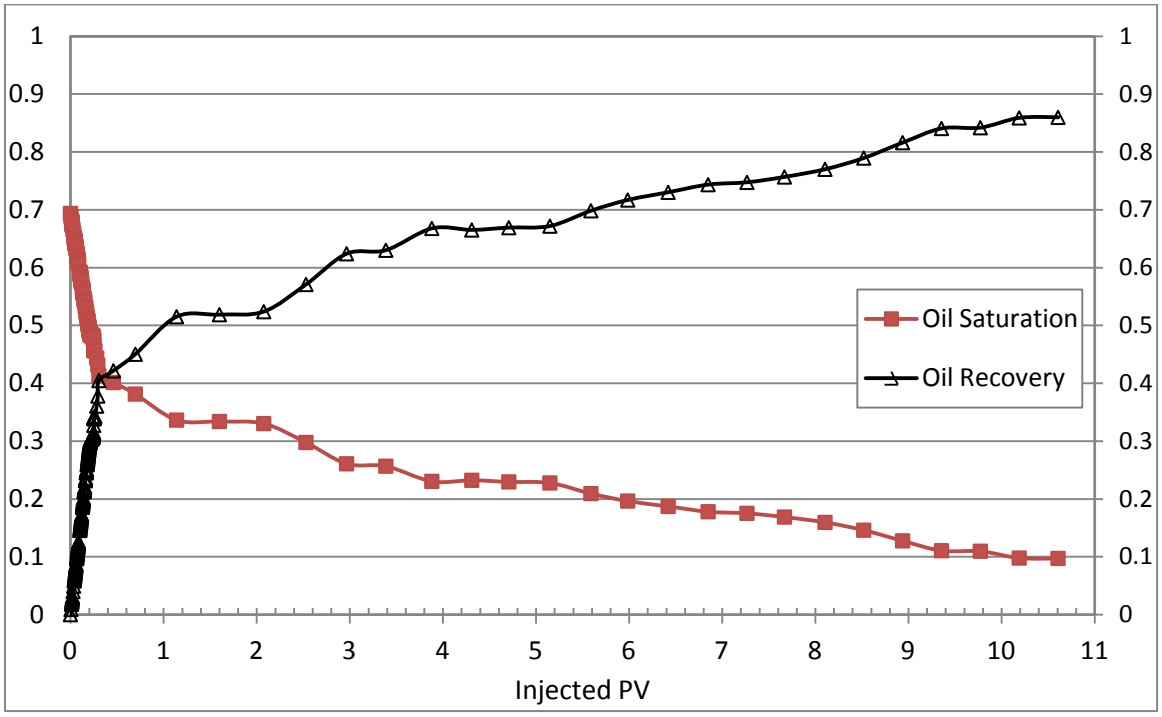

Figure 4.22: Recovery vs. PVs of water injected for A8-10

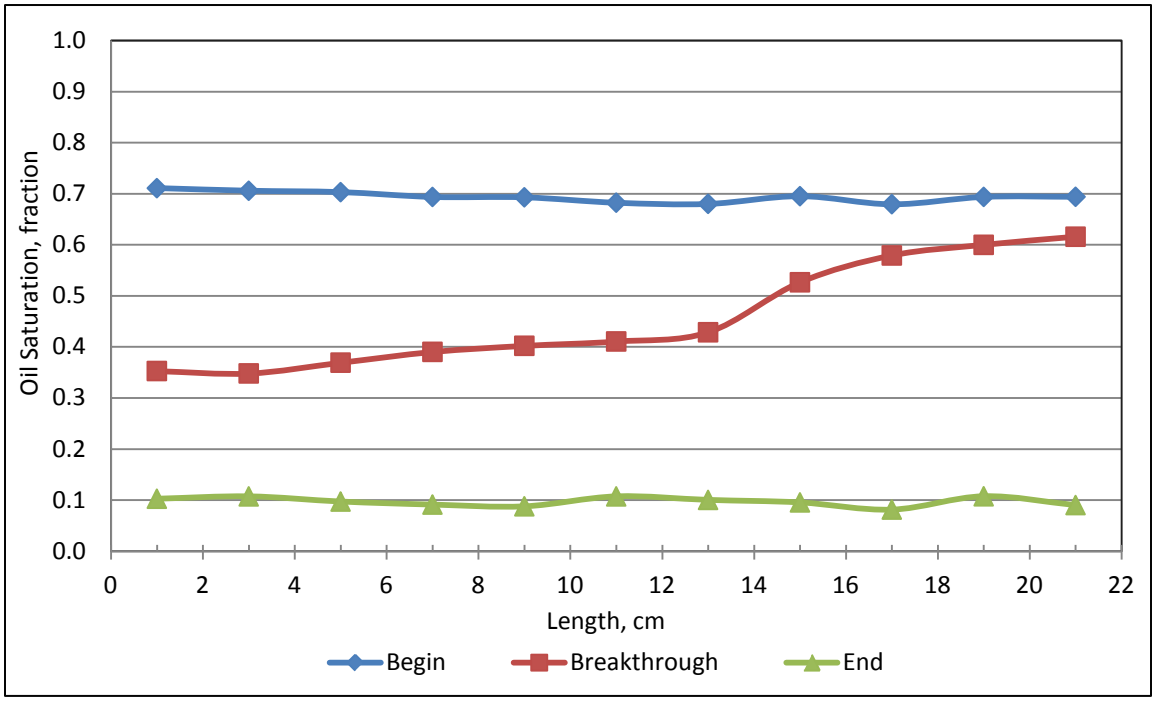

Figure 4.23: Oil saturation profiles during waterflooding for A8-10

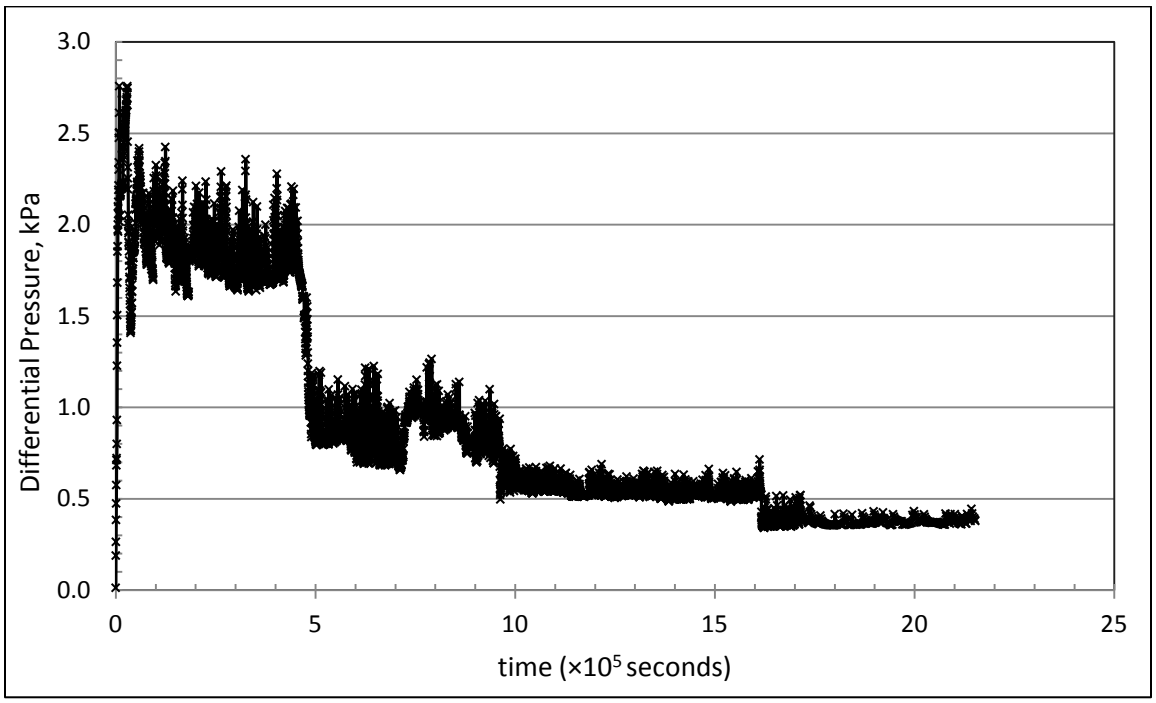

Figure 4.24: Differential pressure response for A8-10

In this case, the time when water breakthrough happened was around 58,800 seconds. And the RF at that time was about 0.34. The final recovery was 0.86, and the water permeability at the end of waterflooding was 2.8 D. The relative permeability to water at residual oil saturation was 0.17. In Figure 4.21, there is also a short horizontal stage on the curve of oil recovery versus time. That means there was a short shut-in period.

Figure 4.23 shows oil saturation profile. The differential pressure collected during waterflooding is presented in Figure 4.24.

4.1.7 Results of A8-100

In this case, the same fluid samples were used as that in section 4.1.6. The water injection rate was constant, and it was 100µl/hr.

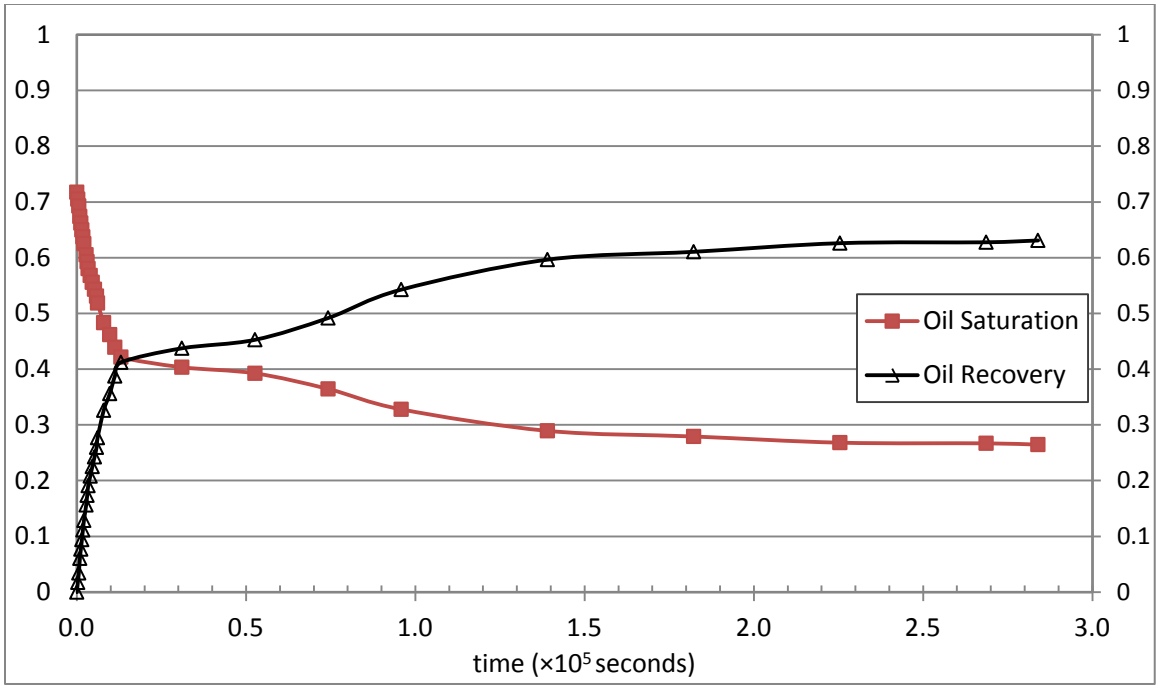

Figure 4.25: Recovery vs. time for A8-100

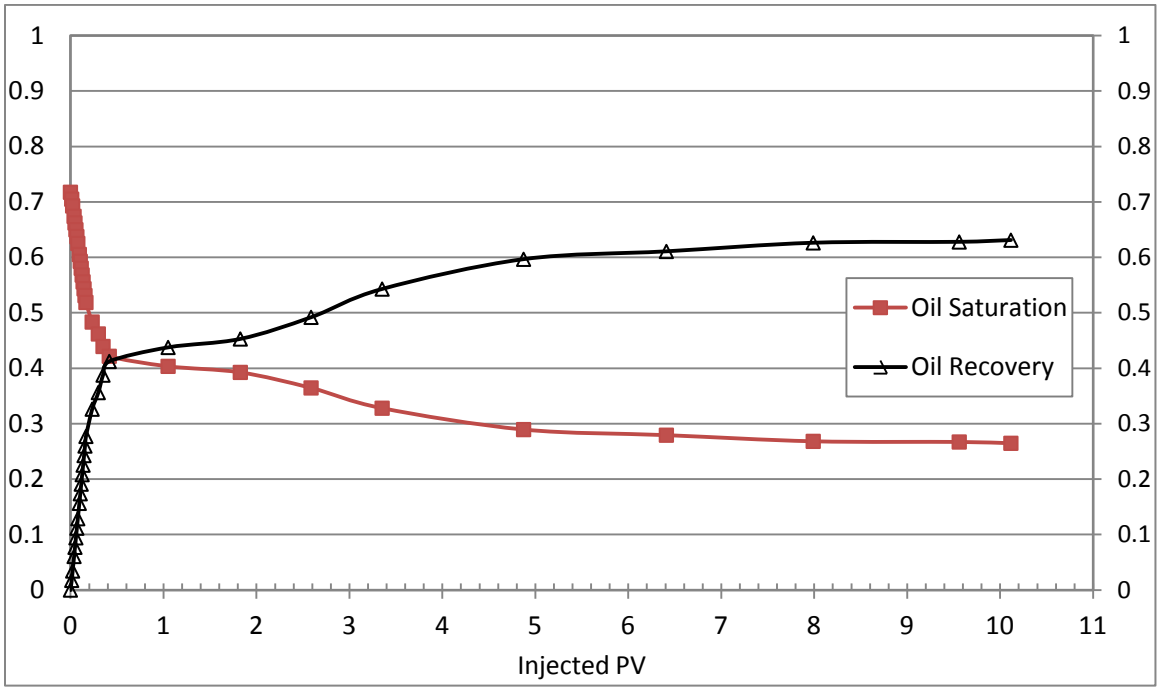

Figure 4.26: Recovery vs. PVs of water injected for A8-100

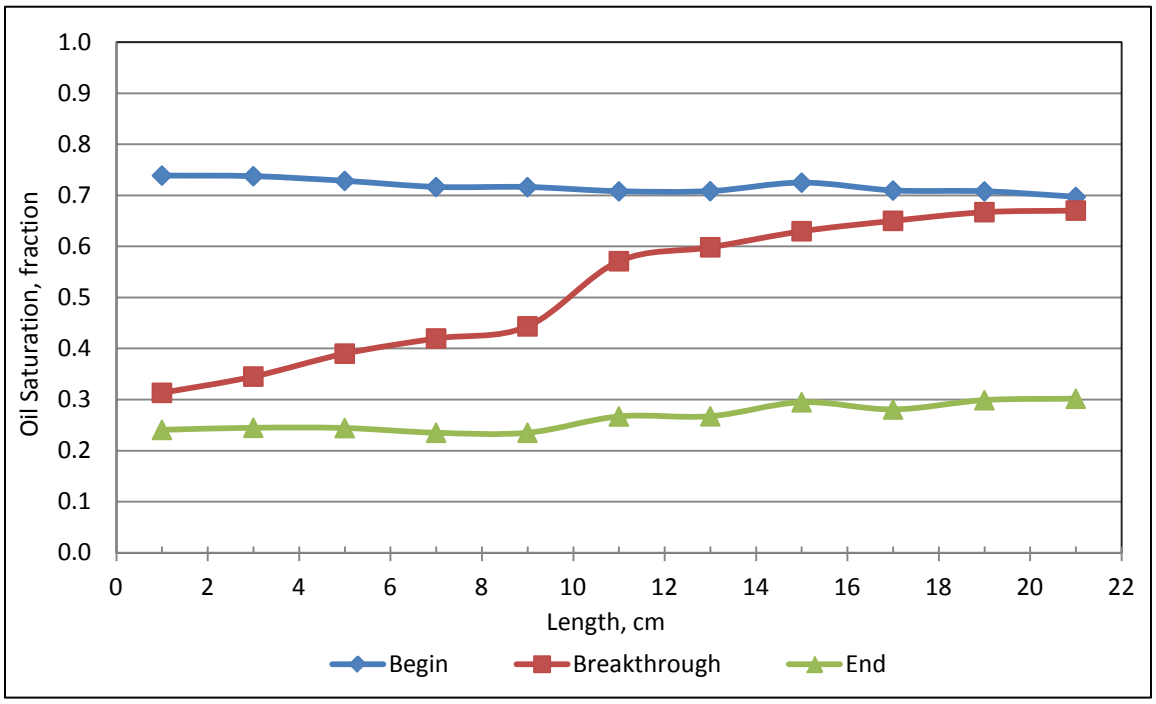

Figure 4.27: Oil saturation profiles during waterflooding for A8-100

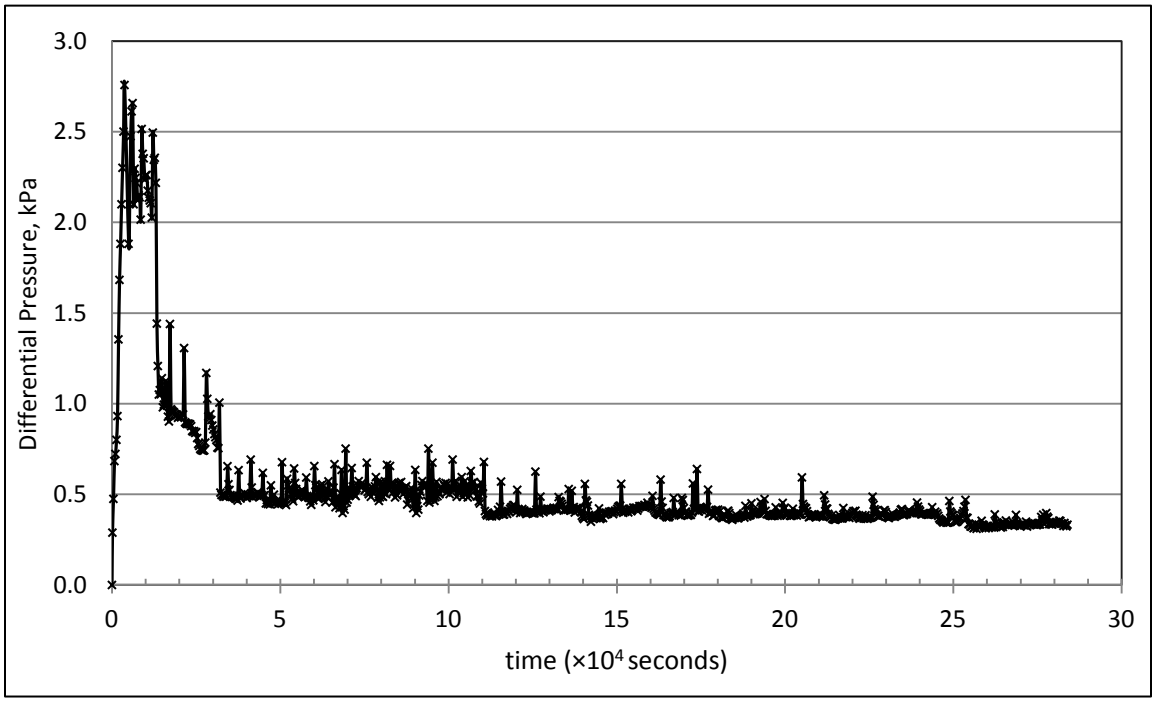

Figure 4.28: Differential pressure response for A8-100

In this case, the time when water breakthrough happened was around 6,141 seconds. And the RF at that time was about 0.277. The final recovery was 0.63, and the water permeability at the end of waterflooding was 3.0D. The relative permeability to water at residual oil saturation was 0.18. Actually, there were 5 shut-in periods before water breakthrough. They cannot be shown on the curve as these periods were as short as several minutes.

Figure 4.27 shows oil saturation profile. The differential pressure collected during waterflooding is presented in Figure 4.28.

4.1.8 Results of A10-10

In this case, the most viscous oil sample was used. A10 stands for the combination of water sample #A and oil sample #10. The viscosity ratio was μ_o/μ_w=561. The water injection rate was constant, and it was 10µl/hr.

In this case, the time when water breakthrough happened was around 38,889 seconds. And the RF at that time was about 0.3004. The final recovery was 0.79, and the water permeability at the end of waterflooding was 2.6D. The relative permeability to water at residual oil saturation was 0.16. Actually, there were 8 short shut-in periods before water breakthrough.

Figure 4.31 shows oil saturation profile. The differential pressure was not collected due to technical problems.

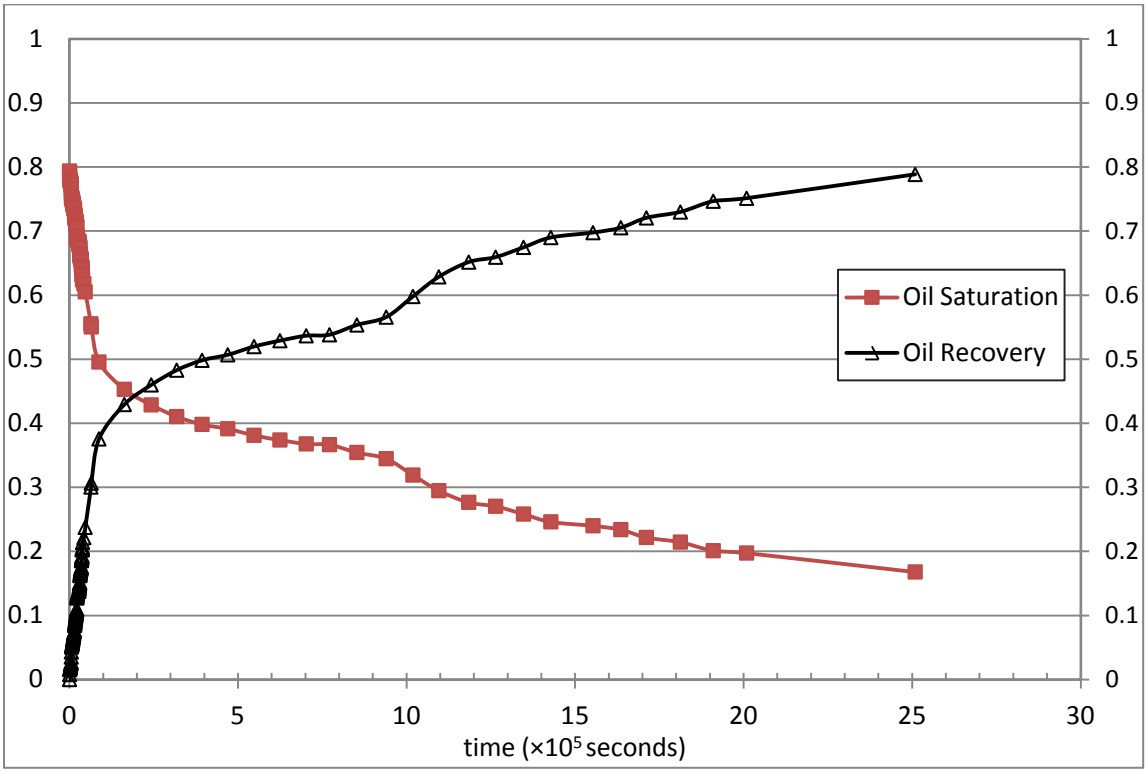

Figure 4.29: Recovery vs. time for A10-10

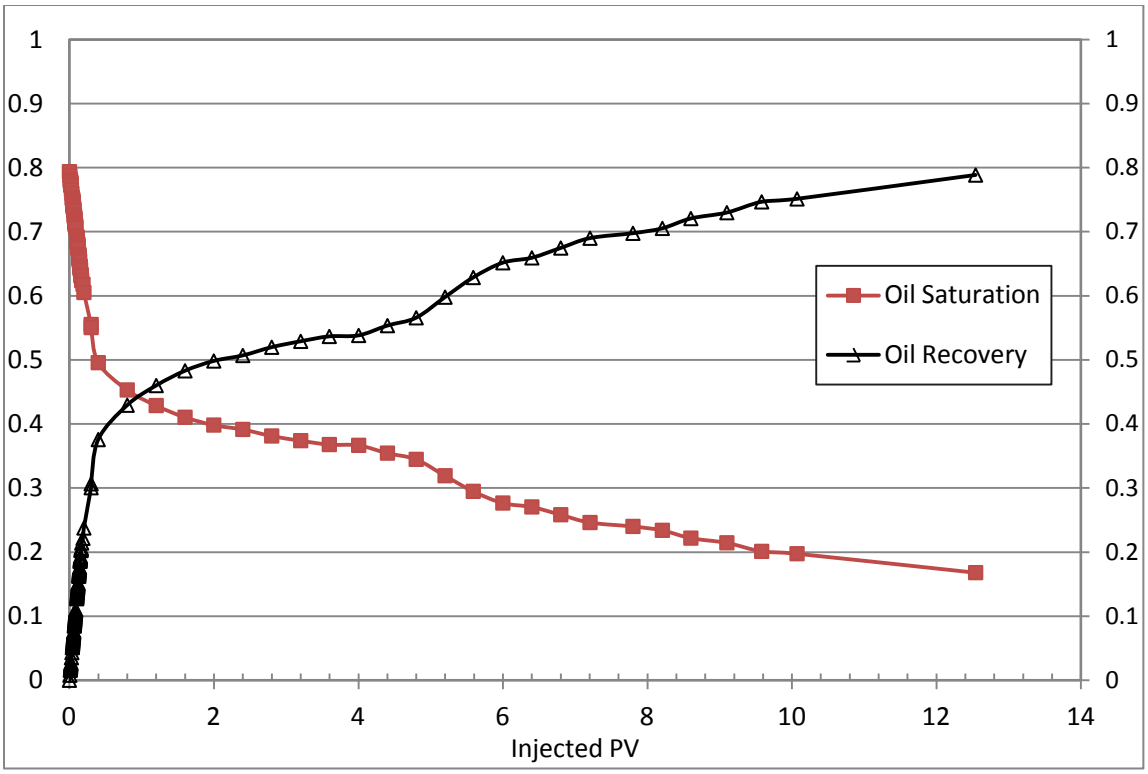

Figure 4.30: Recovery vs. PVs of water injected for A10-10

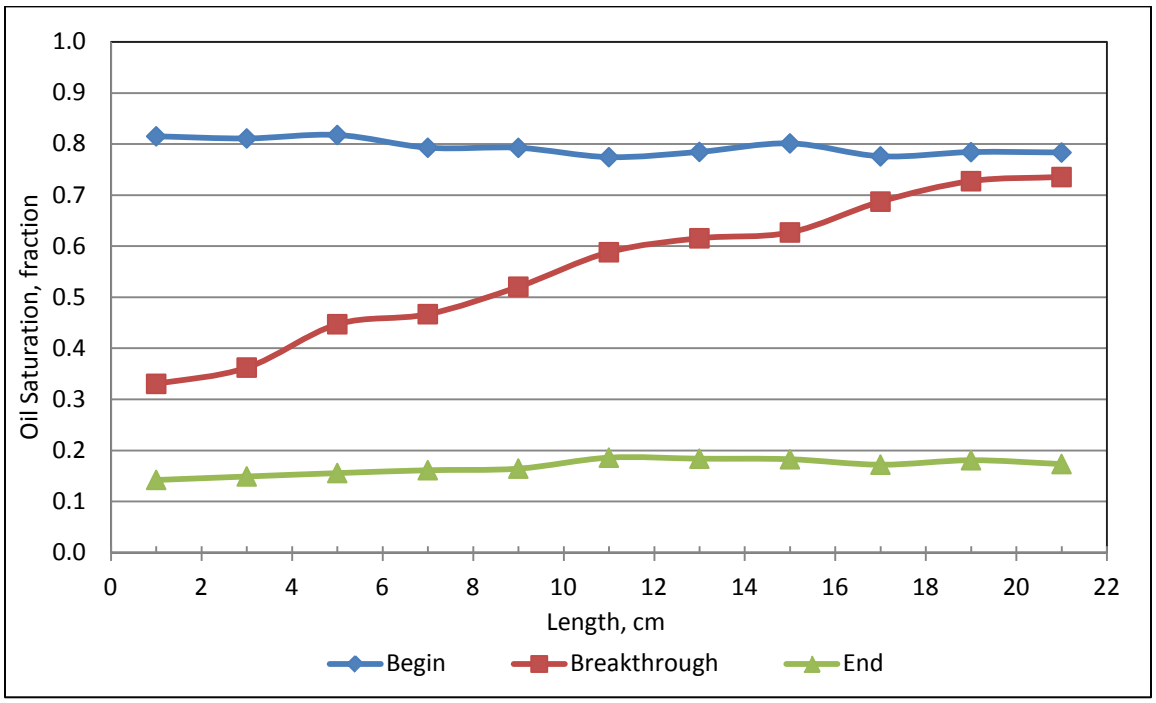

Figure 4.31: Oil saturation profiles during waterflooding for A10-10

4.1.9 Results of Spontaneous Imbibition Experiment

In the experiment of spontaneous imbibition, the fluids combination of water sample #A and oil sample #5 was used. Water was not injected. On the contrary, water imbibed into the micromodel. As shown in Figure 3.8 and 3.9, water imbibed into the micromodel from the left port, and oil flowed out of the micromodel through the right port. In order to trigger this flow pattern, an extremely small differential pressure was built by raising 0.5 cm higher of the left water level than the liquid level at the right side. When water began flowing into the small pore throat, the differential pressure was removed by adjusting the water level at the left side. And this point was considered as the zero time point. After that, the water began to imbibe into the micromodel by capillary forces exclusively.

The rate of spontaneous imbibition was much slower than that of forced imbibition. Figure 4.32 shows the production response of spontaneous imbibition. The capillary forces which were the only kind of force that controlled the spontaneous imbibition process was very weak, and the number of small pore bodies and throats were finite, these two reasons may result in the low spontaneous imbibition rate.

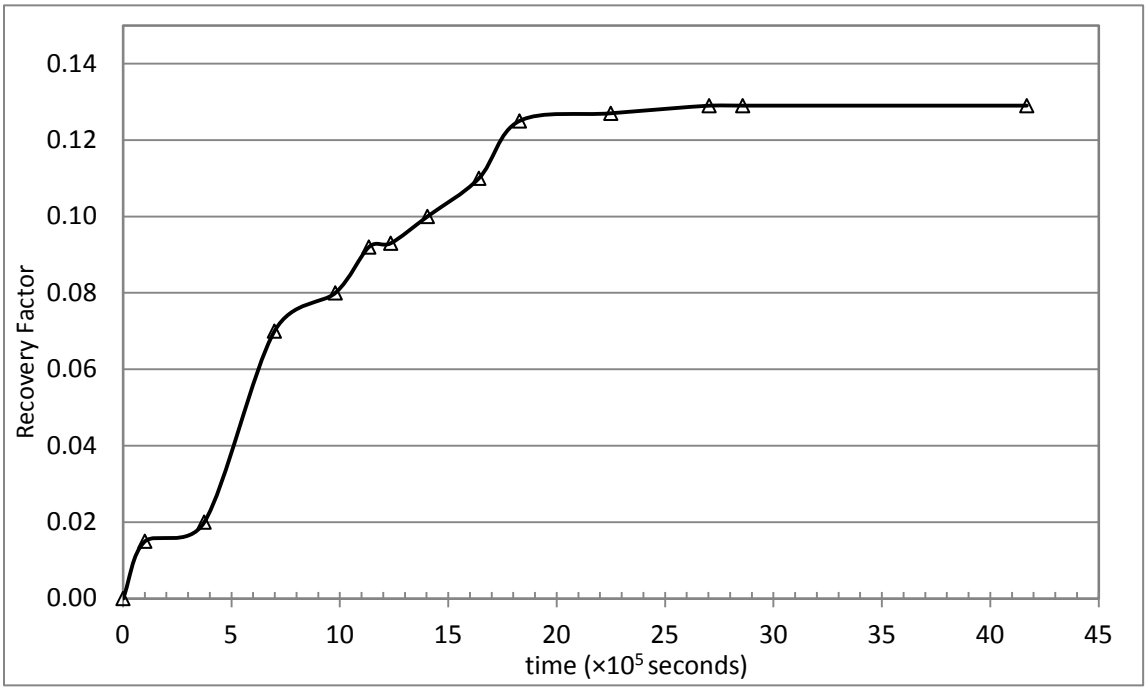

Figure 4.32: Recovery vs. time for spontaneous imbibition

Compared with the forced imbibition experiments, the recovery factor curve in Figure 4.32 goes upward slowly. It reached the highest value at the time 2,703,600 seconds. The final recovery was pretty low, it was just 12.9%. Water just imbibed a small part of the micromodel. There are two reasons for the poor recovery. One is that the resistance for oil phase to flow out of the micromodel through the inlet end is smaller than that through the outlet end, so oil phase tends to flow in the opposite direction. The other one is that

the testing time is no long enough for water to imbibe entire micromodel. More analysis about free spontaneous imbibition is presented in Chapter Five.

4.1.10 Summary

Totally, nine experiments including eight forced imbibition experiments and one spontaneous imbibition experiment have been conducted.

Table 4.1: Summary of individual experiment (forced imbibition only)

μ_o/μ_w	inj. Rate, µl/hr	S_{oi}	$S_{o\text{-}bt}$	R_{bt}	PV@Sor	S_{or}	R_{final}	Kw@S_{or}, Darcy
11.1	10	0.8238	0.5086	0.3734	8.60	0.1338	0.8352	3.0259
	100	0.7726	0.4903	0.3653	12.20	0.1361	0.8238	3.3175
	100-10	0.8429	0.5386	0.3610	6.54	0.1560	0.8149	2.8126
	500-10	0.8397	0.5718	0.3190	10.45	0.1399	0.8333	3.4398
	1000-10	0.8032	0.5695	0.2909	11.27	0.1420	0.8232	3.1291
95.3	10	0.6938	0.4568	0.3415	10.61	0.0972	0.8598	2.8025
	100	0.7175	0.5187	0.2771	10.11	0.2647	0.6310	3.0088
561.1	10	0.7938	0.5553	0.3004	12.54	0.1680	0.7884	2.6103

In the series of forced imbibition experiments, the recovery factors at the point of water breakthrough were in the range of 0.27 to 0.37. The recoveries were in the range of 0.63 to 0.86. The water effective permeability at the end of waterflooding was in the range of 2.6D to 3.4D. Shut-in period was applied in some cases because of the pressure limitation. Water injection rate was kept constant in some cases but varied in others. According to the pressure response, oil samples with higher viscosity were not able to be tested using this micromodel as the pressure limitation.

Additional analysis, such as comparisons between forced imbibition and spontaneous imbibition, effects of fluid properties and operation parameters on imbibition rate, water imbibition mechanisms and image analyses are presented in the next section and next chapter.

4.2 Effect of Time on Water Imbibition

The rate of water imbibition was variable with time. In Figure 4.33, recovery factor is plotted as a function of square root of time. This figure shows that there is a correlation between recovery factor and square root of time. For all the curves in the figure, the water injection rates were 10µl/hr (frontal velocity of 0.0672 m/day). Only post-breakthrough data were compared. Even through the slopes are different, the curves are linear (within the experimental errors) with respect to the square root of time. The water imbibition rate, which is proportional to the derivative of recovery factor, is inversely proportional to the square root of time. This confirms that after water breakthrough, the oil production under low water rate condition is mainly due to water imbibition.

Iffly et al. (1972) pointed out that the formula of "$\ln R \propto t$" is better than "$R \propto \sqrt{t}$" when correlated recovery with time. On the contrary, the latter is better to describe the imbibition process in this research. Compared to Iffly's research, the experiment condition in this thesis was significantly different. Siltstone cores with height of 5 – 200cm were used in Iffly's research, so the relative influence of gravity and capillarity was taken into account. Only spontaneous imbibition was tested and some experiments

lasted through twelve months in Iffly's research. However, in this micromodel experimental study, the effect of gravity was ignored, both forced and spontaneous imbibition was tested, and the longest experiment only lasted one and half months. These differences had influence on water imbibition.

In Figure 4.33, the points would eventually flatten out if experimental time was long enough. The recovery factor for each test will stop increasing when irreducible oil saturation is reached. At that time, the residual oil will be trapped under the control of capillary forces.

It must be noted that there are plateaus on the curves in Figure 4.33. Actually, these plateaus existed only in the situation of low water injection rate. Explanation to this phenomenon was presented in section 4.4.

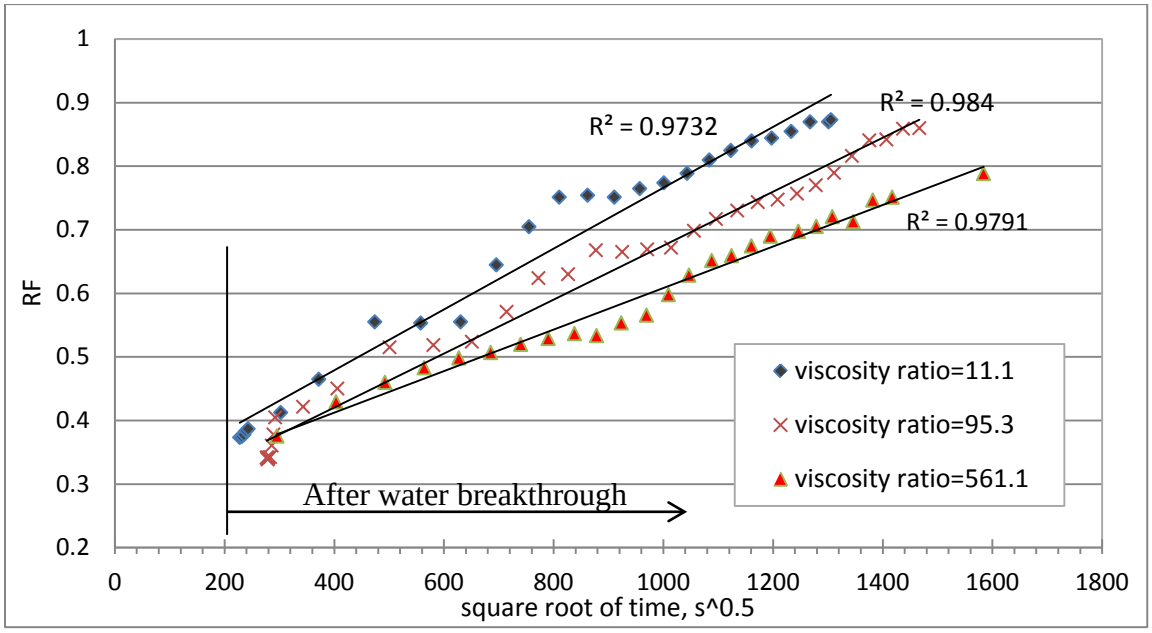

Figure 4.33: Recovery factor vs. square root of time

4.3 Effect of Oil Viscosity on Water Imbibition

The effect of viscosity ratio on spontaneous imbibition in facture-matrix systems has been thoroughly investigated in the literature. Some different correlations for the mean viscosity of oil and water were used to evaluate its effect on water imbibition. However, these different correlations had the similar format as Equation 2.9. All these correlations showed that there was an essential relationship between water imbibition rate and a function of oil and water viscosities.

For three cases in Figure 4.33, when using a first order equation to relate RF to the square root of time ($RF = a\sqrt{t} + b$), the values of intercept '*b*' are very close (~ 0.28) for all three oil viscosities. However, the values of slope '*a*' are very different. The slope is a measure of the rate of oil production with time, after breakthrough.

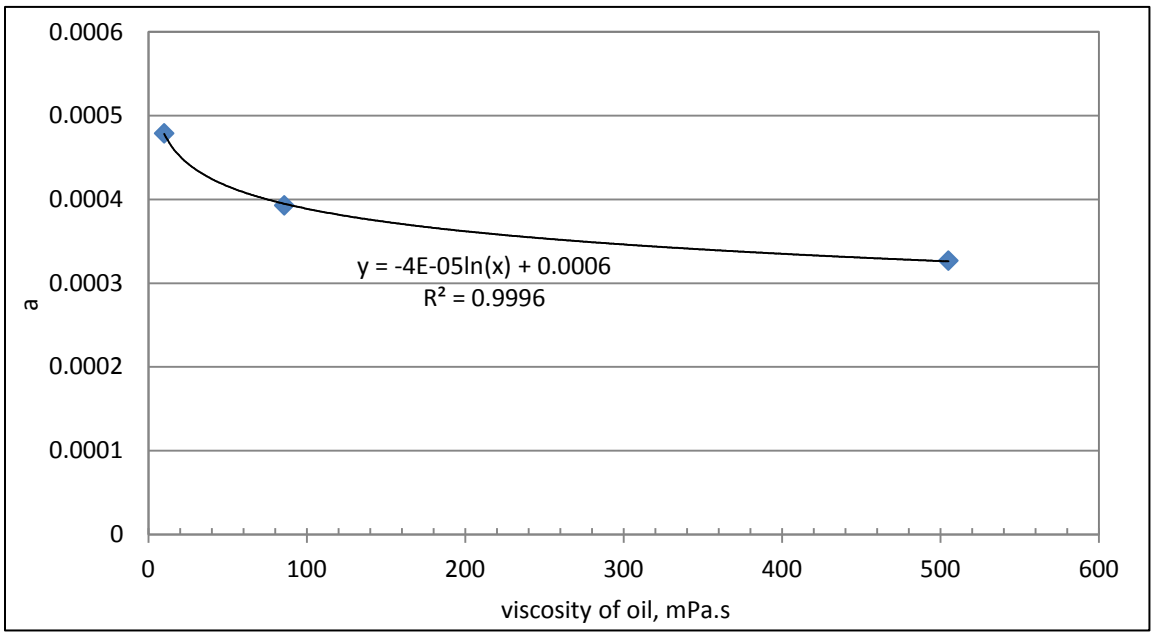

Figure 4.34: Slope vs. oil viscosity

Figure 4.34 plots the slope versus the oil viscosity and shows that the slope decreases with increasing oil viscosity. In other words, when waterflooding is performed for higher viscosity oils, the oil production decreases per pore volume of injected fluid at the same rate (i.e. fluids are produced at higher water cuts). This figure may be indicative of a potential upper limit to fluid viscosity that is waterfloodable. However, what is evident in this figure is that the relationship between the slope and the oil viscosity is non-linear. As viscosity increases by a factor of 50 (from 11 to 561mPa·s), the slope drops by only a factor of 1.5. In post-breakthrough oil production, therefore, recovery of oil is not directly related to the viscous forces (oil viscosity) in the system.

The results shown in Figure 4.35 are plotted as recovery versus PVs of water injected. For all these 3 cases, the water injection rates were all the same: 10μl/hr. For the oil sample with higher viscosity, water breakthrough happened earlier than that of less viscous oil; and had the smaller recovery factor at the point of water breakthrough. The exact values were shown in the Table 4.1. After water breakthrough, at the situation of low water injection rate, oil can still be recovered by water imbibition. The same amount of oil if not more could be produced after water breakthrough as that produced before water breakthrough. And there were only slight differences between the incremental recoveries among these three cases. For the oil samples with higher viscosity, considerable recoveries also could be reached. However, more PVs of water had to be injected. For example, the points of crossing with the line RF=0.8 were different. The PVs at 80% RF was equal to 6 for the lowest viscosity ratio, 8.6 for the medium viscosity ratio, and higher than 12 for the highest viscosity ratio.

Figure 4.36 shows time spent (PVs injected) for different cases to get certain recovery factor. For all these three cases, the water injection rates were 10µl/hr. The R-squared values for all the recovery factors except 0.7 were very close to 1. At a smaller recovery factor, such as 0.2, the curve of PVs versus oil viscosity would be a straight line as it was at the pre-breakthrough stage. The data indicate a definite relationship between oil viscosity and time required for water imbibition for recovery factors below 0.7. This implies that imbibition rate does vary with oil viscosity for the ranges and experimental configurations tested here, even though the relationship is non-linear with viscosity.

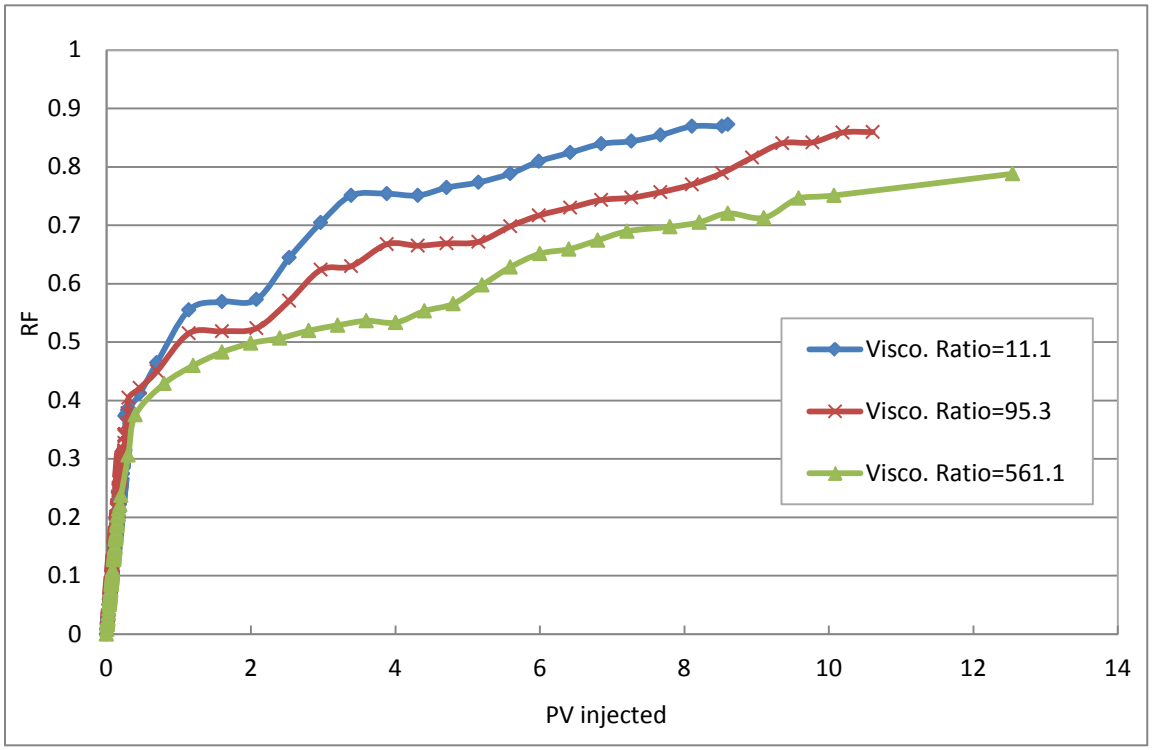

Figure 4.35: Recovery factor vs. PVs injected

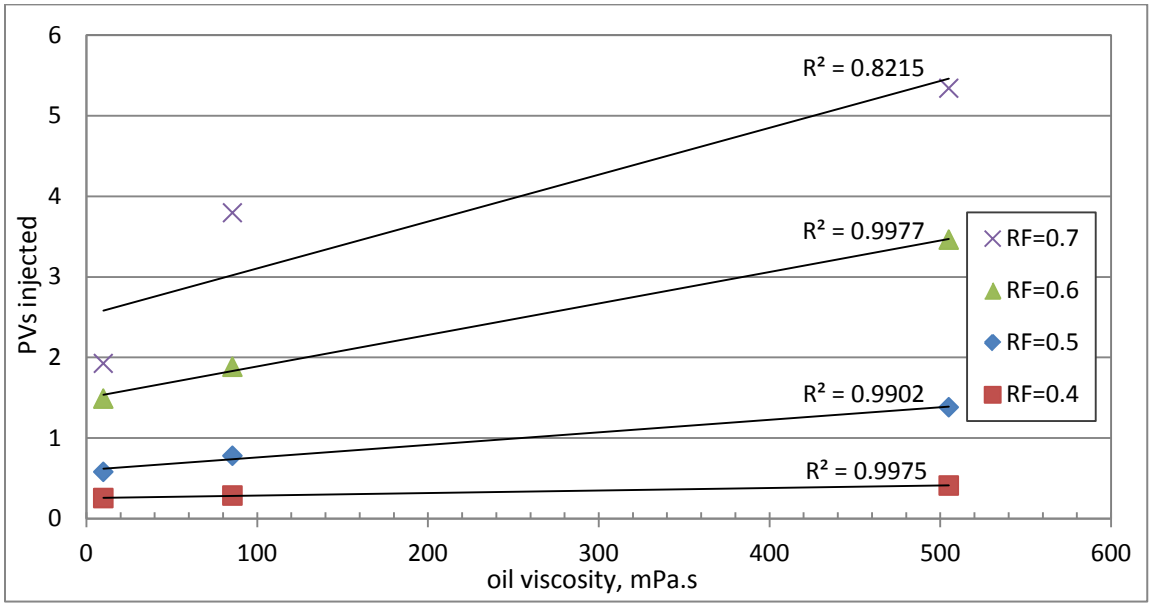

Figure 4.36: Imbibition time vs. oil viscosity

4.4 Effect of Injection Rate on Water Imbibition

In this thesis, 10µl/hr, 100µl/hr, 500µl/hr and 1000µl/hr were set as the water injection rates. The corresponding frontal velocities were 0.0672m/day, 0.672 m/day, 3.36 m/day and 6.72 m/day. The corresponding capillary numbers were 3.05×10^{-8}, 3.05×10^{-7}, 1.52×10^{-6} and 3.05×10^{-6}. It has to be emphasized that, the whole intersection area was assumed to be the effective flow path when calculating the average velocity. Actually, this was wrong. As the waterflooding process was two-phase flow, the effective flow area was smaller than the whole intersection area. As a result, the local capillary number should be larger. In all cases of different injection rates, some typical characters of water imbibition such as water film thickening and snap-off were observed All in all, according to the range of capillary number and experimental observation, the waterfloods were expected to be in the regime of capillary dominated flow, at least in a conventional oil understanding.

The injection rate is one of the most important operation parameters in heavy oil waterflooding. And the investigation about the operation strategy is always an interesting topic. According to the previous investigations, the high injection rate normally resulted in fast oil recovery, and high water cut. The low injection rate normally resulted in relatively small water cut. Generally, because of high water cut, the later stage of the heavy oil waterflooding usually acted like circulation of water. Beside the effects of high or low injection rate, in the literature, cyclic water injection rate was believed to benefit oil production.

4.4.1 High Rate or Low Rate

In Figure 4.37, the results were plotted as the oil production responses of the same oil sample to different water injection rates. As the injection rates of some cases were changed after 6.67 PVs, just the responses to the period of pre-6 PVs were considered for comparison. At the end of 6 PVs injected, slower water injection rates resulted in higher oil recovery. Especially for the lowest injection rate of 10μl/hr, the recovery factor even exceeded 0.8, and was still increasing at the end point. Note, however, that this figure plots oil recovery on the basis of pore volumes injected. For this viscosity ratio of oil/water, going from 10 – 100 μl/hr (a ten-fold increase) only marginally reduces the ultimate recoverable oil. Therefore, on the basis of time instead of PV injected, it may still be more beneficial to flow at intermediate rates in order to accelerate oil production, at least in this level of viscosity ratio.

The recovery factors were very close for the cases of relatively high water rates: 500µl/hr and 1,000µl/hr. based on the performances, the injection rates 10µl/hr and 100µl/hr were considered as low rates; and the 500µl/hr and 1,000µl/hr were considered as high rates.

The Figure 4.38 shows the results for the lower injection rate cases. There were some plateaus on all the curves, and this is especially evident for the lowest injection rate. These plateaus indicated that the recovery factors increased in a stepwise manner and that time was needed for oil to be dislodged from the continuous remaining oil in place. At low injection rates and after water breakthrough, the differential pressure was extremely low, so the viscous forces had weak influence on the process, and the capillary forces were believed to play the dominant role.

At high injection rates (Figure 4.37), the recovery curves appear more gradual. After water breakthrough their slopes decreased significantly, indicating that most of the injected water was simply channeling through preformed water pathways. The curves were almost horizontal when they reached high recovery factors. The performances of these curves were quite different from those of low injection rates.

Capillary forces are always present in immiscible displacement systems. At low water injection rates the time scale is much longer and impact of the capillary forces may become more significant (i.e. more water is used for imbibition and less water simply cycles through the system). However, low injection rates imply long operation time and that may result in unattractive economics.

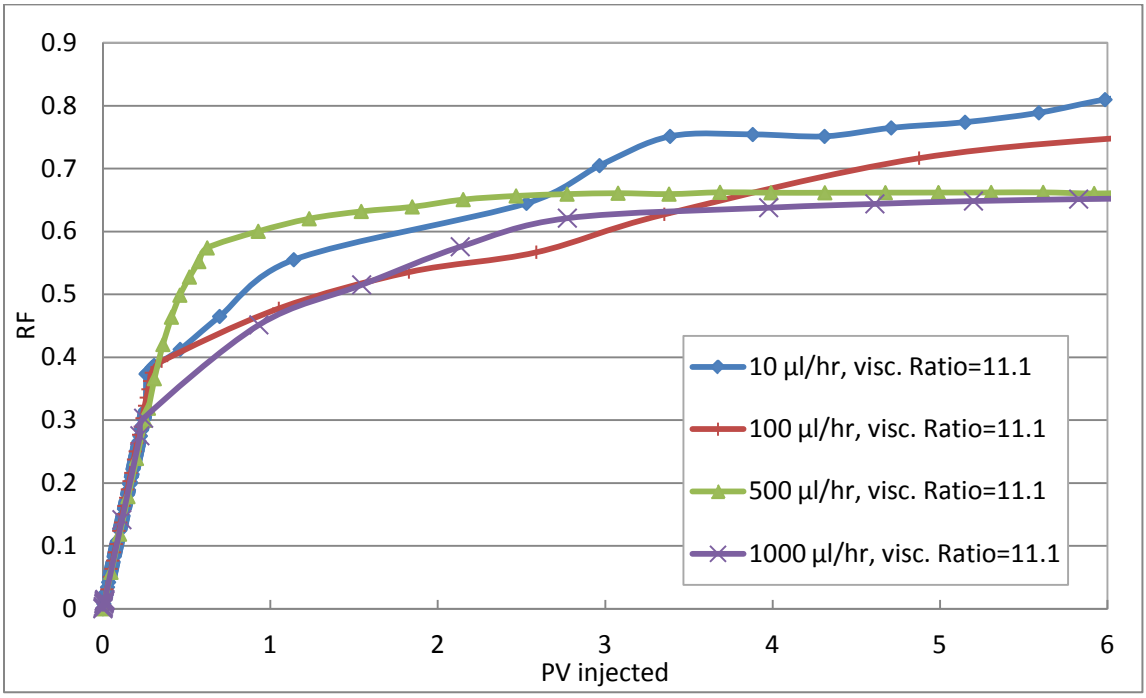

Figure 4.37: Recovery factors at different water injection rate

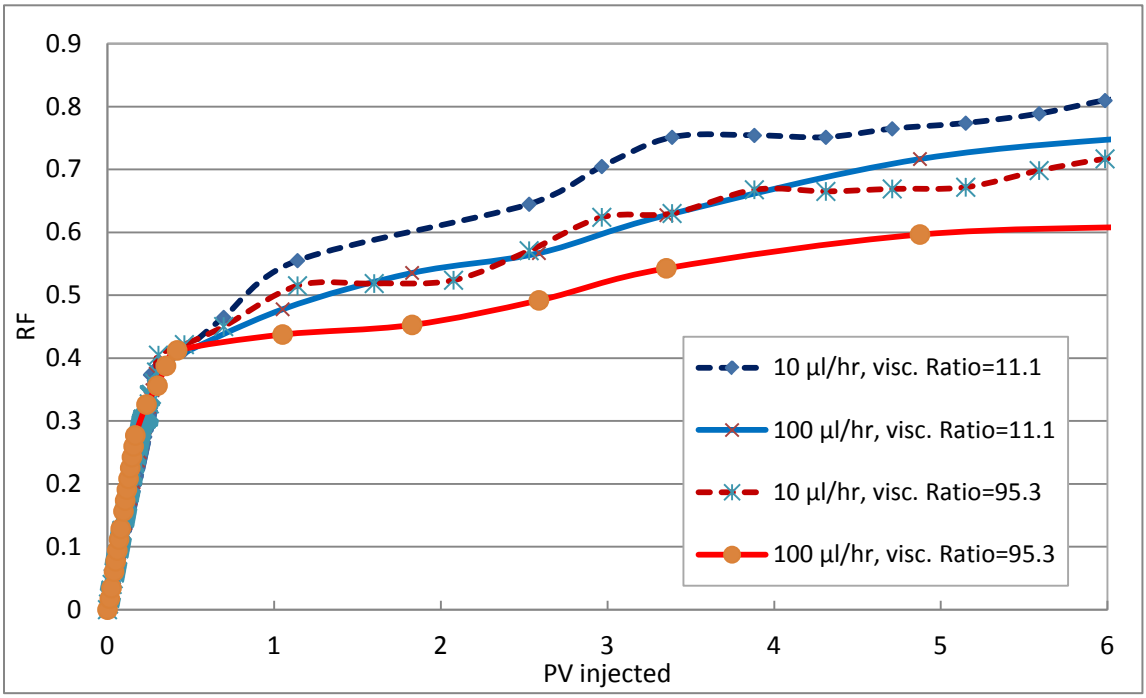

Figure 4.38: Recovery factors of low injection rate cases

4.4.2 Shut-in Period

During the experiments, it was essential to maintain low pressure drops to sustain the integrity of the micromodel. Thus the pump would stop automatically when the differential pressure exceeded an upper limit set value. At this point, the shut-in period began. The system would be shut in until pressure dropped, and the pump would only be re-started manually.

The production responses of the cases that had shut-in periods are shown in Figure 4.39. The red stars show the time when the shut-in periods finished. For the case of 1,000µl/hr, there is a horizontal stage on the curve indicating a long shut-in period. There were 5 shut-in periods before water breakthrough for the case of viscosity ratio 95.3; and there were 8 short shut-in periods for 561.1 before water breakthrough. These periods are not clear on the curves as they were just a few minutes long. In the case of 1,000µl/hr, significant oil production occurred right after the point of re-injecting. For 2 other cases, the incremental recoveries after red stars were insignificant as the shut-in periods were very short.

The dashed line in Figure 4.39 is the prediction of recovery factor without shut-in periods for the case of 1,000µl/hr. The generation of this dashed line was based on the assumption that the decline curve at the post-breakthrough stage was exponential. If the prediction value was accurate, the incremental recovery factor due to shut-in should be 0.11. This indicates that the shut-in periods could significantly benefit oil recovery. This is the evidence of capillary re-distribution of fluids in this water-wet micromodel. Short

shut-in periods do not provide enough time for any significant re-distribution to occur. Thus, the benefits of capillary-driven fluids re-distribution will only be seen for fields that are shut in for extended periods of time.

Note that Figure 4.39 also compares different fluid viscosities; further studies are needed in order to determine if these same increments can be expected for higher viscosity oils. Intuitively, one would expect to see less of an impact from this re-distribution as oil viscosity increases. However, the fact that it happens in the absence of flow relates back to the influence of capillary forces at low flow rates: when injection rates are low enough to allow for capillary imbibition to be significant, this should lead to improvements in producing water cuts.

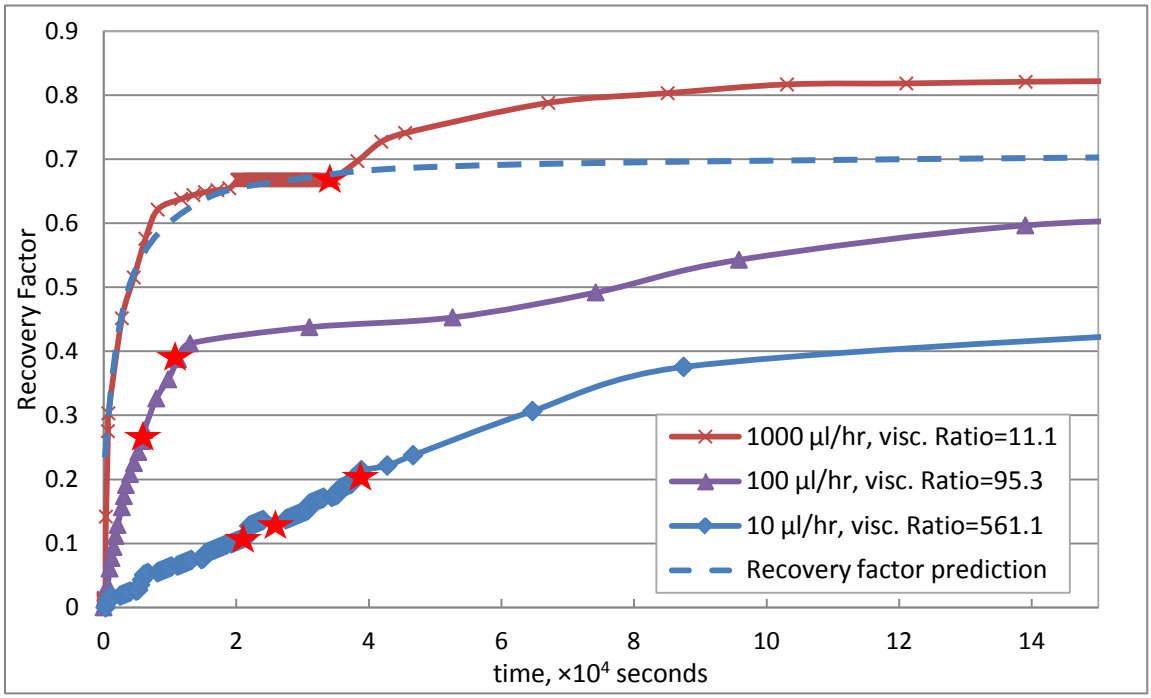

Figure 4.39: Production responses of shut-in period

4.4.3 Switching to Low Rate

The results shown in Figure 4.40 plotted as oil production responses of three cases which experienced injection rate reductions. For this figure, the oil viscosity is 10.0mPa.s. The red stars show the points of switching to the low rate of 10µl/hr.

For the case of 1,000-10µl/hr, the switching to low injection rate occurred right after the end of shut-in period. The recovery factor increased suddenly from the red star, as the injection rate was decreased by a factor of 100 and the impact of capillary forces now became much more evident. There was only one increasing stage. For the cases of 100-10µl/hr and 500-10µl/hr, there was more than one plateau on each curve, which meant there was more than one recovery factor increasing stage for each case. There was a delay between the point of rate reduction and the point of recovery factor increasing, especially for the case of 500-10µl/hr. That meant that time was needed for the system to respond to switching to low rate.

Compared with Figure 4.39, the production response in the situation of switching to low rate implies the same trend as that of shut-in periods. Essentially dropping rate allows time for capillary re-distribution of fluids to occur and this shows up as improved oil recovery.

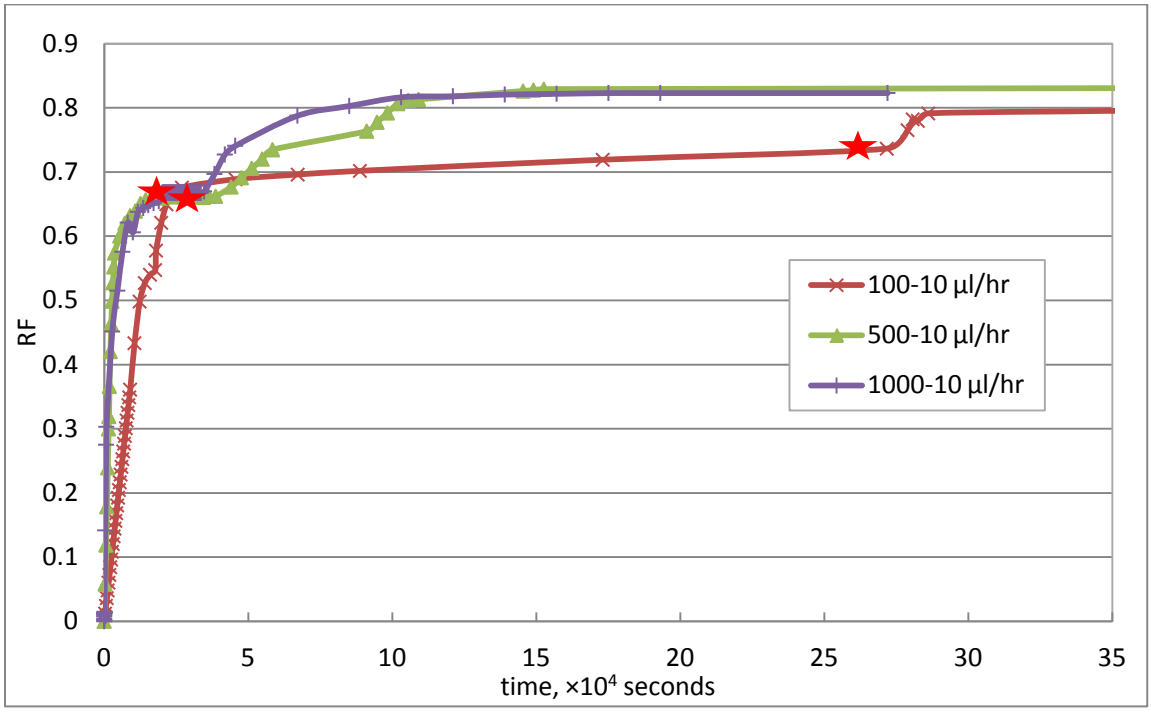

Figure 4.40: Production responses after switching to low injection rate

4.4.4 Summary of Effect of Water Injection Rate

The water injection rate was set at four levels: 10µl/hr, 100µl/hr, 500µl/hr and 1,000µl/hr. The first two levels are considered as low rates, and the last two levels are considered as high rates. In all cases, the flows were in the regime of capillary flow even at the highest water rate. In some cases, the water injection rates were constant. In other cases, shut-in or injection rate reduction was implemented.

High injection rate resulted in fast oil recovery in terms of actual time. However, large PVs of injected water were required to get a given final recovery factor after breakthrough. Especially in the later stages, the waterflooding process performed like water circulation. Low injection rates resulted in relatively higher water efficiency. However, again long production times were required. Shut-in periods and switching to

low rates can significantly benefit oil recovery. The recovery factor increasing stages were observed after re-injecting or rate decreasing. There was no oil production during the shut-in period, and there was a long low oil production period after switching to low rate. All rate schemes had advantages and disadvantages. In order to acquire high recovery factor and better economics, the water rate should be optimized.

4.4.5 Water Rate Strategy

When designing an operation strategy, the final oil recovery and economic feasibility are two most important indicators. On the basis of previous results in this section 4.4, a water strategy of cyclic water injection rate for heavy oil waterflooding is recommended: try to get a high breakthrough recovery via low rate injection at initial phase; increase the injection rate to a high level but below the rock fracture limit; reduce injection rate gradually to a low level when water cut is beyond a level; increase and decrease water rate repeatedly; shut-in water injection well when water cut is very high. The reason of shutting in well or reducing injection rate is to offer time for water imbibition and fluids redistribution. This strategy could lead to high efficient water imbibition and high oil recovery.

4.5 Mechanisms of Water Imbibition

Pore scale visualization was used to visually study the occurrence of some oil recovery mechanisms. These pore level mechanisms included film thickening, snap-off, oil refilling and emulsification. Water fingering and water imbibition before water breakthrough were also observed. The direction of water imbibition after water

breakthrough varied with water injection rate. These mechanisms are illustrated in this section through a sequence of images.

4.5.1Water Fingering

Viscous fingering was first reported by Engelberts and Klinkenberg (Engelberts et al, 1951). It usually occurs when the viscosity of the displacing fluid is much less than that of the displaced fluid. The initiation and growth of viscous fingers is believed to be caused by instabilities at the interface between the displacing and displaced fluids.

In a waterflooding where the viscosity of oil is much higher than that of water, the displacement front is not even. The displacement front is not stable as the displacing water will tend to finger through the displaced oil. Figure 2.1 shows a schematic of viscous fingering.

Perkins and Johnston (Perkins et at., 1969) reported that many viscous fingers formed at the condition of unfavourable viscosity ratio and high injection rate. They also reported that the growth of fingers depended on the severity of the unstable flood front. The severity is controlled by many factors such as mobility ratio, injection velocity and rock wettability. Instability number was proposed by Peters and Flock (Peters et al., 1981). This number defines the condition under which a frontal perturbation will grow and become a viscous finger. More analysis and discussion about instability number is presented in Chapter Five.

Willhite (1986) pointed out that capillary forces may oppose the development of fingers and may dampen fingers' propagation in strongly water-wet rocks.

Figure 4.41 shows the distribution of oil and water at breakthrough. For this figure, the oil viscosity is 85.8mPa.s, and water injection rate is 10µl/hr. The red zone is occupied by oil; the blue zone is the water zone. The viscous fingers initially formed at the entrance of the micromodel. As water was injected, the fingers deteriorated into a zone of graded saturation. The area in blue shadow is an illustration showing the water path. Due to water fingering, water broke through the micromodel quickly, leaving a large un-swept area. Especially in the situation of high injection rate and high viscosity ratio, water fingering would be much more severe. Compared to light oil waterflooding, the breakthrough recovery of heavy oil is low. Water has moved through the paths of least resistance, leaving a relatively high S_{or} even in the swept zone. The large bypassed area is the main target for later water imbibition.

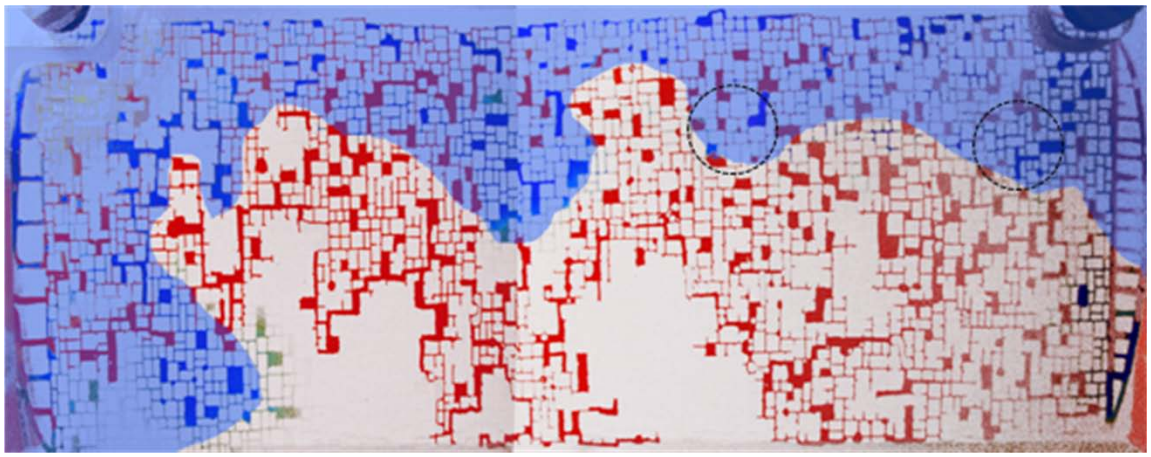

*In this figure, the micromodel was first saturated with colourless distilled water. The water which was used for displacing oil was dyed blue. The green area ahead of water front was where dye diffused. The inlet is located at left side.

Figure 4.41: Schematic of water fingering (A8-10)

In the figure, the area in the two dashed line circles is not on the water pathway. In the left circle, the water film thickening and snap-off can be observed. In the right circle, a cluster of small pores which is surrounded by large pores were invaded by water. Thereafter, water was imbibed into these two circles by capillary forces. The direction of the water imbibition was backward. This kind of imbibition was counter-current imbibition. From this point of view, capillary forces can keep viscous fingers from growing.

4.5.2 Direction of Water Imbibition after Water Breakthrough

Right after water breakthrough, the differential pressure between the injection port and production port decreased significantly. Thereafter, the viscous forces would instantaneously be weakened and might be no longer dominant driving forces. However, water would continue imbibing into the oil zone under the effect of capillary forces. The direction of water imbibition after water breakthrough for low injection rate was different to that for high injection rate.

4.5.2.1 Low Water Injection Rate

Figure 4.42 shows the distribution of water and oil at different time. This case is the same case as illustrated in Figure 4.41. The top picture shows the whole view of the micromodel at the time of breakthrough. The lower left picture shows the enlargement of the part in the dashed rectangular. The lower right picture shows the water front location after 24.9 hours (compared with the lower left picture). The water channel has moved from the left side of the rectangle to the center of the zone, of interest, and then water

moves to the top of the model and finds a path along the top row of pores. In the dominance of viscous forces water would then continue along these same pathways, perhaps stripping oil along the water channels. In this figure, water is observed to have also moved away from the formed low resistance pathways and has accessed some of the other regions of the model, which previously did not consist of continuous water pathways. This is evidence of water moving transversely to the channels, most likely due to capillary imbibition.

As shown in the circle of lower right picture, the water front moved downward. Simultaneously, a large pore at the upper right of the circle was invaded by water. According to these observations, the direction of water imbibition right after water breakthrough was perpendicular and parallel to the water channels. This sidewise imbibition can improve aerial sweep efficiency.

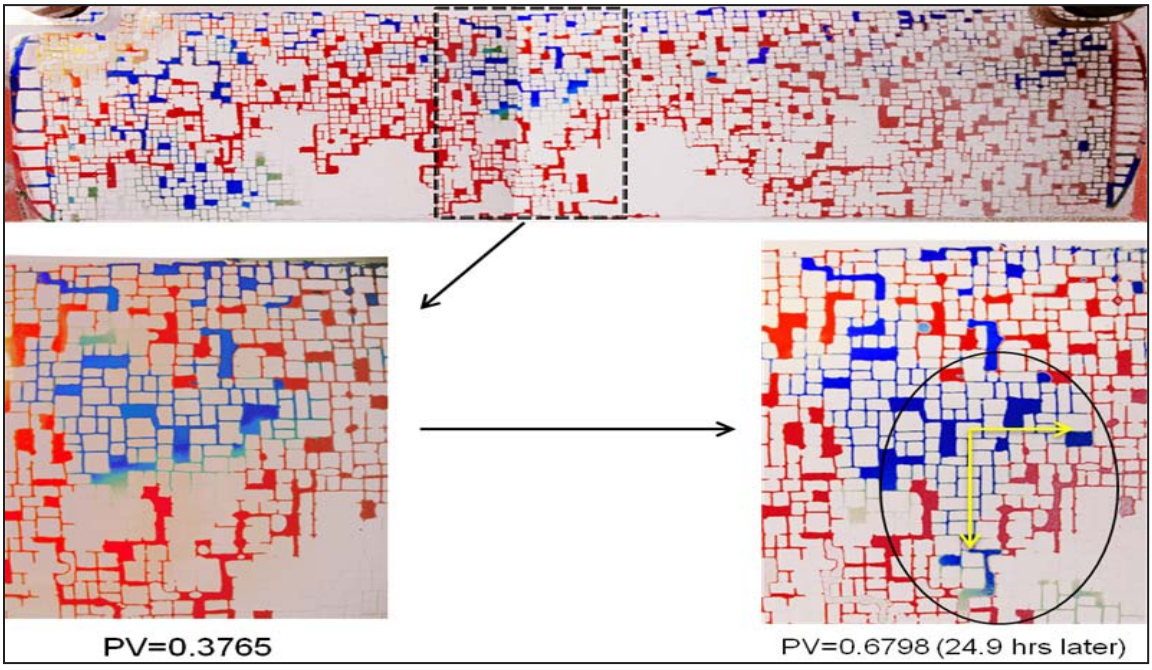

Figure 4.42: Direction of imbibition after water breakthrough for A8-10

4.5.2.2 High Water Injection Rate

Figure 4.43 shows the distribution of water and oil for the case of A5-500. The water injection rate is 500μl/hr, and the viscosity ratio is 11.1. The picture at top is the whole view of the micromodel at the time of water breakthrough. The middle and lower pictures show the enlargements of the area in yellow dashed line and in red solid-line circles separately. The pictures at right side show the water front locations at S_{or}. In the figure, the water front moves mainly forward. At the bottom of the middle pictures, there is a large pore which was at the tip of one water finger at breakthrough. It is fully occupied by water in the left picture. However, in the right picture, it is only half occupied by water. Oil flowed into this pore from surrounding narrow pores. Water imbibed into these narrow pores and squeezed oil out of there. This is the process of oil refilling which is presented in section 4.5.3.3. According to above observations, at high water injection rate, the direction of water imbibition after water breakthrough is parallel or approximately parallel to the water pathway. Thereafter, co-current is the main manner imbibition in high injection rate waterflooding.

Actually, the direction of water imbibition was determined by the pore structure, water injection rate and local wettability. Essentially, there was no difference between co-current imbibition and counter-current imbibition.

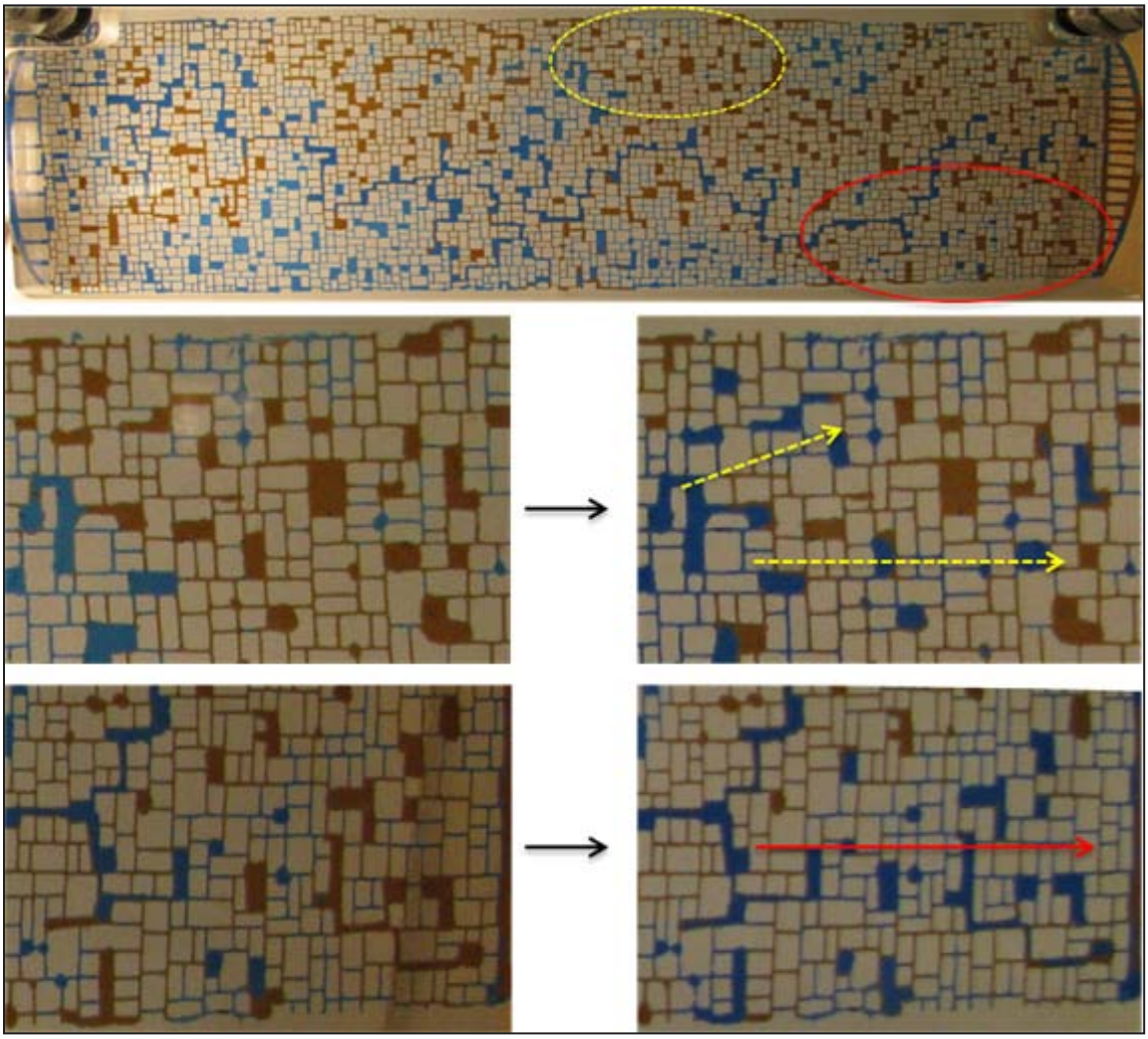

Figure 4.43: Direction of imbibition after water breakthrough for A5-500

4.5.3 Film Thickening, Snap-off and Oil Refilling

In Figure 4.44, there are a series of pictures, which are captured from the same part of the micromodel. The area in view is at right side of the rectangular in Figure 4.42. For this case, the water injection rate is 10µl/hr, and the viscosity ratio is 95.3. The upper left picture was captured slightly before water breakthrough. The lower right one was captured at residual oil saturation.

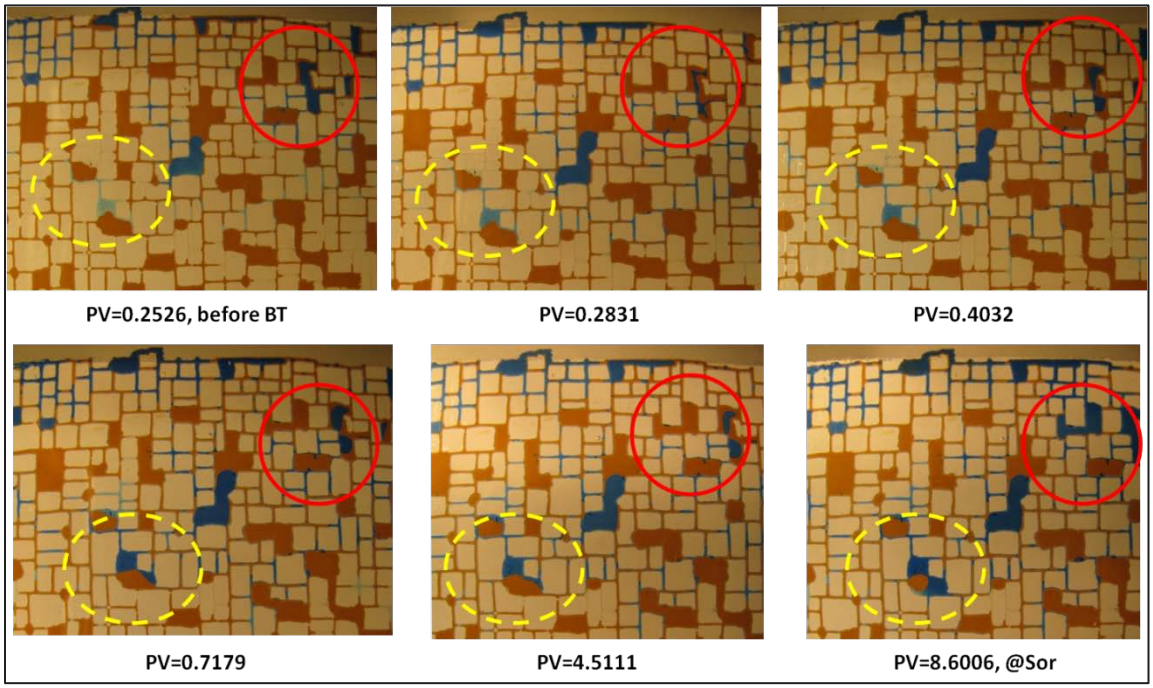

Figure 4.44: Schematic of film thickening, snap-off and oil refilling

4.5.3.1 Film Thickening

The type of films coating solid walls determines porous media wettability. And the thickness of films determines whether or not porous media can be altered from the initial state of wettability (Radke et al., 1992). In this thesis, the wettability of the micromodel was treated to water wet with a standard procedure. In all micromodel pictures, thin water films coating pore walls showed that micromodel was water wet.

In the yellow dashed line circle of interest, there is a large pore which is half filled by water in the upper left picture. This pore contained bypassed oil during the initial waterflood. In this pore, the water film close to wall was thickening as PV number was increasing. As the water film thickened, the oil saturation within this pore dropped. Especially in the lower right picture, this pore was almost completely occupied by water.

This is oil production through the thickening of water films. According to observation, water film thickening was mainly occurred in relatively large pores.

4.5.3.2 Snap-off

In Figure 4.44, there was a relatively large pore at the upper left of the yellow dashed-line circle. In that pore, the water flowed from a narrow pore throat, and into other narrow pore throats. However, the main part of the pore was by-passed. Only the water film coating the walls served as water path. At the bottom of the red solid-line circle, there was a large pore in where the occurrence of snap-off was also observed.

For these two pores where snap-off occurred, there was a same feature in common: the aspect ratio of pore body to pore throat was high. For the situation when pore body to pore throat aspect ratio was close to 1, the occurrence of snap-off was not observed.

4.5.3.3 Oil Refilling

In Figure 4.44, in the red solid-line circle, there was a large and long pore at the right side. This pore was on the water path. It was the key node that connecting injection port and production port at the time of water breakthrough. In the upper left picture, that pore was almost occupied by water. However, in the upper middle picture, after injecting 0.2831 PV water, oil flowed into that pore and the area where was occupied by oil expanded. In the upper right and lower left pictures, the oil area shrank. In the lower middle picture, the oil area increased again. And in the lower right picture, the oil area decreased again. Actually, in the last picture, the whole pore was almost occupied by water completely. The area of oil in that pore decreased and increased again and again,

this was the process of oil re-saturate or oil refilling. These experimental observations were in agreement with previous findings reported by Dong et al. (2005), who stated that oil refilling of water channels provided favourable conditions for waterflooding.

Water imbibition after water breakthrough was complex. Water channels were growing, developing and combining with time. The process cannot be simplified as a combination of two separated flows: oil flowed from oil zones into water channel and through the channel oil flowed into production port.

The mechanism of oil refilling appears to be important to oil recovery. After water breakthrough, the flow resistance through water channel was very low. Thereafter, the waterflooding tended to circulate water. Oil refilling can block water channel and increase flow resistance. Therefore, it can prevent water cut from steeply increasing and improve sweep efficiency.

In the literature, oil refilling was proposed as a result of the displacement of oil by gas injected (Dong et al., 2005). The re-saturating the water path with gas-in-oil foams was proposed by Vittoratos et al. (2006). In Vittoratos' research, the gas phase was from the solution gas when the pressure declined below the oil's bubble point. However, in this experimental study, no gas was injected. The effect of solution gas can be ignored as well. Therefore the mechanism of oil refilling in this research has nothing to do with gas phase. The oil which refilled water path was from the surrounding small pores into where

water has imbibed. This process was controlled by capillary forces. Water and oil moved in opposite directions. Thus, it performed like counter-current imbibition.

More analysis about the correlation between oil refilling and differential pressure variance is presented in section 4.6.

4.5.4 Viscous Instability vs. Imbibition

Figure 4.45 shows the penetration of water into oil area and migration of oil filaments. In this case, the injection rate was 1,000µl/hr, and viscosity ratio was 11.1. Picture #1-#4 shows the fluid distributions for PV# is equal to 0, 0.2906, 0.3416, and 1.8478 separately.

In the figure, the displacement front is very unstable. There were three factors led to unstable front: capillary forces, adverse mobility condition and high injection rate. As water only penetrated relatively large pores where both resistance force and capillary forces were weak, viscous forces dominated the penetration process.

At the left bottom of each picture, there is a large pore. In the picture #2, water flows into the centre of that pore under the effect of viscous forces. In the picture #3, water almost occupies the full pore except the thin oil filaments coating the wall. The micromodel looks like oil wet. However, if the figure is magnified, it would reveal that there is a tiny thin water film between the wall and the oil filaments in that pore. Besides, the water-oil-solid contact angle is less than 90 degree in un-swept area. Therefore, the micromodel is water wet in fact. In the picture #4, the pore is completely occupied by water. What

forces drove the oil filaments out of that pore is an interesting question. The water flow rate in that pore was very low as that pore was not on the water pathway even though it connected with water pathway. The water flow rate was too slow to drag oil filaments out of the pore. So the forces cannot be viscous forces. The only possible mechanism is water imbibition under the control of capillary forces. In picture #3 and #4, water imbibes into the narrow pore throats connecting to that pore. The water film thickening and water film lubrication maybe the main mechanisms.

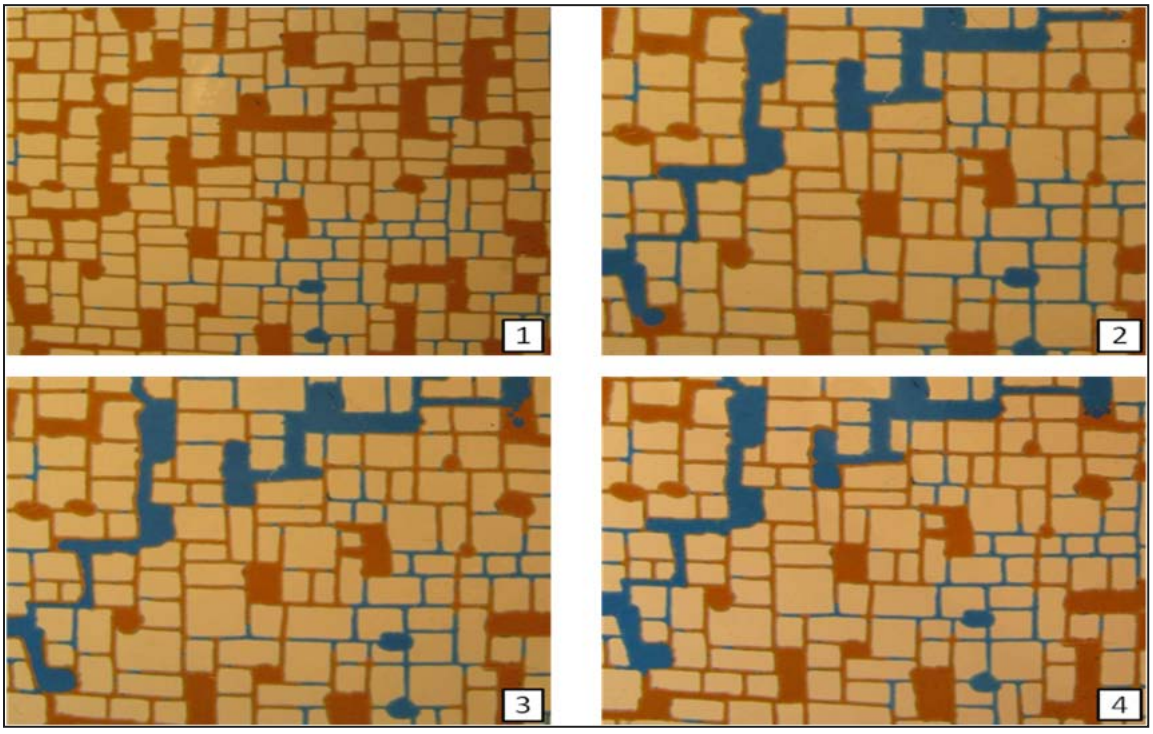

Figure 4.45: Schematic of viscous instability (A5-1000)

Above all, viscous instability usually occurred in large pores. Due to viscous instability, sweep efficiency was poor and significant area was by-passed. Water imbibition helped to improve sweep efficiencies of waterflooding and displace by-passed oil.

4.5.5 Emulsification

Figure 4.46 shows the existence of water-in-oil emulsions. Water-in-oil emulsions can also be observed in Figure 4.45 (in a large pore at top right corner of picture #3 and #4). The emulsions tended to accumulate in large pores, even though they existed in both large and small pores. Actually, in the experiments, emulsification occurred in every test. The emulsification was severe in some tests. The process of emulsification was complex. Further investigation is needed to figure out the mechanism of emulsification and its effect on waterflood performance.

Vittoratos (Vittoratos, et al., 2006 and 2010) has also observed the presence of emulsions in their Alaska heavy oil floods, and W/O emulsions were observed during NMR studies of produced fluids from heavy oil waterfloods (Mai, 2008). It is interesting that these emulsions form even in the absence of added surfactants. This is an indication of the unstable nature of this displacement, whereby water will force its way into the center of some large pores even during an imbibition process. Subsequently, oil films will encapsulate this water, and the emulsions remain stable due to the viscosity of the continuous oil phase. Figure 4.46 indicates schematically how these emulsions may lead to IOR during waterflooding. The emulsion is theoretically more viscous than the oil itself, and this can lead to blockage of some pores, and further re-distribution of fluids away from swept zones. However, this is currently only an observation. Emulsification and emulsion viscosity in porous media are entire separate avenues of research. It is currently not proven that these emulsions can aid in IOR.

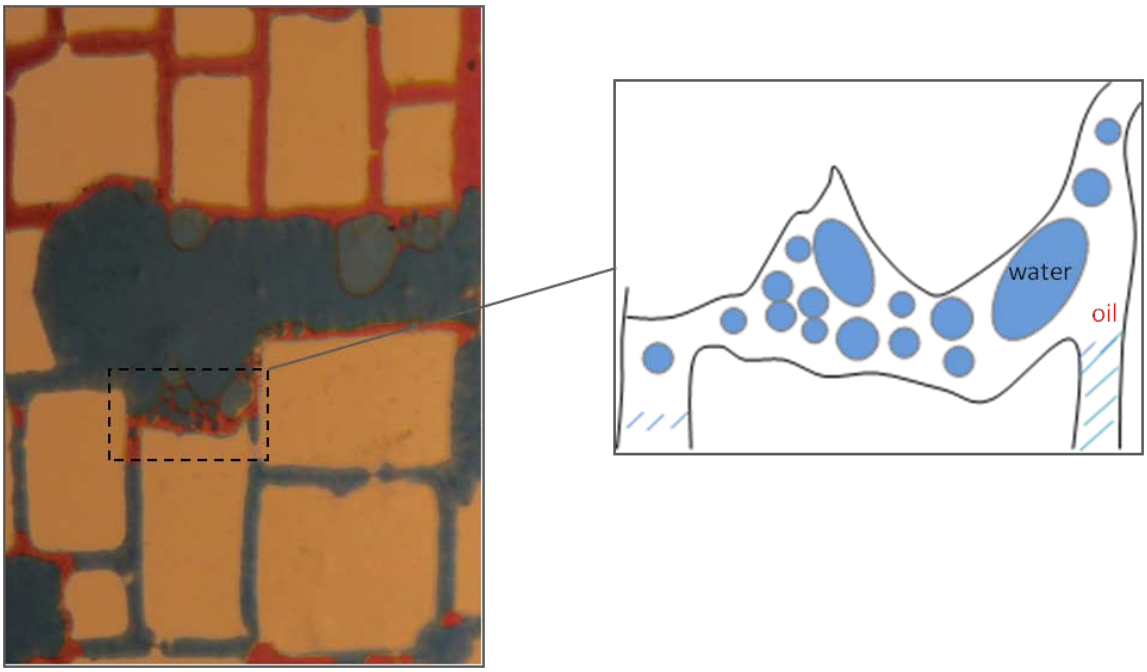

Figure 4.46: Water in oil emulsions (A8-10)

4.6 Differential Pressure Variance and Imbibition Mechanisms

In this chapter, Figure 4.4 and other six figures show the differential pressure responses of six different waterfloods. Appendix III illustrates the differential pressure analysis in detail. Table III.1 shows the average volume per drop is 0.048ml, and the average differential pressure variance is 0.065kPa. It must be noted that only water phase was used in water drop experiments in Appendix III. In fact, second phase (oil phase) should have influence on liquid drop volume, time interval of two drops and differential pressure variance. Considering the IOIP (initial oil in place) was only 0.5-0.8ml, there was only water production at most of the time after water breakthrough. Therefore, above results were eligible to be used as a reference.

According to above results, the average time per drop for the injection rate of 10μl/hr is 17280 seconds (~ 4.8 hrs). In Chapter 4, Figure 4.5 shows the differential pressure response of A5-10 during the period of $12\text{-}13\times10^5$ seconds. If it is assumed that only water drop at the outlet has influence on pressure variance, there should be only 5.8 drops for that period. However, there are 17 peaks on the curve in Figure 4.5. And the differential pressure variance is 0.2 ~ 0.5kPa which is much greater than 0.065kPa. Therefore, except liquid drop at the outlet, there should be other factors that lead to differential pressure variation.

Among the mechanisms discussed in this chapter, oil refilling and viscous instability can result in higher differential pressure. Other mechanisms' effect on differential pressure was not studied in this thesis.

Figure 4.47 and Figure 4.48 plot both oil production and differential pressure response on a same time scale. By making a comparison of differential pressure response with oil production, there was a good correlation between these two kinds of data. These peaks on the differential pressure curve can be approximately correlated with oil production. However, as oil propagation in the micromodel also resulted in pressure variation, these two kinds of data did not match very well.

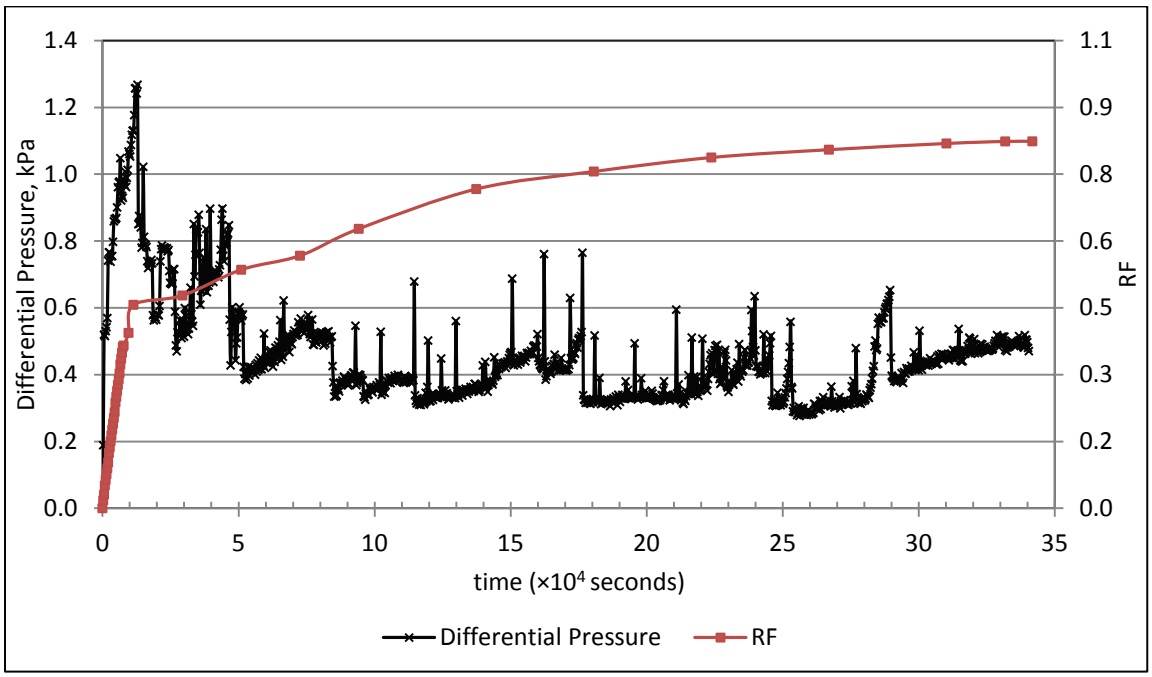

Figure 4.47: Comparison of oil production and differential pressure (A5-100)

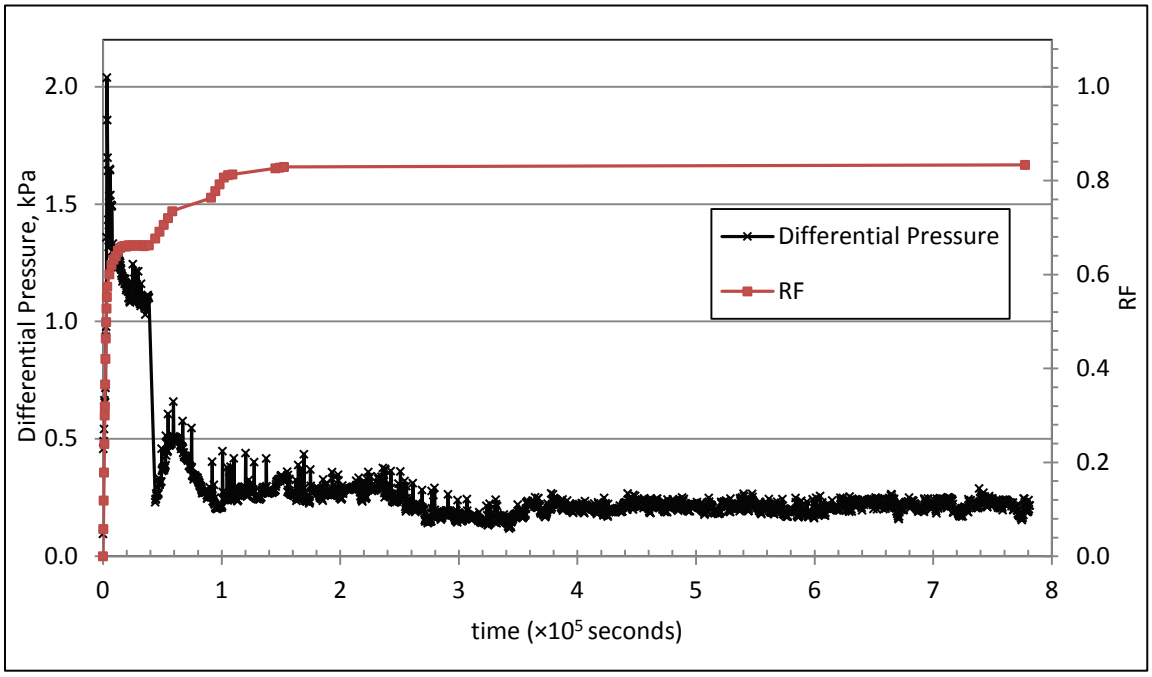

Figure 4.48: Comparison of oil production and differential pressure (A5-500)

For the case A5-500, water injection rate reduction happened at 44,048 seconds. A lot of peaks exist on the curve after water rate reduction. That means significant amount of oil was produced during the long slow water injection period.

4.7 Summary

This chapter presented the results of eight forced imbibition experiments and one spontaneous imbibition experiment. The production responses were presented individually. The differences among these experiments were compared and discussed. These differences include the fluid properties, operational parameters, recovery factors at the point of water breakthrough, final oil recovery and end point permeability measurements.

This chapter also discussed the effects of time, oil viscosity and water injection rate, on water imbibition. For the effects of water injection rate, three different water injection strategies, which were constant injection rate, with shut-in period and switching to low injection rate, were tested.

Numerous visual observations of heavy oil waterflooding performance through micromodel were presented in this chapter. The detailed descriptions of the mechanisms of water imbibition, which were extracted from photographs, were provided.

In large pores, viscous instability and imbibition can be easily distinguished. However, in small pores, it’s difficult to distinguish the effects of different kinds of imbibition

mechanisms. At pre-breakthrough stage, forced imbibition is the dominant mechanism as the differential pressure is usually much higher than that at post-breakthrough stage. Whereat post-breakthrough stage, the pressure variation indicated that not only spontaneous imbibition dominated the long low injection rate process, but also forced imbibition helped to improve imbibition efficiency. To evaluate the efficiency of imbibition, any contributions to improve areal sweep efficiency and microscopic displacement efficiency should be taken into consideration. In this research, water film thickening, snap-off and oil refilling were three important mechanisms that let water imbibition work. Among these three mechanisms, oil refilling was the most important one.

CHAPTER FIVE: FORCES BALANCE AND APPLICATION

In Chapter Four, it was demonstrated that water imbibition was enhanced at low water injection rates. Waterflooding before water breakthrough was considered to be dominated by viscous forces as differential pressure was high. After water breakthrough, the process was considered to be controlled by the combination of capillary forces and viscous forces. In this chapter, water injection rates were classified into a high and a low range. As discussed in Chapter Four, 10µl/hr and 100µl/hr are considered as low rates, 500µl/hr and 1000µl/hr are considered as high rates. The instability number and capillary number are discussed in this chapter, because they are two general parameters comparing the influences of viscous forces and capillary forces. The result of spontaneous imbibition experiment is used in this chapter.

5.1 Overview

The Instability Number is used to evaluate the stability of the displacement process. It is usually used to correlate the breakthrough recovery with parameters such as mobility ratio, displacement velocity, capillary forces, gravitational forces, rock permeability and wettability, system geometry and dimensions.

The Capillary Number is the ratio of viscous forces over capillary forces. It is usually used to correlate the breakthrough recovery and final recovery with parameters: displacement velocity, fluid viscosity, interfacial tension, rock wettability and so on.

The theories of instability number and capillary number are basically a balance of forces. The difference between instability number and capillary number lies in that the instability number has taken gravitational forces and system dimensions into consideration.

5.2 Instability Number

5.2.1 Instability Number Theory

Peters and Flock (Peters and Flock, 1981) defined the Instability Number (I_{sr}) as that shown in Equation 5.1, and used this number to evaluate the stability of waterflooding. In this equation, the effect of imbibition on the growth of viscous fingers is controlled by a wettability constant C^*.

$$I_{sr} = \frac{(M-1)v\mu_w D^2}{C^* \sigma K_{wor}} \qquad \text{Eqn (5.1)}$$

Where K_{wor} is permeability to water at the irreducible oil saturation S_{or}

C^* is wettability constant

v is the interstitial velocity (m/s)

D is diameter of the sandpack (m)

M is mobility ratio.

Bentsen (Bensten, 1985) derived a new version of the instability number for a rectangular system, and it was shown in Equation 5.2-5.4:

$$I_{sr} = \frac{\mu_w v(M-1-N_g)}{K_{wor}\sigma_e} \frac{M^{5/3}+1}{(M+1)(M^{1/3}+1)^2} \frac{4h^2b^2}{h^2+b^2} \qquad \text{Eqn (5.2)}$$

$$\sigma_e = \frac{1}{2} A_c \phi (1 - S_{wi} - S_{or}) \overline{r_m} \qquad \text{Eqn (5.3)}$$

$$N_g = \frac{(\rho_w - \rho_o) \cdot g \cdot \cos\alpha \cdot K_{wor}}{\mu_w v} \qquad \text{Eqn (5.4)}$$

Where N_g is the gravity number

σ_e is the effective or the pseudo-interfacial tension

b and *h* are dimensions of the rectangular model

A_c is the area under the capillary pressure curve

$\overline{r_m}$ is the average macroscopic mean radius

α is the dip angle; in a horizontal system, it's equal to zero, this results in a value of N_g=0

ρ_w is the density of water; ρ_o is the density of oil

g is the gravitational acceleration.

Compared to Equation 5.1, Equation 5.2 is much more complicated. It introduces the effective interfacial tension and gravity number into the correlation. Using effective tension instead of wettability number is more feasible. However, as lacking of enough data, only Equation 5.1 can be used in this research.

5.2.2 Instability Number vs. Breakthrough Recovery

In Equation 5.1 two parameters (wettability constant and diameter) were still not available from the experiments. The wettability constant C^* has different values for different rocks having different wettability, which determines the effect of water

imbibition on the growth of water fingers. However, as the same experimental procedure and micromodel were used, these two parameters could be ignored or just be assumed as constants. Considering the value of 306.25 was assigned for a water wet media by Peters (Peters and Flock, 1981), the wettability constant (dimensionless) was assigned a value of 300 in this thesis. The diameter was assigned a value of 0.02289m which was derived from cross-sectional area of the micromodel ($D = 2 \cdot \sqrt{\frac{Width \cdot Height}{\pi}}$). K_{ro} at S_{wi} was considered as 1.0 for every case. K_{rw} at S_{or} was gathered in every experiment. Based on above assumptions, instability number was calculated using the equation 5.1. The results were listed in Table 5.1.

Table 5.1: Summary of instability number

μ_o mPa.s	water rate µl/hr	v m/s	IFT mN/m	M	K_{wor} Darcy	I_{sr} dimensionless
10	10	7.77E-07	14.6	60.87	3.03	0.41
10	100	7.77E-06	14.6	55.56	3.32	3.44
10	100-10	7.77E-06	14.6	65.64	2.81	4.82
10	500	3.89E-05	14.6	53.62	3.44	16.02
10	1000	7.77E-05	14.6	58.93	3.13	38.76
85.8	10	7.77E-07	13.3	565.19	2.80	4.63
85.8	100	7.77E-06	13.3	525.76	3.01	40.08
505	10	7.77E-07	15.5	3568.75	2.61	26.96

Peters (Peters and Flock, 1981) found that immiscible displacement is stable when I_{sr} < 13.56; and it is "pseudo stable" when I_{sr} > 900; and it is in the transition zone when 13.56 < I_{sr} < 900. According to above conclusion and results, the case of A5-10, A5-100, A5-100-10 and A10-10 were in the stable range. The others were in the transition zone in where waterfloods were becoming increasingly unstable.

Figure 5.1 shows the relationship between breakthrough recovery and instability number. It can be seen that, as the instability number increases, the breakthrough recovery decreases. It is obvious that the breakthrough recovery is strongly related to instability number. The three points at upper left part are almost on a horizontal line, which means breakthrough recovery is independent of instability number in that zone. When instability number increases, the breakthrough recovery decreases continuously. By making a comparison between cases of same viscosity ratio but different injection rates, it can be found that breakthrough recovery decreased with increasing water velocity. Besides, for cases having same injection rate, breakthrough recovery also decreased with increasing mobility ratio.

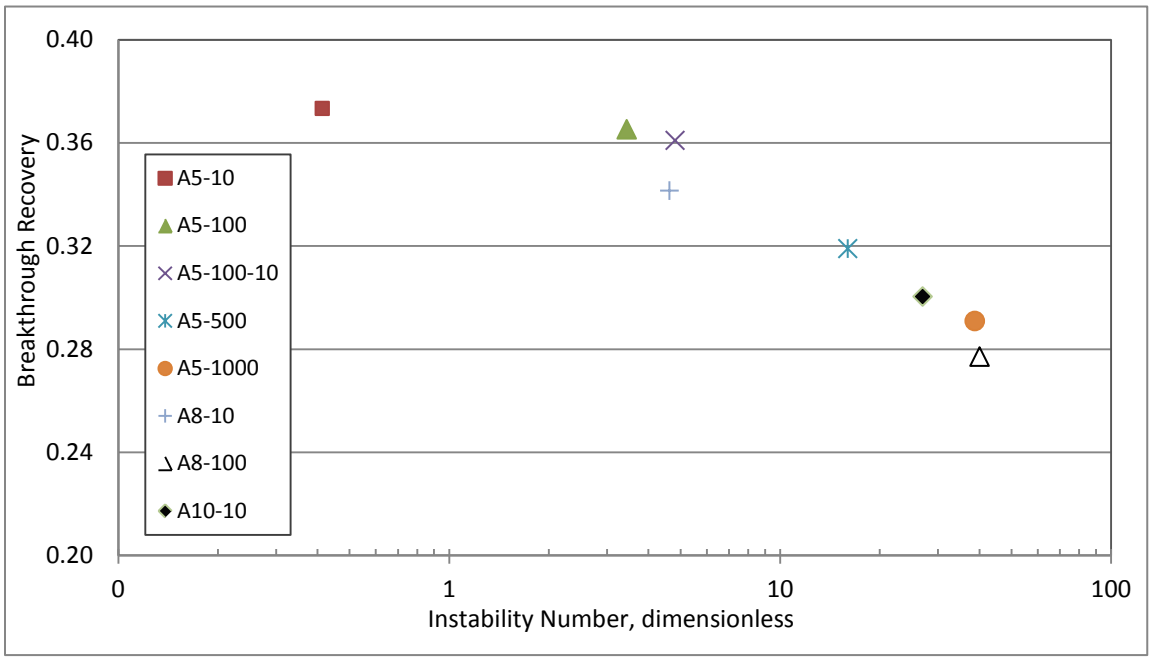

Figure 5.1: Breakthrough recoveries as a function of instability number

5.2.3 Instability Number vs. Final Recovery

Although instability number theory was only designed to predict the displacement performance until water breakthrough, it may also be eligible to predict the behaviour after water breakthrough.

Figure 5.2 plots the final recoveries as a function of instability number. Instability numbers were calculated using the same equation as that used in section 5.2.2. It can be seen that as the instability number increased, the final recovery decreased. This figure indicates that as flooding becomes more unstable, instability number does have influence on not only the breakthrough recovery, but also on the final recovery.

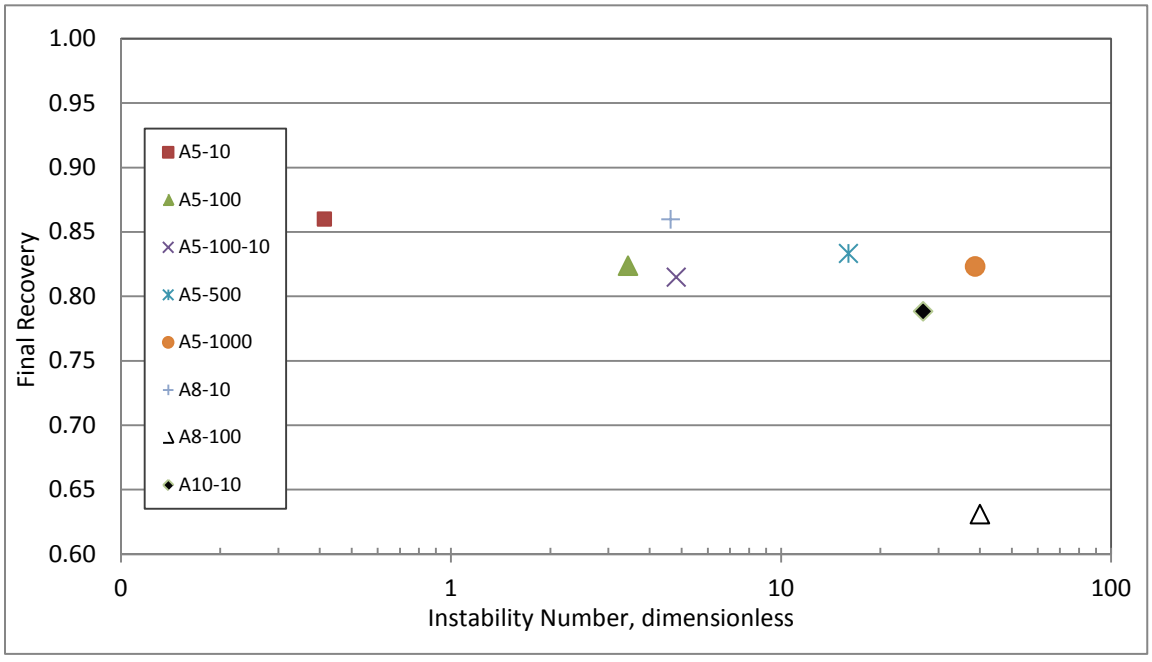

Figure 5.2: Final recoveries as a function of instability number

On semi-logarithmic scale, all points except the point A8-100 in Figure 5.2 exhibit a linear relationship between final recovery and instability number. The final recovery of

A8-100 was very low. That may resulted from the high instability number and absence of shut-in or injection rate reduction periods. It must be noted that the R-squared value of the rest seven points is only 0.41, that means the relationship is very weak. Therefore, the final recovery of heavy oil waterflooding is just roughly attributed to the instability number.

5.3 Capillary Number

5.3.1 Abrams' Capillary Number

5.3.1.1 Theory

Capillary Number, N_{ca}, which is proportional to the ratio of viscous forces over capillary force. It is a dimensionless number that describes the relative importance between viscous forces and capillary forces in an immiscible displacement. It is commonly defined as:

$$N_{ca} = \frac{\text{Viscous Force}}{\text{Capillary Force}} = \frac{v\mu_w}{\sigma_{ow}} \qquad \text{Eqn (5.5)}$$

Or

$$N_{ca} = \frac{v\mu_w}{\sigma_{ow}\cos\theta} \qquad \text{Eqn (5.6)}$$

Where, v is the interstitial velocity (m/s)

μ_w is the water viscosity (mPa.s)

σ_{ow} is interfacial tension (mN/m)

θ is the contact angle.

In the literature, there are more than ten forms of Capillary Number or displacement ratio correlating groups. However, all formats except Abrams (Abrams, 1975) ignored the possible difference between oil and water viscosity.

In conventional oil waterflooding, the breakthrough recovery increases as capillary number increases in the condition of water wet (Abrams, 1975). However, this conclusion does not apply to heavy oil waterflooding because of adverse mobility ratio. So, Abrams took the influence of the oil viscosity into account by introducing an extra viscosity term into previous capillary number:

$$N_{ca} = \frac{v\mu_w}{\sigma_{ow}\cos\theta}\left(\frac{\mu_w}{\mu_o}\right)^{0.4} \qquad \text{Eqn (5.7)}$$

The Equation 5.7 shows that, as the oil viscosity increases, capillary number will decrease apparently. Therefore, this will result in reduced breakthrough recovery. It must be noted that in Abrams' experiments, the oil viscosity only varied from 0.4mPa.s to 30.5mPa.s.

5.3.1.2 Application

An attempt was made to correlate incremental (post-breakthrough) oil recovery with above capillary number model. This was based on the assumption that, after water breakthrough, the process of low rate water injection was controlled by the combination of capillary forces and viscous forces, which are shown in the capillary number.

Figure 5.3 shows the capillary numbers calculated by using Abrams' correlation. The relationship between incremental recovery and capillary number is not monotonic. Mai (Mai, 2008) attributed this phenomenon to high oil viscosity, being outside the range of what was measured by Abrams. In Figure 5.3, it is only for the lowest oil viscosity (10.0mPa·s), which is within the range of viscosities tested by Abrams, that the expected relationship between recovery factor and N_{ca} is observed. For higher viscosity oils in Figure 5.3, as N_{ca} increases (higher rates) oil recovery actually decreases due to the adverse effects of water channeling. In these systems, improved recovery is seen only for low values of N_{ca}, indicating that capillary forces are helping to provide production of oil in these systems. Therefore, in heavy oil systems a capillary-number based approach to understanding recovery should focus on the benefits of capillary forces, rather than their trapping tendencies.

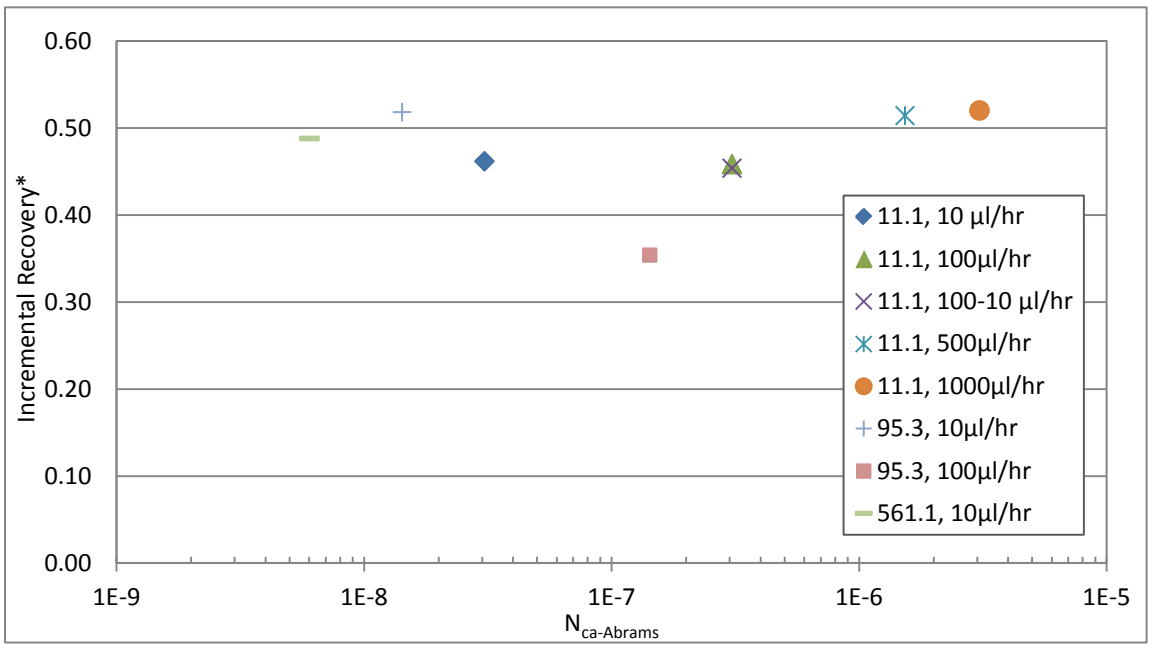

*Incremental recovery (ΔR) is equal to final recovery minus breakthrough recovery

Figure 5.3: Incremental recovery vs. $N_{ca\text{-}Abrams}$

5.3.2 Dong's Complete Capillary Number

5.3.2.1 Theory

Dong (Dong et al., 1998) presented a Complete Capillary Number (*CA*). In a waterflood, *CA* is equal to the ratio of water injection rate to the initial rate of free spontaneous imbibition:

$$CA = \frac{\upsilon}{\upsilon_{free-spo-im}} = \frac{q_t}{q_{free-spo-im}} \qquad \text{Eqn (5.8)}$$

Where, v is the Darcy velocity determined by water injection rate (m/s)

$v_{free\text{-}spo\text{-}im}$ is the initial Darcy velocity in free spontaneous imbibition (m/s)

q_t is the constant pumping rate (cm^3/s)

$q_{free\text{-}spo\text{-}im}$ is the initial displacement rate in the free spontaneous imbibition (cm^3/s).

According to Dong's conclusion: capillary forces control the waterflood process and the saturation profile is uniform if $CA<<1$; and viscous forces control the waterflood process and there is a step on the saturation profile if $CA>>1$. It must be noted that, in order to determine the value of *CA* in a waterflood, two experiments have to be carried out at the same experimental conditions. Otherwise, the comparison rule between two experiments is changed (Dong et al., 1997 and 1998).

5.3.2.2 Application

The initial displacement rate in free spontaneous imbibition ($q_{free\text{-}spo\text{-}im}$) was derived from oil production curve of the spontaneous imbibition experiment. In Figure 5.4, there is a step at the initial part of oil production curve. In fact, oil production during this period

was not due to water spontaneous imbibition. As mentioned in previous chapters, a tiny differential pressure was imposed at the inlet of the micromodel at early stage. Meanwhile, the residual oil in the connecting space (dead volume) was entering the micromodel. Therefore, the differential pressure and residual oil resulted in a short oil drainage period. Above all, spontaneous water imbibition began after the early short drainage period.

On the curve, there is a dramatically increasing period which is overlapped with the red straight line. That period is the first part of spontaneous imbibition. The line whose slope is 0.0154 in Figure 5.4 shows the beginning of free spontaneous imbibition. Based on the slope, initial oil saturation, properties of the micromodel and $q_{free\text{-}spo\text{-}im}$ were calculated.

The Complete Capillary Number (*CA*) was calculated using Equation 5.8. The results were listed in Table 5.2. As only oil sample with viscosity of 10.0mPa.s was used in the free spontaneous imbibition experiment, experiments testing oil of different viscosities (i.e. except A5) were unable to acquire Complete Capillary Numbers.

Table 5.2: Results of *CA* calculation

Viscosity Ratio	Injection Rate	Free Spon.-Imbi. Rate	*CA*
/	µl/hr	µl/hr	dimensionless
11.1	10	0.366	27.3244
	100		273.244
	500		1366.22
	1000		2732.44
95.3	10	/	/
	100	/	/
561.1	10	/	/

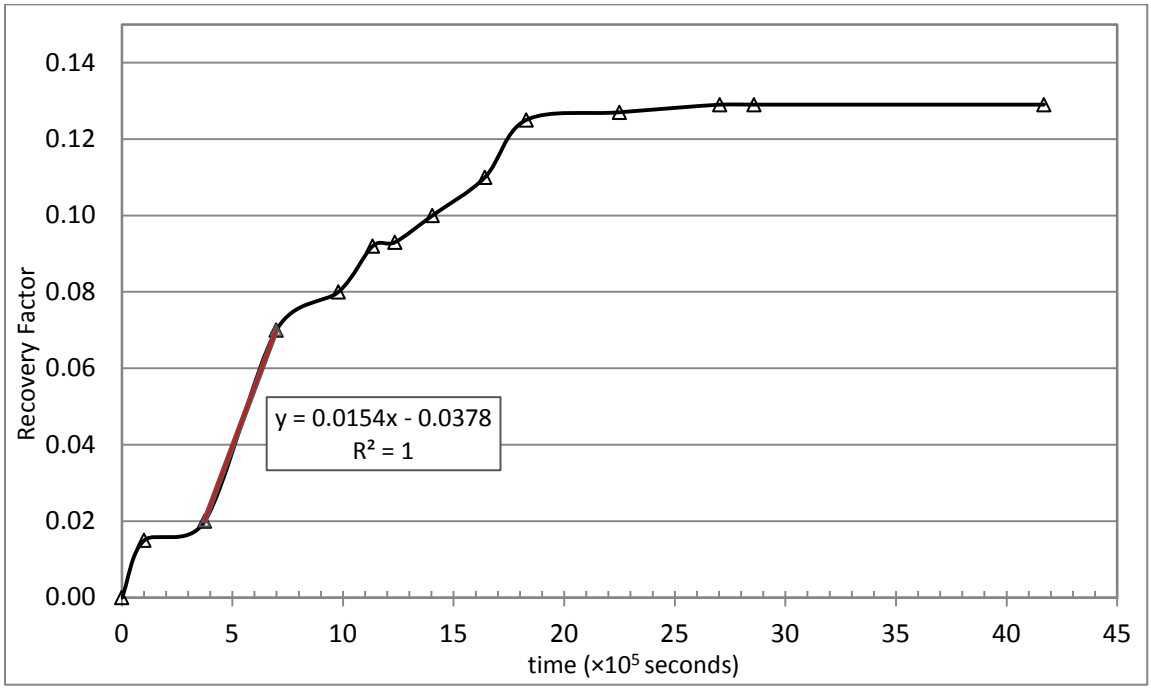

Figure 5.4: Recovery vs. time for spontaneous imbibition

The figures of oil saturation profiles were presented in Chapter Four. By comparing these figures, it can be observed that the oil saturation of A5-10 decreased relatively uniformly along the entire length of the micromodel. It also can be found that there were steps on oil saturation profiles of A5-500 and A5-1000. However, for A5-100, the oil saturation profiles were not uniform, but no obvious step as well.

According to above observation, these conclusions can be drawn: For $CA \leq 27.3$, capillary forces control. For $CA \geqslant 1300$, viscous forces control. For $27.3 < CA < 1300$, there is a transition zone in this scope.

As mentioned above, the boundary value of *CA* is 1.0 in Dong's research. However, in this experimental study, the boundary value should be around 273 if it exists. The

difference of the boundary values may result from the experimental material. In Dong's study, sand packs were used. They were more complex and representative compared to the micromodel.

CHAPTER SIX: CONCLUSIONS AND RECOMMENDATIONS

In this thesis, the important hypothesis was that capillary forces are significant in heavy oil water system, and the incremental recovery after water breakthrough is mainly due to displacement from water imbibition. The visual etched glasses micromodel was used in experimental study. The mechanisms during water imbibition were observed and analyzed. However, it is not possible to quantify the contribution of every mechanism on oil production. The effects of time, oil viscosity and water injection rate on water imbibition were studied. Finally, the instability number and capillary number were used to correlate with oil production and oil saturation profile.

Well, this research still had some limitations, such as the small 2D micromodel cannot represent sand rock perfectly, and the operation pressure is low. In order to improve the understanding of heavy oil waterflooding process, further study is needed. Some recommendations for future study are also given in this chapter.

6.1 Conclusions

The main conclusions reached in this study are listed below:

- After water breakthrough, the recovery factor is proportional to the square root of time.
- There is a definite relationship between oil viscosity and time required for water imbibition when recovery factor is below 0.7. Imbibition rate does vary with oil viscosity.

- The effects of injection rate on imbibition rate are complicated. At low injection rate, waterflooding becomes more efficient, and a significant amount of oil is produced discontinuously; therefore the recovery factor increases in a stepwise manner. Shut-in periods and switching to low injection rate can benefit oil production.
- In heavy oil waterflooding, water breaks through the micromodel quickly because of water fingering. After water breakthrough, capillary forces become significant, and water injection rate should be reduced to improve the waterflood efficiency.
- In the cases of low rate water injection, water imbibes into the original oil region perpendicularly to the water channel.
- Water film thickening, snap-off and oil refilling are the main mechanisms that let water imbibition work. Emulsions exist in every test; and in some tests emulsification is severe.
- The instability number theory was found to be a good method to predict breakthrough recovery for heavy oil waterflooding.
- When predicting oil recovery as a function of the ratio of viscous forces over capillary forces, it is evident that different trends are presented for oils of varying viscosity. For relatively low mobility ratio systems, the traditional capillary number based approach seems to work as a means for understanding how to enhance production of oil. As the viscosity ratio becomes more adverse, capillary forces actually assist in recovery of oil, and recovery becomes inversely related to the capillary number.

6.2 Recommendations

The main recommendations made for future study are listed as below:

- The balance that must be achieved in a heavy oil waterflooding process is that of high ultimate recovery of oil at low rates vs. fast production of oil at higher rates. Capillary driven mechanisms such as film thickening and oil re-filling are relatively slow processes, so the influence of the *in-situ* emulsions should also be studied. The key to successful oil production after water breakthrough is to mobilize the significant fraction of bypassed oil that is still continuous at the point of water breakthrough. This could be done through some combination of emulsification and imbibition of water, and other strategies to improve mobility ratio (e.g. polymer flooding) can also be attempted in future studies, so long as they do not negate the positive impact of these capillary forces.
- In order to test the oil samples with higher viscosity at higher injection rate and higher pressure, new micromodels that can bear higher pressure should be used.

REFERENCES

- Abrams, A., “The Influence of Fluid Viscosity, Interfacial Tension, and Flow Velocity on Residual Oil Saturation Left by Waterflood”, SPE Journal, 15(5), October 1975, p.437-447.
- Adams, D.M., “Experiences with Waterflooding Lloydminster Heavy-Oil Reservoirs”, Journal of Petroleum Technology, 34(8), August 1982, p.1643-1650.
- Alikhan, A.A. and Farouq-Ali, S.M., “Current Status of Nonthermal Heavy Oil Recovery”, presented at the Rocky Mountain Regional Meeting, Salt Lake City, May 23-25, 1983.
- Anderson, W. G., “Wettability Literature Survey- Part 2: Wettability Measurement”, Journal of Petroleum Technology, November 1986, p.1246 - 1262.
- Aronofsky, J.S., Masse, L. and Natanson, S.G., “A Model for the Mechanism of Oil Recovery from the Porous Matrix Due to Water Invasion in Fractured Reservoirs”, Trans. AIME, 213, 1958, p.17 - 19.
- Bennion, D.B., Chan, M.Y.S., Sarioglu, G. and Courtnage, D., “The In-Situ Formation of Bitumen-Water-Stable Emulsions in Porous Media during Thermal Stimulation” SPE 25802, 1993.
- Bentsen, R.G., “A New Approach to Instability Theory in Porous Media”, SPE Journal, October 1985, p.765 - 779.
- Blair, P.M., “Calculation of Oil Displacement by Counter-current Water Imbibition”, SPE Journal, 4 (3), September 1964, p.195 - 202.
- Brice, B. W. and Renouf, G., “Increasing Oil Recovery from Heavy Oil Waterfloods”, SPE 117327, 2008.

- Buckley, S.E and Leverett, M.C., “Mechanisms of Fluid Displacement in Sands”, Trans. AIME, 146, 1942, p.107 - 116.
- Chen, T., Chakraberty, T., Cullen, M.P., Thomas, R.A. and Sleben, M.C., “Laboratory and Field Evidence of Emulsion Flow in Porous Media”, CIM/AOSTRA 1991 Technical Conference in Banff, April 21-24, 1991.
- Chen, T., Yuan, J.Y., Serres, A.J. and Rancier, D.G., “Emulsification of Water into Bitumen in Co-injection Experiments”, Journal of Canadian Petroleum Technology, Special Edition, 1999, 38(13), p.1 - 6.
- Dong, M. and Dullien, F.A.L., “A New Model for Immiscible Displacement in Porous Media”, Transport in Porous Media, p.185-204, 1997.
- Dong, M, Dullien, F.A.L. and Zhou, J., “Characterization of Waterflood Saturation Profile Histories by the 'Complete' Capillary Number”, Transport in Porous Media, 31(2), p.213-237, May 1998.
- Dong, M., Foraie, J., Huang, S. and Chatzis, I., “Analysis of Immiscible Water-Alternating-Gas (WAG) Injection Using Micromodel Tests”, Journal of Canadian Petroleum Technology, 44(2), February 2005, p.17 - 25.
- Dullien, F.A.L., “Porous Media Fluid Transport and Pore Structure”, Academic Press Inc., New York, USA, 1979.
- Engelberts, W.F. and Klinkenberg, L.J., “Laboratory Experiments on the Displacement of Oil by Water from Packs of Granular Material”, 3rd World Petroleum Congress, May 28 - June 6, 1951.
- ERCB (Energy Resources Conservation Board, Alberta, Canada), Alberta’s Energy Reserves 2009 and Supply/Demand Outlook 2010-2019, 2010.
- Farouq-Ali, S.M., “Non-Thermal Heavy oil Recovery Methods”, SPE 5893, 1976.

- Farouq-Ali, S.M. and Islam, M.R., "Numerical Simulation of Emulsion Flow through Porous Media", the 40th Annual CIM Pet. Banff, Canada, 1989.
- Farouq-Ali, S.M. and S. Thomas, "Enhanced Oil Recovery – What We Have Learned", Journal of Canadian Petroleum Technology, 39(2), February 2000, p.7 - 11.
- Fischer, H. and Morrow, N.R., "Spontaneous Imbibition with Matched Liquid Viscosities", SPE 96812, 2005.
- Fischer, H., Wo, S. and Morrow, N.R., "Modeling the Effect of Viscosity Ratio on Spontaneous Imbibition", SPE 102641, 2006.
- Fischer, H., Wo, S. and Morrow, N.R., "Modeling the Effect of Viscosity Ratio on Spontaneous Imbibition" SPE Reservoir Evaluation & Engineering, June 2008, p.577 - 589.
- Graham, J.W. and Richardson, J.G., "Theory and Applications of Imbibition Phenomena in Recovery of Oil", Journal of Petroleum Technology, 11 (2), February 1959, p.65 - 69.
- Hamon, G. and Vidal, J.V., "Scaling-Up the Capillary Imbibition Process From Laboratory Experiments on Homogeneous and Heterogeneous Samples", SPE 15852, 1986.
- Iffly, R., Rousselet, D.C. and Vermeulen, J.L., "Fundamental Study of Imbibition in Fissured Oil Fields", SPE 4102, 1972.
- Kazemi, H., Gilman, J.R. and Elsharkawy, A.M., "Analytical and Numerical Solution of Oil Recovery from Fractured Reservoirs with Empirical Transfer Functions", SPE Reservoir Engineering, May 1992, p.219 - 227.
- Li, K. and Horne, R.N., "An Analytical Scaling Method for Spontaneous Imbibition in Gas/Water/Rock Systems", SPE 88996, 2004.

- Li, K. and Horne, R.N., “Generalized Scaling Approach for Spontaneous Imbibition: An Analytical Model”, SPE Reservoir Evaluation & Engineering, June 2006, p.251 - 258.
- Ma, S., Morrow, N.R. and Zhang, X., “Generalized scaling of spontaneous imbibition data for strongly water-wet systems”, Journal of Petroleum Science and Engineering, 18, 1997, p.165 - 178.
- Mai, A., “Mechanisms of Heavy Oil Recovery by Waterflooding”, Ph.D. Dissertation, University of Calgary, April 2008.
- Mai, A. and Kantzas, A., “Mechanisms of Heavy Oil Recovery by Low Rate Waterflooding”, Journal of Canadian Petroleum Technology, 49(3), March 2010, p.44 - 50.
- Maini, B. B., “Foamy-Oil Flow”, SPE Distinguished Author Series, October 2001, p.54-64.
- Mattax, C.C. and Kyte, J.R., “Ever see waterflood?”, Oil and Gas Journal, 59, 1961, p.115 - 128.
- Mattax, C.C. and Kyte, J.R., “Imbibition Oil Recovery from Fractured, Water-Drive Reservoir”, SPE Journal, 2 (2), June 1962, p.177 - 184.
- Miller, K.A., “Improving the State of the ART of Western Canadian Heavy Oil Waterflood Technology”, Journal of Canadian Petroleum Technology, 54 (4), April 2006, p.7 - 11.
- Nandez, I.A., “Production Mechanisms in Heavy Oil Waterflooding”, Master’s Dissertation, University of Calgary, September 2010.
- Perkins, T.K. and Johnston, O.C., “A Study of Immiscible Fingering in Linear Models”, SPE Journal, 9(1), March 1969, SPE 2230, p.39 - 46.

- Peters, E.J., and Flock, D.L., “The Onset of Instability During Two-Phase Immiscible Displacement in Porous Media”, SPE Journal, 21(2), April 1981, p.249-258.
- Pooladi-Darvish, M. and Firoozabadi, A., “Experiments and Modelling of Water Injection in Water-wet Fractured Porous Media”, Journal of Canadian Petroleum Technology, 39(3), March 2000, p.31 - 42.
- Radke, C.J., Kovscek, A.R. and Wong, H., “A Pore-Level Scenario for the Development of Mixed Wettability in Oil Reservoirs”, 1992, SPE 24880.
- Rapoport, L.A., “Scaling Laws for Use in Design and Operation of Water-Oil Flow Models”, Trans., AIME (1955) Vol. 201, p.143 - 150.
- Romero-Zeron, L. B., “The Role of Porous Media Wettability on Foamed Gel Propagation and Fluid Diverting Performance”, Ph.D. Dissertation, University of Calgary, October 2004.
- Singhal, A.K., “Improving Water Flood Performance by Varying Injection-Production Rates”, Canadian International Petroleum Conference (CIPC) paper 2009-126, June, 2009.
- Smith, G.E., "Fluid Flow and Sand Production in Heavy-Oil Reservoirs Under Solution-Gas Drive", SPE 15094, 1988.
- Smith, G.E., "Waterflooding Heavy Oils", SPE 24367, 1992, p.18-21.
- Sohrabi, M., Tehrani, D.H., Danesh, A. and Henderson, G.D., “Visualization of Oil Recovery by Water-Alternating-Gas Injection Using High-Pressure Micromodels”, SPE 89000, 2004.
- Tremblay, B., Sedgwick, G. and Forshner, K., “Simulation of Cold Production in Heavy-Oil Reservoirs: Wormhole Dynamics”, SPE 35387, 1997.

- Vittoratos, E.S., “Interpretation of Production Data from Cyclic Steam Stimulation at Cold Lake”, SPE 20527, 1990.
- Vittoratos, E.S., Brice, B.W., West, C.C., Digert, S.A. and Chambers, B.C., “Optimal Heavy Oil Waterflooding: Are the Light Oil Paradigms Applicable?”, 1st World Heavy Oil Conference, Beijing, China, 2006.
- Vittoratos, E.S. and West, C.C., “Optimal Heavy Oil Waterflood Management May Differ From that of Light Oils”, SPE 129545, 2010.
- Wang, R., “Gas Recovery from Porous Media by Spontaneous Imbibition of Liquid”, Master’s Dissertation, University of Wyoming, UMI: EP20660, December 1999.
- Willhite, G.Paul, “Waterflooding”, 1st edition, Society of Petroleum Engineers, Richardson, TX, 1986
- Xie, X. and Morrow, N.R., “Oil Recovery By Spontaneous Imbibition From Weakly Water-wet Rocks”, Petrophysics, 42(4), July-August 2001, p.312 - 322.
- Yuster, S.T. “Theoretical Consideration of Multiphase Flow in Idealized Capillary Systems”, Proceedings of 3rd World Petroleum Congress, 1951, p.437 - 445.
- Zhang, X., Morrow, N.R. and Ma, S., “Experimental Verification of a Modified Scaling Group for Spontaneous Imbibition”, SPE Reservoir Engineering, 11(4), November 1996, p.280 - 285.

APPENDIX I: FLUID PROPERTIES

Density

A density meter which was manufactured by Anton Paar was used for the measurements of both oil and water samples. The measurements were carried out at atmospheric pressure and room temperature of 23^{o}C. According to its manual, the precision of this density meter is $\pm 1\times10^{-4}$ g/cm^3 if the density measured is in the range of 0.5 to 1.5 g/cm^3. The results of density measurement were shown in Table 3.1 and Table 3.2.

Viscosity

For viscosity measurement, a Brookfield Viscometer was used to measure some oil samples which having large viscosities. For low viscous samples, such as brine and other oil samples having low viscosities, glass capillary viscometers were used. The measurements were also carried out at atmospheric pressure and room temperature of 23^{o}C. According to the manual, at the temperature of 20^{o}C, the precision of glass capillary viscometers is ±0.17%. The results of viscosity measurement were also shown in Table 3.1 and Table 3.2.

Contact Angle

Contact angles of oil-water-glass system were measured using drop geometry analysis method. The standard FTA200 equipped with a high resolution camera and a zoom microscope were used to capture the images of oil drops. A built-in computer software was used to acquire the image and conduct the shape analysis and calculation. For each fluid pair, at least 2 measurements were conducted. For the pairs of 1A (stands for water

sample #1 and oil sample #A), 1B and 1C, no contact angle was able to be measured as the oil sample #1 was transparent naphtha. The results of the measurement were shown in Table 3.4 and Figure 3.2.

Figure I.1 shows the images of the sample pair B6. The results of two measurements are consistent. However, the real contact angle should be less than 53^{o}, since the yellow lines don't depict the shapes of oil drops very well. Another main source of the error is from the treatment of the glasses used in the experiments. The glasses were only washed with soap solution and distilled water. However, the micromodel was treated with a complex procedure. Therefore this would result in the discrepancy of wettability conditions.

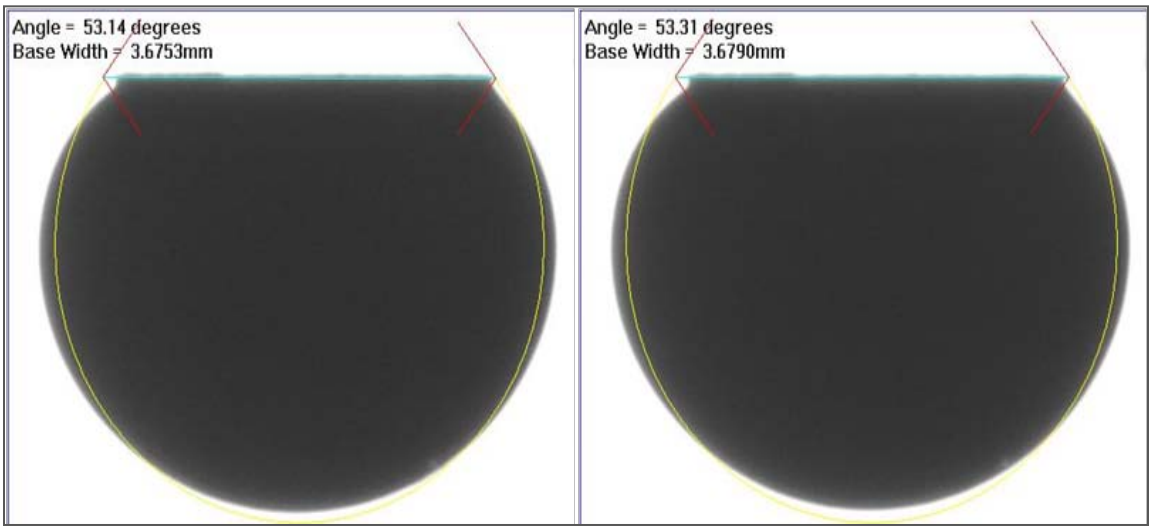

Figure I.1: Oil drop images for contact angle measurement

Interfacial Tension

Interfacial tensions were measured using the spinning drop method. A Kruss SITE04 Spinning Drop Interfacial Tensiometer was used. A small droplet of oil was injected

inside a horizontal tube filled with brine. Then the tube was rotated and the centrifugal force stretched the oil droplet. The degree of stretching was proportional to the interfacial forces between the oil sample and brine sample, and the interfacial tension was calculated using following equation:

$$\gamma = 3.427 * 10^{-7} * \Delta\rho (fd)^3 n_r^{\ 2} \qquad \text{Eqn (I.1)}$$

Where, γ = interfacial tension between oil and water (mN/m)

$\Delta\rho$= density difference (g/cm^3)

f= calibration factor (mm/scale)

d= drop diameter (scale)

n_r= rotation rate (rpm).

The interfacial tensions measured were in the range of 10.5mN/m to 15.7mN/m. The results were shown in Table 3.3 and Figure 3.1.

APPENDIX II: IMAGE ANALYSIS METHOD

This appendix illustrated the procedure of extracting oil or water saturations from the images captured during waterflooding. In order to verify the results of image analysis, saturations were also measured using mass balance method. A comparison between the results of two kinds of methods was made. At last, the possible source of error was discussed.

Saturation Calculation

There are two main steps to calculate oil or water saturation from one picture. The first step is to select the oil zone and water zone. The second step is to calculate the areas of oil zone and water zone. And then the saturation can be calculated based on area fraction.

The first step was conducted using the software: Photoshop. In Figure II.1, the red zone is occupied by oil, and the blue zone is occupied by water.

The second step was conducted using the software: ImageJ. In Figure II.2, only the oil zone was adjusted to black, the other part of the picture was adjusted to white. After colour adjustment, a process of making binary has been done; this process assigned a value “1” to the black pixel and “0” to white pixel. Then the areas of oil zone and water zone were calculated based on the number of pixel. The above procedure is listed as:

1) Colour adjustment: Image – Adjust - Threshold, adjust the RGB channels and set the ROI to white, set the background to black.

2) Binary making: Process - Binary - Make Binary.

3) Area measurement: Analyze - Analyze Particles.

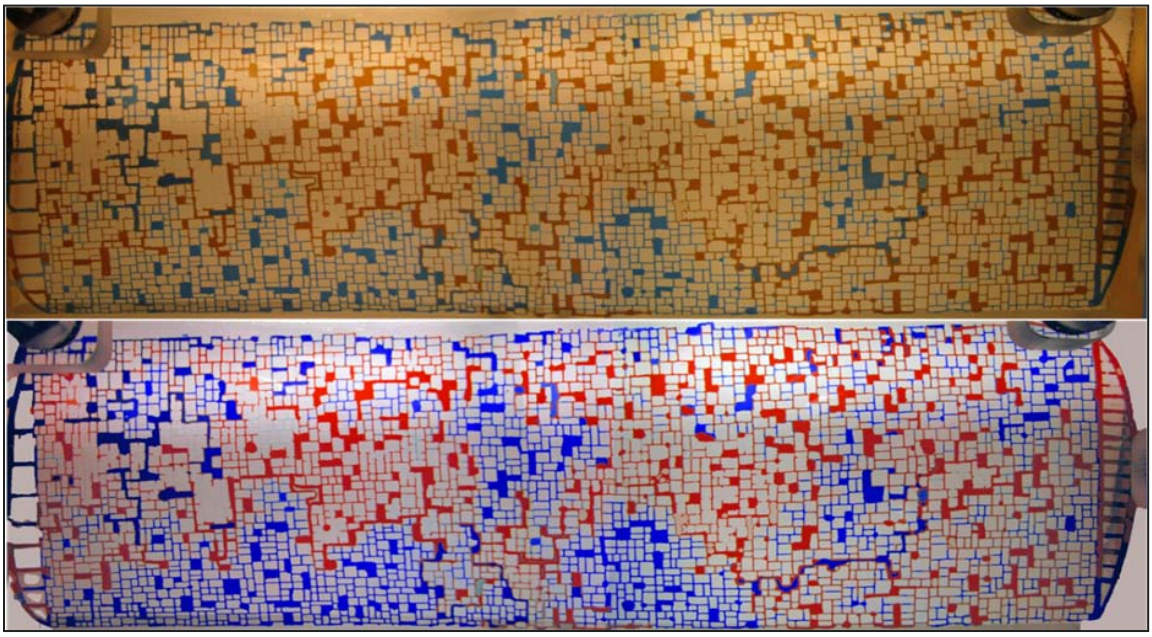

Figure II.1: Oil/water zone selection

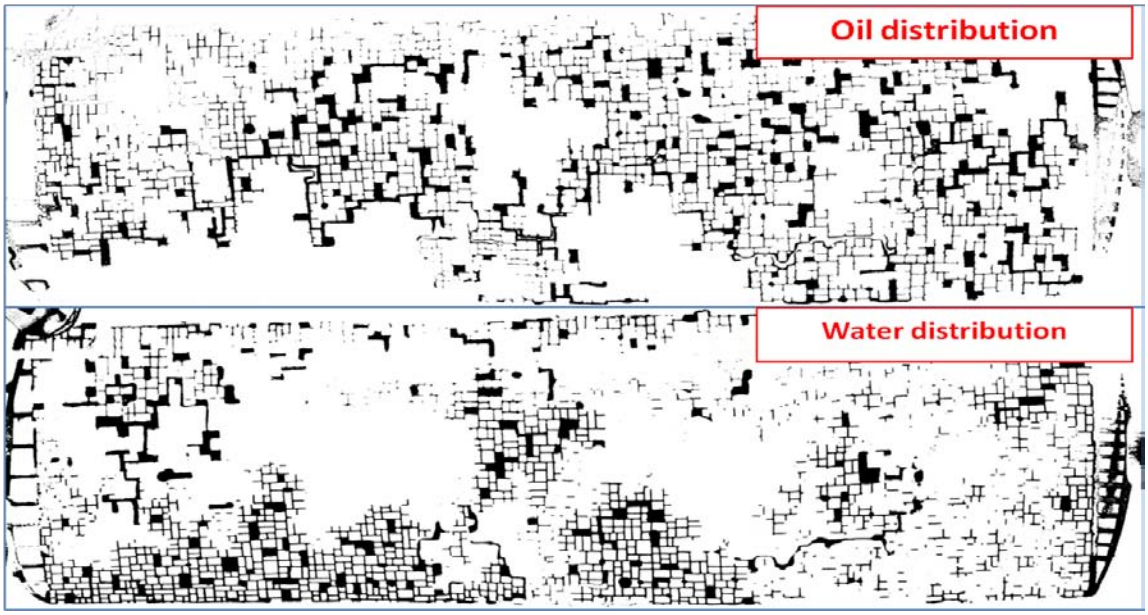

Figure II.2: Oil/water saturation calculation

Assumed the pore space was fully occupied by water and oil, so the oil and water saturation can be calculated when the areas of oil zone and water zone were known. Oil saturation is equal to the fraction of oil zone over the summation of both areas. Water saturation is equal to one minus oil saturation (Equation 4.1). Table II.1 shows the result of saturation calculation.

Table II.1: Result of image analysis process

	Count	Total Area	Average Size	Area Fraction	Saturation
oil	4317	2120142	491.115	13.3	0.4765
water	2690	2329701	866.06	14.6	0.5235

Verification of the Result of Image Analysis

In this section, the saturations calculated with mass balance method are compared to those calculated with image analysis method. The micromodel was initially saturated with blue water, then oil was injected at the rate of 100 µl/hr. Before oil arriving at the outlet, the amount of oil injected into the micromodel and the pore volume were known, so the oil saturation can be calculated.

Table II.2 shows the relative error of the result of image analysis. In the comparison, the values calculated from mass balance were supposed to be true. In fact, the error is small, and the results of two methods show good agreement.

Table II.2: Comparison between image analysis and mass balance

	Oil Saturation, %		Error, %
	Mass balance	Image analysis	
0.5 hr	6.08	6.03	0.82
1 hr	12.17	12.08	0.74
1.5 hrs	18.25	18.3	0.28
2 hrs	24.33	24.4	0.28
2.2 hrs	26.76	26.01	2.82

In the saturation calculation process, the oil/water zone selection was the most important step. Both oil and water zones should be selected carefully. Especially when dealing with the tiny pores, carefulness and patience were both needed.

APPENDIX III: INSIGHT INTO DIFFERENTIAL PRESSURE VARIANCE

Differential pressure data is very important in this research. It reflects flow resistance through the micromodel. Some imbibition mechanisms can be extracted from these data as well. This appendix evaluated the effect of liquid drop at the production end on differential pressure variance. Experiments were conducted at different water injection rates. Based on water injection rate and average time elapsed per drop, average volume per drop was calculated. At last, the possible source of error was analysed.

Experimental design

In order to reduce possible factors resulting in pressure variance, no piston cylinder was used in this experiment. A stop watch was used to measure the time elapsed per one drop. Figure III.1 shows the schematic diagram of this experiment.

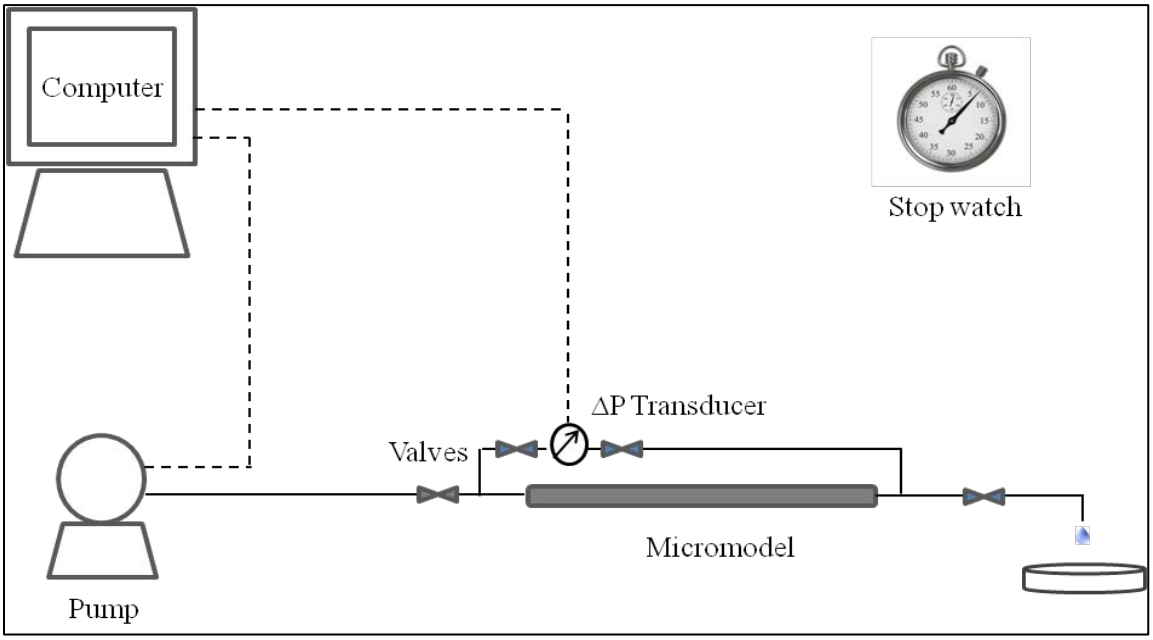

Figure III.1: Water drop experiment

In this experiment, just water sample was tested. The micromodel was saturated and then flooded with distilled water only. At the beginning, the micromodel was cleaned and vacuumed following the procedure as described in section 3.3. Then, the micromodel was instantly saturated with distilled water. At last, waterflooding began. No air bubble was allowed to exist in the micromodel, as it would affect flow resistance.

Result

Figure III.2 shows the differential pressure response of different water injection rates. When both ports of transducer were open to air, the differential pressure should be zero. The line of “open to air” is horizontal and very stable even through its value is not zero. Its value “-0.04kPa” should be used to correct other readings. For other four tests, their values increase and decrease periodically. According to observations, a peak on every curve means the beginning of formation of a drop. The process when a curve is moving downward means a drop is expanding. At the lowest point of every period, the related drop is falling.

The whole process of beginning, expanding and falling is very clear for the tests of 100µl/hr and 500µl/hr. For tests of 1000µl/hr and 2000µl/hr, data points are too sparse to perfectly depict the whole process. The water injection rate 10µl/hr was not tested. However, its tendency can be extrapolated based on above rates tested. Based on these curves and water injection rates, drop volume and differential pressure variance were further analyzed in the next step.

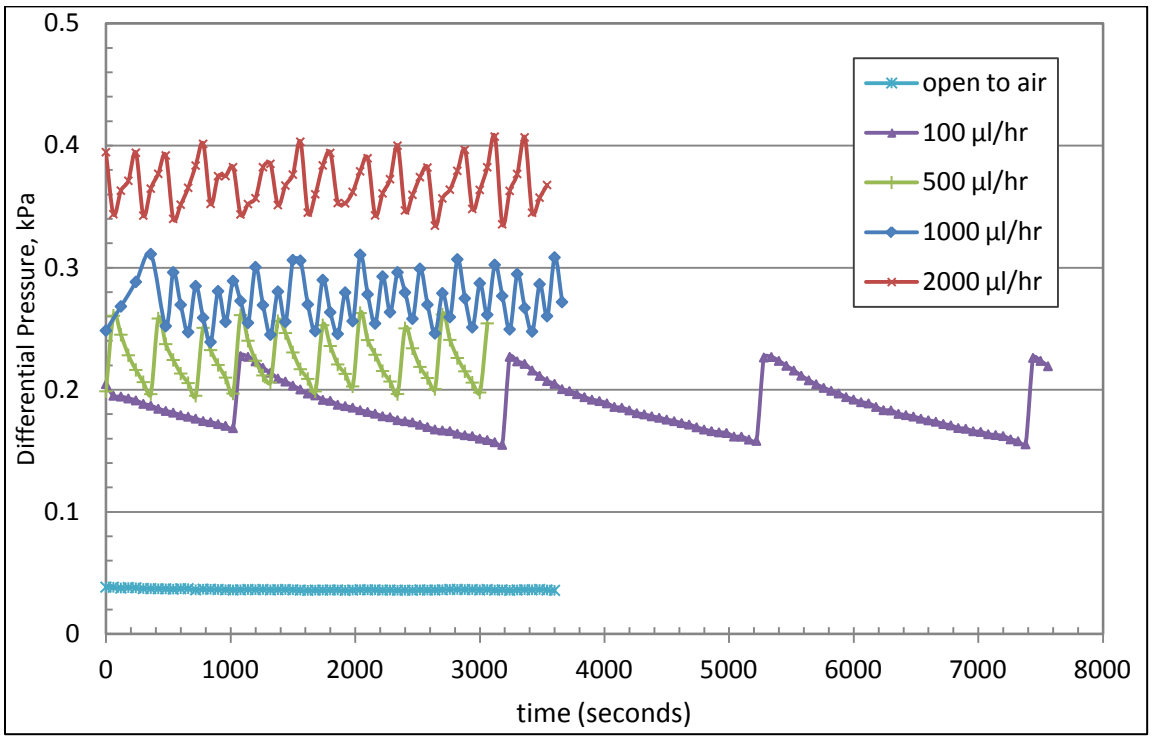

Figure III.2: Differential pressure curves of water drop experiment

Table III.1 shows the results of time, volume and differential pressure calculation. The value of ΔP (differential pressure variance) is equal to maximum of differential pressure minus minimum. As listed in the table, the average volume per drop is 0.048ml, and the average differential pressure variance is 0.065kPa.

Table III.1: Result of water drop experiments

Inj. Rate µl/hr	Ave. Time/Drop second	Vol./Drop ml	Ave. Vol/Drop ml	ΔP kPa	$\overline{\Delta P}$ kPa
100	2040	0.057	0.048	0.0688	0.0653
500	332	0.046		0.0663	
1000	162	0.045		0.0606	
2000	78	0.043		0.0655	

According to above results, the average time per drop for the rate of 10μl/hr should be 17280 seconds (~ 4.8 hrs). And the ΔP should be around 0.065kPa.

In Chapter 4, Figure 4.5 shows the differential pressure response of A5-10. During the period of 12-13×10^5 seconds, there should be only 5.8 drops. However, there are 17 peaks on the curve. And the differential pressure variance is 0.2 ~ 0.5kPa which is much greater than 0.065kPa. Therefore, except liquid drop at the outlet, there should be other factors which may lead to differential pressure variation.